ROZPRAWA DOKTORSKA

Passive microfluidic systems

for development of analytical assays

Adam Stanisław Opalski MSc

Matriculation number 17/2014

Supervisor: Professor Piotr Garstecki

Auxiliary advisor: Ladislav Derzsi PhD

The dissertation was prepared within the International PhD Studies at the

Institute of Physical Chemistry of the Polish Academy of Sciences

ul. Kasprzaka 44/52, 01-224 Warsaw

Warsaw, July 2019

Niech cię nie niepokoją
Cierpienia twe i błędy.
Wszędy są drogi proste
Lecz i manowce wszędy.

O to chodzi jedynie,
By naprzód wciąż iść śmiało,
Bo zawsze się dochodzi
Gdzie indziej, niż się chciało.

Zostanie kamień z napisem:
Tu leży taki i taki.
Każdy z nas jest Odysem,
Co wraca do swej Itaki

Odys

Leopold Staff

Acknowledgements

The Institute of Physical Chemistry is not limited to Garstecki Lab. I would like to express gratitude to all of the current and former workers. I especially acknowledge Łukasz Richter, Marta Janczuk-Richter, Krzysztof Sozański, Kinga Matuła, Jan Guzowski, Robert Buda, Marco Costantini.

Special thanks go to my father, Leszek Opalski, who helped me formulate and express ideas in scientific manner, and introduced me to the world of automation of the data extraction.

Praca, choćby najbardziej doniosła, nie wypełnia całego życia. Chciałbym szczególnie podziękować mojej rodzinie i przyjaciołom za ich miłość, przyjaźń, wsparcie i po prostu za obecność.

Dziękuję serdecznie rodzicom, Leszkowi i Katarzynie, oraz braciom, Krzysztofowi, Marcinowi i Janowi, a także wszystkim przyjaciołom, wymienionym z imienia i nie. Dziękuję Szymonowi i Bogusi Dziewulskim, Alicji Matuszewskiej i Piotrowi Wojtaszewskiemu za wspólną grę w brydża i wypady na żagle, Danielowi Paprockiemu i Pawłowi Mitkowskiemu za wspólną historię tworzoną od pierwszego roku studiów, ekipie ursynowskiej za niezliczone miłe chwile (nawet przy śpiewaniu) oraz Karolinie Włodydze za to że ze mną wytrzymuje z uśmiechem, sprawiając że i ja uśmiecham się częściej.

Funding

List of publications and patent applications

Publications related to the topic of the dissertation:

1) F. Dutka, **A. S. Opalski** and P. Garstecki, *Nano-liter droplet libraries from a pipette: step-emulsificator that stabilizes droplet volume against variation in flow rate.,* Lab on a Chip, 2016, 16, 2044–2049.

2) **A. S. Opalski**, T. S. Kaminski and P. Garstecki, *Droplet Microfluidics as a Tool for the Generation of Granular Matters and Functional Emulsions,* KONA Powder Part. J., 2019, 36, 50–71.

3) **A. S. Opalski**, K. Makuch, Y.-K. K. Lai, L. Derzsi and P. Garstecki, *Grooved step emulsification systems optimize throughput of passive generation of monodisperse emulsions,* Lab on a Chip, 2019, 19, 1183–1192.

4) **A. S. Opalski**, K. Makuch, L. Derzsi and P. Garstecki, *Split or slip - passive generation of monodisperse double emulsions with cores of varying viscosity,* in preparation

5) **A. S. Opalski**, A. Ruszczak, Y. Promovych, M. Horka, L. Derzsi and P. Garstecki, *Combinatorial antimicrobial susceptibility testing in microwells prefilled by non-contact printing,* in preparation

Other publications:

1) **A. S. Opalski**, I. Grabowska-Jadach and S. Oszwaldowski, *Biological Activity of Surface Modified Nanocrystals,* Current Nanoscience, 2018, **14**, 307–312.

Patent applications:

1) **A. S. Opalski**, K. Makuch, Y.-K. Lai, L. Derzsi, and P. Garstecki, *Układ mikroprzepływowy,* Polish patent application P.425543, submitted on 15.05.2018

Contributions

This dissertation includes the experimental results of two finished research projects, each ending with peer-reviewed publications, and one that has not yet been published. In one of the publications I am the co-author and in the other one I am the first author of the publication. I am also a first author of a peer-reviewed review publication.

F. Dutka, **A. S. Opalski** and P. Garstecki, *Nano-liter droplet libraries from a pipette: step-emulsificator that stabilizes droplet volume against variation in flow rate,* Lab on a Chip, 2016, 16, 2044–2049.

Main contribution: PG, FD and AO worked on the concept of the project. FD and AO conducted experiments and analyzed the results. FD, AO and PG together interpreted the results and wrote the manuscript.

A. S. Opalski, K. Makuch, Y.-K. K. Lai, L. Derzsi and P. Garstecki, *Grooved step emulsification systems optimize throughput of passive generation of monodisperse emulsions,* Lab on a Chip, 2019, 19, 1183–1192.

Main contribution: PG, KM, LD and AO worked on the concept of the project. AO and KM developed the architecture of microfluidic system. AO and YKL conducted experiments. AO, YKL and KM analyzed the results. AO, KM, YKL, LD and PG interpreted the results and wrote the manuscript.

A. S. Opalski, T. S. Kaminski and P. Garstecki, *Droplet Microfluidics as a Tool for the Generation of Granular Matters and Functional Emulsions,* KONA Powder Part. J., 2019, 36, 50–71.

Main contribution: PG, TK and AO worked on the concept of the project. AO and TK researched the literature. AO, TK and PG wrote the manuscript.

All results included in this dissertation are presented with the consent of all of the co-authors. All projects were conducted under the guidance of prof. Piotr Garstecki, the supervisor of my doctoral studies.

Contents

10

11

List of used symbols and abbreviations

A	area
Bo	Bond number
Ca	capillary number
CNC milling	Computerized Numerical Control milling
CV	coefficient of variation
DCM	dichloromethane
DE	double emulsion
DIW	deionized water
d_n	nominal droplet size
FC	fluorocarbon
G^σ	surface free energy
G_f	energy of formation
HFE	hydrofluoroether
ΔP	Laplace pressure
O/W	oil in water emulsion
PC	polycarbonate
PCR	polymerase chain reaction
PDI	polydispersity index
PDMS	poly(dimethylsiloxane)
PE	poly(ethylene)
PEG	poly(ethylene glycol)
PFPE	perfluoropolyether
PTFE	poly(tetrafluoroethylene)

PVA	poly(vinyl alcohol)
Q	volumetric flow rate
Q_{drip}	flow rate providing dripping droplet formation
Re	Reynolds number
S	entropy
SD	standard deviation
U	velocity
We	Webber number
W/O	water in oil emulsion
W/O/W	water in oil in water emulsion
α	coefficient of droplet size insensitivity to flow rate variations
γ	surface tension
θ	contact angle
λ	viscosity ratio
μ	absolute viscosity

Streszczenie (abstract in Polish)

Mikrofluidyka kropelkowa to interdyscyplinarna dziedzina nauki zajmująca się wytwarzaniem, manipulacją i wykorzystaniem kropelek w mikroskali. Kropelki wytwarzane są w mikrokanałach specjalnych urządzeń mikroprzepływowych. Architektura mikrokanałów, czyli rozmiar i rozmieszczenie mikrokanalików w urządzeniu mikroprzepływowym, ma wielki wpływ na rozmiar i rozrzut rozmiarów wytwarzanych kropelek.

We wnętrzu każdej kropli można przeprowadzić różne operacje, od reakcji chemicznych po prowadzenie hodowli komórkowej. Duża liczba przedziałów reakcyjnych oferowana przez emulsje pozwala na przeprowadzenie w nich eksperymentów w wielu powtórzeniach. Emulsje są często wykorzystywane do celów analitycznych, takich jak amplifikacja kwasów nukleinowych czy badania przesiewowe toksyczności leków. Metody kropelkowe zrewolucjonizowały nauki bioanalityczne, przez umożliwienie przeprowadzenie badań wcześniej technicznie niemożliwych ze względu na liczbę potrzebnych przedziałów. Przykładem takich badań jest na przykład sekwencjonowanie genomów pojedynczych komórek w dużych populacjach. Krople wykorzystywane w metodzie analitycznej powinny być monodyspersyjne – jednolite pod względem wielkości – by zapewnić kropli stabilność i umożliwić porównanie wyników z różnych kropli. Pasywne metody mikrokropelkowe produkują monodyspersyjne emulsje, niestety z małą wydajnością. Intuicyjne rozwiązanie problemu wydajności, polegające na zwiększeniu tempa emulsyfikacji, prowadzi do zmian rozmiarów kropli i rozrzutu tych rozmiarów.

Celem przedstawionej pracy była optymalizacja pasywnych architektur mikroprzepływowych w celu i) zmniejszenia zależności rozmiaru produkowanych kropli od tempa emulsyfikacji, ii) zwiększenia wydajności produkcji kropli oraz iii) produkcji emulsji wielokrotnych w sposób pasywny. Spodziewanym wynikiem było opracowanie urządzeń mikroprzepływowych wydajnie produkujących monodyspersyjne krople, nadające się do wykorzystania w celach analitycznych.

Niniejsza rozprawa doktorska została podzielona na trzy części: wstęp, wyniki, spis piśmiennictwa. Pierwsze cztery rozdziały wprowadzają Czytelnika w temat

rozprawy. W rozdziale pierwszym opisane zostały emulsje i ich właściwości. W rozdziale drugim przedstawione zostały informacje dotyczące mikrofluidyki kropelkowej, ze szczególnym uwzględnieniem pasywnych metod produkcji kropli. W trzecim rozdziale pracy sformułowałem cele badawcze. Czwarty rozdział pracy zawiera spis wykorzystanych w pracy materiałów oraz opis metod. Rozdziały od piątego do siódmego opisują eksperymentalną część pracy. W rozdziale piątym opisałem jak, poprzez modyfikację geometrii emulsyfikatora stopniowego, można zmniejszyć zależność między rozmiarem produkowanej kropli a tempem podawania rozpraszanego płynu. W szóstym rozdziale przedstawiłem jak zwiększyć wydajność produkcji kropli poprzez modyfikację architektury pasywnego urządzenia mikroprzepływowego. Rozdział siódmy poświęciłem opisowi pasywnego wytwarzania emulsji podwójnych w układzie mikroprzepływowym. W ostatnim, ósmym, rozdziale pracy podsumowałem otrzymane wyniki, przedstawiłem wnioski z przeprowadzonych projektów oraz zarysowałem możliwe perspektywy wykorzystania pasywnych technik kropelkowych do rozwoju metod analitycznych.

Abstract

Droplet microfluidics is an interdisciplinary field of science dealing with production, manipulation and use of the droplets at the microscale. Droplets are produced in microchannels of engineered cartridges called microfluidic devices. Architecture of microfluidic device, a way the microchannels are placed in the microfluidic device, greatly influences the size of the generated droplets and uniformity of their sizes.

Inside each of the droplet of the emulsion a number of operations can be carried out, for example conducting the chemical reaction or culturing cells. Large number of compartments offered by emulsions allows performing assays with many repetitions. Emulsions are useful in analytical schemes such as nucleic acid amplification or drug toxicity screening. Droplet microfluidics revolutionized the field of bioanalytics, allowing performing assays previously unattainable due to technical limitations of number of compartments. Example of such assay is sequencing genomes of single cells in large bacterial populations. Droplets required for analytical methods should be monodisperse – uniform in size – to provide the emulsion stability and allow direct comparison of results from distinct droplets. Passive droplet microfluidic techniques offer tightly monodisperse emulsion, though at quite low throughput (droplets production rate). The intuitive solution is to increase the flow rate of the emulsified liquid in order to increase the throughput. However, increasing the flow rate of the to-be-dispersed (droplet) phase in standard passive droplet generating junctions results in changing the emulsion size and uniformity.

The aim of this dissertation was optimization of passive droplet microfluidic architectures in order to i) decouple the produced droplet volume from the flow rate of the droplet phase, ii) increase the throughput of the device, and iii) explore possibility of producing complex emulsions using step emulsificator. The expected outcome was creation of an emulsificator that would produce monodisperse emulsions useful for development of analytical assays in wide range of flow rates.

The dissertation consists of three main sections: introduction, results, and literature. First four chapters offer introduction to the subject of the dissertation. Chapter 1 introduces emulsions and their properties. Chapter 2 provides description of the droplet microfluidics, with emphasis on passive droplet generation schemes. In

Chapter 3 research objectives of my dissertation are revealed. Chapter 4 includes description of the materials and methods used in the described experiments. Chapters 5-7 describe selected experimental results of the projects I researched. In Chapter 5 I described how to decouple droplet volume from flow rate of the droplet phase in step emulsificator. In Chapter 6 I present how I upscaled the production of monodisperse emulsions from the step emulsificators by modifying the microfluidic device architecture. In Chapter 7 I describe passive production of double emulsions in the microfluidic device. Chapter 8 concludes the dissertation with the summary, conclusion and perspectives of use of developed step emulsificators in development of analytical schemes.

Motivation and aim of the dissertation

Nowadays, medical diagnostics is a rapidly developing field both due to the increased demand and due to new technological solutions. The aim is straightforward – to get better, cheaper, faster and more informative diagnostics and aid disease prevention and treatment. To tackle such challenges, new approaches to diagnostics were invented. One of them is a concept of digital assays – splitting a sample into numerous compartments, so each compartment contains either one or zero molecule or cell of interest. Then, the same operation is performed on all of the compartments simultaneously, e.g. amplification of the nucleic acid confined within the compartment. In empty compartments nothing happens, but in the occupied microreactors the reaction occurs and it can be detected [1–4]. This allows for precise quantification of the initial concentration of the tested agent (e.g. pathogen infecting the patient[5]), as well as identification and extraction of agents of interest from a whole pool of sample (e.g. a single cancer cell or bacterium out of thousands present in the blood sample[5,6]).

Diagnostic assays can be performed in classical way, in Petri dishes, in lab tubes or in micro-titer plates. However, their throughput is limited, and costs and sample requirements are high. Another way to run digital assay is to employ droplet microfluidics that can cut workload, time of operation and cost of the assay. Exemplary comparison of running an extensive screen of bacterial mutants by robot-based methods and ultrahigh-throughput microfluidic droplet method is presented in Table 1.

Droplet microfluidics is a field of science dealing with microscopic volumes of fluids engulfed in another liquid and confined within microchannels. Such discrete volumes of liquids, emulsions, can be used as containers and microreactors. Volumes of droplets are small (usually in nano- or picoliter scale, but even attoliters are attainable[9]), lowering the cost, enhancing the throughput and dynamic range of assays performed within. This is why emulsions, single and multiple, may serve as versatile tool for advances in science, in commercial applications, and medical diagnostics[7].

Table 1 Comparison of robotic and microfluidic-run assay and their cost. Adapted from Agresti et al[8]

	Robot	Microfluidic drops
Total reactions	5×10^7	5×10^7
Reaction volume	100 μL	6 pL
Total volume	5,000 L	150 μL
Reactions/day	73,000	1×10^8
Total time	~2 years	~7 h
Number of plates/devices	260,000	2
Cost of plates/devices	$520,000	$1.00
Cost of tips	$10 million	$0.30
Amortized cost of instruments	$280,000	$1.70
Substrate	$4.75 million	$0.25
Total cost	$15.81 million	$2.50

Passive microfluidics is a set of microfluidic techniques that utilize surface forces to produce emulsions of to-be-dispersed phase in outer phase. Passive microfluidics methods contrast to active microfluidic techniques that are based on shearing droplets from the stream of to-be-dispersed phase by flow of the continuous phase. The droplet generation process in passive emulsification is controlled mainly by the surface forces, that in turn can effectively be 'tamed' by tight geometrical confinement. Thus, geometry of the passive microfluidic devices determines the throughput and quality of the generated emulsions. Passive microfluidics features multiple advantages over active methods, such as easy parallelization, low energy input, and high monodispersity of produced emulsion. Monodispersity is a crucial parameter of emulsion from application point of view. Monodispersity characterizes the size uniformity of produced droplets. The smaller the variability of droplet size, the better as the droplets are more stable and can serve as reliable microreactors[11].

This dissertation researches use of passive microfluidic methods for droplet generation. I aimed to deliver robust microfluidic step emulsificators that would produce monodisperse single and double emulsions. I set out to investigate in details process of formation of single and double emulsions in passive microfluidic step emulsificators. The goal of that investigation was to introduce novel microfluidic geometries that generated droplets useful for development of analytical assays.

19

I. INTRODUCTION

This section introduces the Reader to fundamentals of the emulsions (Chapter 1), and droplet microfluidics and droplet applications in analytical assays (Chapter 2). The introduction is based on literature review and my peer-reviewed publication, *Droplet Microfluidics as a Tool for the Generation of Granular Matters and Functional Emulsions*, **A. S. Opalski**, T. S. Kaminski and P. Garstecki, *KONA Powder Part. J.*, 2019, 36, 50–71., DOI: 10.14356/kona.2019004 [9]. Chapter 3 lists all of the materials and methods I used throughout my experiments.

1. **Emulsions**

This chapter introduces the emulsions. Fundamental properties of emulsions are explained to orient the reader in the subject of the dissertation.

1.1. General information

International Union of Pure and Applied Chemistry (IUPAC) defines an emulsion as *'A fluid colloidal system in which liquid droplets and/or liquid crystals are dispersed in a liquid. The droplets often exceed the usual limits for colloids in size. An emulsion is denoted by the symbol O/W if the continuous phase is an aqueous solution and by W/O if the continuous phase is an organic liquid (an 'oil'). More complicated emulsions such as O/W/O (i.e. oil droplets contained within aqueous droplets dispersed in a continuous oil phase) are also possible. Photographic emulsions, although colloidal systems, are not emulsions in the sense of this nomenclature'*[10]. Emulsions are in high demand, due to their uses in various industries[11], as well as in research[12] and diagnostic assays[13]. In essence, emulsification of fluid allows to create more compartments to investigate, as shown schematically in Figure 1. What is more, emulsions bear many similarities with granular matter, as both comprise discrete pieces of matter immersed in an interstitial fluid, and hence are of interest to powder and particle engineers[9,14]. More complicated emulsions, called multiple emulsions are sets of nested drops. They differ from single emulsions, called just 'emulsions' in some properties due to the more complex structure[15,16].
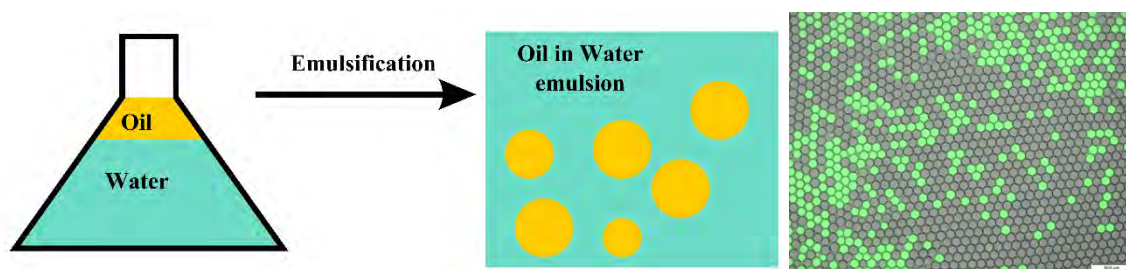
*Figure 1 **Left:** Schematic representation of emulsification – turning two separate phases into an emulsion. **Right:** Water in oil emulsion under fluorescent microscope. Some droplets contain fluorescent dye, fluorescein isothiocyanate. Image is a courtesy of Simona Bartkova PhD, and Professor Ott Scheler, Tallinn University of Technology.*

Emulsion size is usually characterized by the mean diameter of the droplets, usage of droplet radius or volume is less common. Emulsions typically range from single to hundreds of micrometers in diameter, while microemulsions range from 1 to 100 nanometers[17]. Emulsion size also comprises index of droplet size distribution. Common measure of uniformity of droplet population is a coefficient of

variation of droplet diameters, CV (standard deviation of the diameters of the droplets in emulsion divided over mean diameter of emulsion in population). The value of CV=5% is used as an arbitrary yet common threshold that distinguishes uniform population from non-uniform one, with uniform ones called monodisperse and non-uniform polydisperse. Another name found in literature for the population description is polymer-derived term polydispersity index (PDI). While CV is widely accepted measure of monodispersity, some researchers claim that other statistical value should be employed. US-based National Institute of Standards and Technology defines monodisperse population as one with an unimodal distribution about a median value, where at least 90% of the measured objects lies within 5% of the median size[21]. Even though the term monodisperse is not recommended by IUPAC[10], it is broadly used to describe a population considered uniform (CV<5%)[18–20]. In this dissertation I refer to such uniform populations as monodisperse and use CV as measure of uniformity of emulsion.

1.2. **Interfacial forces**

Liquid-liquid interface is defined as the boundary between bulks of two liquid phases, with different properties than any of the bulk phases. An useful quantity to describe thermodynamics of the interface is the interfacial tension, γ, which can be defined as the measure of change of free energy of interface surface when changing interfacial area, under given conditions[21].

$$\gamma = \left(\frac{\partial G^{\sigma}}{\partial A}\right)_{T,n_i}$$

Equation 1 Interfacial tension.

Where:

γ – surface tension [N/m],

G^{σ} - the surface free energy [J],

A – area [m^2],

T, n_i – constant temperature [K] and composition of the system [mol].

Surface tension stems from the cohesive forces of the molecules at the interface. Liquid molecules at the liquid-liquid interface are held together by cohesive forces and each molecule is pulled in every direction equally by the neighbors. At the interface between two immiscible fluids molecules are pulled only by neighboring molecules from the inside of the interface (inside of the droplet). In order to minimize the energy the interface curves into a sphere, and this is why interfacial tension is usually referred to as a measure of tendency to curve the interface to minimize the surface area[22]. Interfacial tension is a crucial factor in the droplet stability[23], which is described in details in the next sections.

The curvature of the droplet interface introduces another physical phenomenon, a difference of pressures across the interface – the Laplace pressure (ΔP). In the equilibrium state this pressure is balanced by the surface tension. Balance of forces is described by the Young-Laplace equation:

$$\Delta P = P_{inside} - P_{outside} = \gamma \left(\frac{1}{R_1} + \frac{1}{R_2} \right)$$

Equation 2 Young-Laplace equation[22,24].

Where:

ΔP – Laplace pressure [Pa],

P_{inside} – pressure inside the curved interface [Pa],

$P_{outside}$ - pressure outside the curved interface [Pa],

γ – surface tension [J/m^2],

R_1 and R_2 – principal radii of curvature [m].

1.3. **Wetting**

Wetting is the ability of the solid surface to maintain contact with a continuous liquid due to molecular interactions[24]. Wetting can be defined as the function of the surface tension and contact angle between the fluid and the solid and is schematically presented in Figure 2. Contact angle θ can be calculated by using the Young relation:

$$\gamma_{SG} = \gamma_{SL} + \gamma_{LG} * \cos \theta$$

Equation 3 Young relation.

Where:

γ_{SG} – interfacial tension between solid substrate and the gaseous medium,

γ_{SL} – interfacial tension between the solid substrate and the liquid drop,

γ_{LG} – interfacial tension between the liquid drop and the gaseous medium,

θ – contact angle between the solid and liquid phase.

For contact angle <90^0, wetting of the surface by the liquid is favorable. For contact angle >90^0, wetting is unfavorable – fluid minimizes the contact area with solid. For contact angle~90^0 liquid partially wets the substrate, which makes the precise control over liquid very challenging. Droplet microfluidic devices work controllably if the walls of the microchannel are wetted by the continuous phase and not wetted (even partially) by the droplet phase. This is why wetting of the channel walls by both phases should be perfectly controlled in order for the system to work in a stable and predictable manner. Preferential wall wetting by immiscible liquids determines which phase is the continuous phase and which one will be droplet phase. Any multiple emulsions with oil as the outer phase (W/O or higher order e.g. O/W/O emulsions), are made in hydrophobic devices (or fluorophilic if fluorinated oil is used)[25], and oil in water O/W (or multiple W/O/W) emulsions are formed in hydrophilic devices[26,27]. Microfluidic devices might contain zones of different wetting properties, often used for double emulsion formation[28].
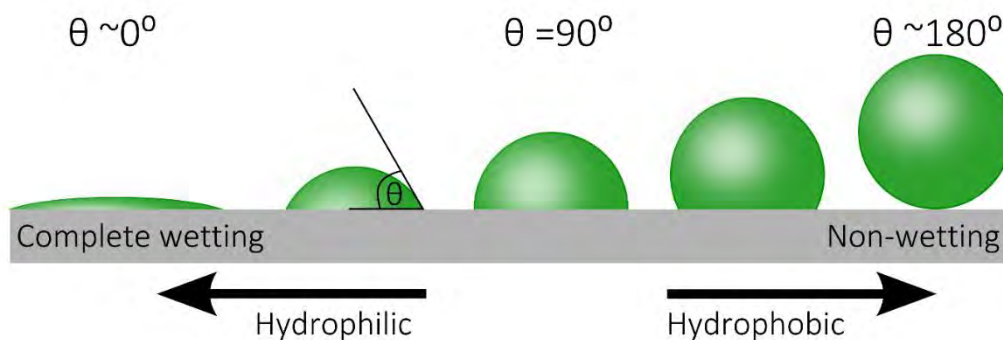
Figure 2 Schematic illustration of phenomena of hydrophilicity and hydrophobicity and partial wetting of the surface as a function of the static contact angle of the aqueous droplet phase on the solid substrate. Adapted from [9]*.*

1.4. Surfactants

Surfactant is a term for surface-active agent, an amphiphilic molecule that has different moieties with affinities for different immiscible phases, e.g. water and fluorinated oil. If surfactant is present in one phase, which forms an interface with the phase that the surfactant has the affinity to, the surfactant molecules are driven to the interface. Adsorption of surfactant to the interface modifies its properties. Most importantly, the interfacial tension is lowered, but also the interactions between the phases and internal flows within droplets are influenced[19,29]. The number of free surfactant molecules in the solution is determined by critical micellar concentration (CMC). When the concentration is higher than CMC, all of the excess of surfactant molecules self-assemble into structures called micelles[24].

Two-phase system is in thermodynamic equilibrium when the phases are separated. Thus, if one phase is dispersed in another, the system is out of equilibrium and a force arises to reach the equilibrium. Emulsions are metastable, due to interfacial tension counteracting the sample homogenization. Surfactant-stabilized emulsions are more resistant to coalescence than surfactant-free emulsions, even though they are not immune to it[30]. The increase of emulsion stability is the key advantage of use of surfactants.

The most common composition of continuous phase used in droplet microfluidics comprises fluorinated liquid and a biocompatible fluorosurfactant. For other liquids

one must use suitable surfactant which is often a challenge[19,31]. Typically, the surface tension value of aqueous sample-fluorinated oil with surfactant is of order of few mN/m – much smaller than surface tension of water-fluorinated oil without surfactant (5.2×10^{-4} N/m) or water-air (7.2×10^{-4} N/m) systems[32].

Choice of surfactant for the emulsion is critical. Common water-soluble emulsificators are sodium dodecylsufate (SDS) or Triton®X--100. Two widespread hydrocarbon oil-soluble surfactants are Span and Ebil 90. In case of use of fluorinated oil, most widespread are tri-block copolymers, with two ends of the chain being fluorinated (fluorophilic, e.g. Krytox®-based), and with hydrophilic middle segment, e.g. chain of poly(ethylene glycol[19,33]. Novel and promising approaches to stabilize emulsions without the use of surfactants are based on the use of nanoparticles in the so-called Pickering emulsions [34,35], or to design surfactant-free emulsions[36].

1.5. **Droplet stability**

The lifetime of emulsion ranges from fractions of second to years – it depends on the droplet stability. Droplet stability depends on a number of factors, such as droplet population size distribution, density difference between the droplets and the continuous phase, attractive and repulsive forces, surface tension and properties of used surface active agents. Droplet can be subjected to a number of breakdown processes, such as: creaming, sedimentation, flocculation, phase inversion, coalescence and Ostwald [22]. All of the processes might happen at the same time. Creaming and sedimentation are processes in which external force (gravitational or centrifugal) acting on the droplets exceeds the Brownian motion and causes the droplets to migrate to top (creaming) or bottom (sedimentation) of the container. Rate of movement depends on the density gradient and size of the droplet, the larger the droplet the faster the movement. Flocculation is a process of droplet aggregation, without changing the size of individual droplets as a result of van der Waals attractions exceeding repulsion forces. Ostwald ripening stems from mutual solubility of the liquid phases comprising emulsion. Curvature effects result in smaller droplets having larger solubility than larger droplets, which in time leads to disappearance of smaller droplets and diffusion of their molecules to the bulk and subsequent deposition on the larger droplets. Coalescence is a process in which the liquid film between two or more droplets thins and is disrupted and fusion of involved droplets

happens. Phase inversion is described as dispersed phase and the outer phase changing their roles – outer phase becomes dispersed in the previously-dispersed-phase. This process might lead to formation of (usually polydisperse) double emulsions[22].

Emulsions are sometimes called macroemulsions to distinguish them from microemulsions. Microemulsions (diameter 1 to 100 nanometers) are distinct class of emulsions due to their unique properties – they are isotropic, optically transparent and, unlike macroemulsions, thermodynamically stable dispersions of fluid in another fluid. Presence of surfactant is required for microemulsion formation[41]. The reason of stability is the thermodynamic spontaneity of microemulsion formation, stemming from negative interface formation energy ($\Delta G_f < 0$)

$$\Delta G_f = \gamma * \Delta A - T\Delta S$$

Equation 4 Gibbs energy of interface formation.

Where:

ΔG_f – change of Gibbs energy of formation [J],

γ – surface tension [N/m],

ΔA – change of interfacial area during emulsification [m^2],

T – temperature [K],

ΔS – change of entropy [J/K].

The condition $\Delta G_f < 0$ is met if the surface element of the equation is small and the entropic element is large. Presence of surfactant at the interface decreases the surface tension, and consequently the value of the first part of the Equation 4 Favorable entropic contributions arise from: i) high dispersion entropy from mixing the phases, ii) surfactant diffusion in the interfacial layer and iii) monomer-micelle surfactant exchange. In case of microemulsions, the entropic component gets greater than interfacial component and results in negative Gibbs energy, providing thermodynamic stability. Additionally, it also means that such emulsions will form on their own, without input of additional energy by mixing[37].

In case of three-phase system (such as a water droplet on solid substrate surrounded by air, or double emulsions), balance of forces between phases can be expressed in form of set of Young relations, called the Neumann triangle (see Figure 3):

$$\gamma_{AB} \cos \theta_B + \gamma_B + \gamma_A \cos(\theta_A + \theta_B) = 0$$

$$\gamma_{AB} \cos \theta_A + \gamma_A + \gamma_B \cos(\theta_A + \theta_B) = 0$$

Equation 5 Neumann triangle - balance of forces acting on the three-phase contact line

Where:

γ_{AB} – interfacial tension between phases A and B,

γ_A – interfacial tension between phase A and environment,

γ_B – interfacial tension between phase B and environment,

θ_A – contact angles of phases A,

θ_B – contact angles of phase B.

Interfacial tensions between phases define whether the multiple droplets will be completely engulfed by one another ($\gamma_A > \gamma_B + \gamma_{AB}$ or $\gamma_B > \gamma_A + \gamma_{AB}$), will be completely separated ($\gamma_{AB} > \gamma_A + \gamma_B$) or partially engulfing each other (droplets share interface, are both exposed to the outer phase and none of the previous inequalities hold)[38]. Special form of multiple droplet, Janus emulsion, is formed when two (or more) droplets are in contact, but do not engulf each other completely (see Figure 3). It has been shown that the systems can be design even to dynamically reconfigure the emulsion (make the core and shell switch places), by tuning interfacial tension of the fluids[39].
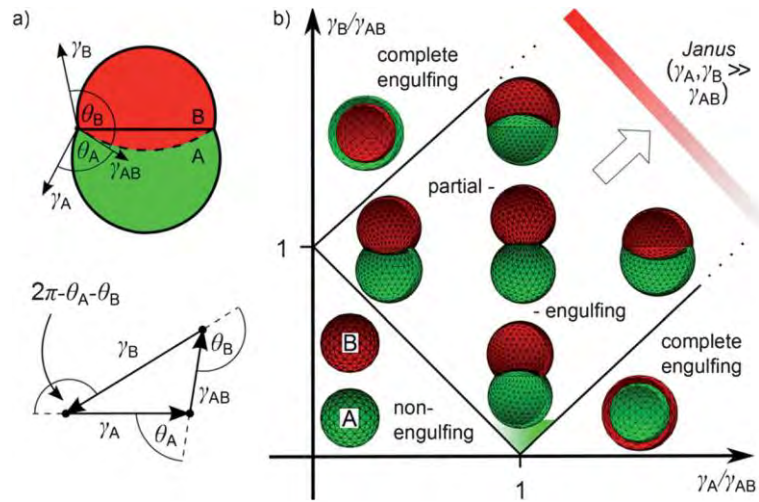
Figure 3 (a) Droplet composed of two phases with contact angles θ_A and θ_B(top) and the Neumann's triangle (bottom). (b) Stability diagram – all morphologies of the emulsion composed of two equal droplets. Adapted from [38].

1.6. **Dimensionless numbers**

Two dynamic forces that are important in hydrodynamics of emulsions are viscous forces and inertial forces. Viscous drag forces are parallel to the flow direction, while the inertial forces are perpendicular to the flow direction. Viscous forces are quantified by viscosity, defined as ratio of shear stress to the velocity of the fluid, and commonly referred to as the measure of resistance of a fluid to deformation. Inertial forces describe the lift induced by the flow past the surface of a body[40,41].Fluid dynamics reports ratios of some forces in the system as dimensionless numbers.

Reynolds (Re) number is a ratio of inertial to viscous forces. Re number defines whether the flow is turbulent (Re>~2300 or more) or laminar (Re<~2300)– exact values of laminar-turbulent transition depend on the system conditions[45]. In microfluidic devices due to small dimensions and velocities $Re \in (0,100)$, only laminar flow occurs in vast majority of conditions [42].

$$Re = \frac{\rho * U * d}{\mu}$$

Equation 6 Reynolds number.

Where:

ρ – fluid density [kg/m³],

U – fluid velocity [m/s],

d – typical length scale of the system (e.g. hydraulic diameter) [m],

µ – dynamic viscosity of the fluid [Pa × s].

From microfluidic point of view, the capillary number (Ca) is the most important factor. Ca is the dimensionless number representing the ratio of viscous forces versus interfacial tension forces. Capillary number is essential when considering events happening at a microscale in the microfluidic channels, e.g. Ca determines the regimes of droplet formation in droplet microfluidics[43,44]. Ca is defined as

$$Ca = \frac{\mu * U}{\gamma}$$

Equation 7 Capillary number.

Where:

µ - dynamic viscosity of the fluid [Pa × s],

U – characteristic velocity of the fluid [m/s];

γ – surface tension [N/m].

Weber number (We) results from combining Reynolds and capillary numbers, and it is a measure of inertial forces to surface forces. In microfluidics it is usually negligible, but can play role in some processes relying in part on inertia - such as jetting in co-flowing fluids[45] or one-step double emulsion formation[46].

$$We = Re * Ca = \frac{\rho * U^2 * d}{\gamma}$$

Equation 8 Weber number.

Where:

Re – Reynolds number,

Ca – capillary number,

ρ – density [kg/m^3]

U – characteristic fluid velocity [m/s]

31

d – typical length scale of the system (e.g. hydraulic diameter) [m],

γ – interfacial tension [N/m].

Bond number (Bo), sometimes called Eötvös (Eo) number compares gravitational forces to surface tension. Bond number is not often used, as rarely does gravity play significant role in microfluidic systems[20].

$$Bo = Eo = \frac{\Delta\rho * g * d^2}{\gamma}$$

Equation 9 Bond (Eötvös) number.

Where:

$\Delta\rho$ – density difference between liquids [kg/m^3]

g – gravitational acceleration [m/s^2]

d – typical length scale of the system (e.g. hydraulic diameter) [m],

γ – interfacial tension [N/m].

Viscosity ratio is defined as the ratio of dynamic viscosities of used phases. It is not 'named' as a number, however it is often used as a handy measure to describe the viscosity relation of two phases.

$$\lambda = \frac{\mu_d}{\mu_c}$$

Equation 10 Viscosity ratio

Where:

μ_d – viscosity of dispersed phase [Pa × s],

μ_c – viscosity of continuous phase [Pa × s].

2. **Droplet microfluidics**

This chapter introduces the droplet microfluidics. A background of droplet microfluidics is presented, as well as state of the art microfluidic systems and their applications for development of analytical assays.

2.1.   **General information**

Microfluidics is an interdisciplinary field intersecting engineering, physics, chemistry, nanotechnology, biology and material sciences[23]. Microfluidics studies the fluid properties at the microscale, including development of tools to study and utilize the physical phenomena. Microfluidic techniques are based on the precise handling of small volumes of fluids confined to miniature channels with typical dimensions from one to hundreds of microns. As mentioned before, the small dimensions guarantee the laminar flow of liquids and provide precise control over the transport of fluids[47,48]. The channels are usually microfabricated in inexpensive substrate (e.g. polymeric plate), making most of microfluidics chips disposable[49,50].

Historically, the beginning of the microfluidic were studies on capillary electrophoresis systems[51,52]. Then the main research focus switched to single-phase continuous-flow systems in which liquids flowed through the network of microfluidic channels. In such systems small portions of fluids are injected to device in a specified order, they are mixed, and incubated under various conditions[12,53]. Flow is usually applied and controlled via the use of pneumatic microvalves (pressure-driven flow), pumps (displacement-driven flow) or with the use of specific physical phenomena such as, e.g. electro- wetting or electro-kinetic flow[52,54,55]. The breakthrough point for microfluidics was the development of the microfluidic large-scale integration, which is a fluidic equivalent of a technology routinely used in the electronic industry. Large scale integration allowed for massive parallelization in the execution of biological assays and chemical reactions in complex microscopic hydraulic architectures[56,57]. Single-phase microfluidics has its limitations, such as Taylor-Aris dispersion (parabolic flow profile in the microchannel) which results in unequal residence times of substrates in single-phase microfluidic reactors, and possibility of microchannel contamination by the sample and cross-contamination between [53,58–61].

Next step in development of microfluidic techniques came with segmenting the flow of the sample into emulsions comprising discrete volumes dispersed in the second immiscible fluid. Emulsions are investigated and used by droplet microfluidics, in which two or more immiscible fluids are transported, manipulated and investigated in the network of microfluidic channels. Great advantage of the droplet microfluidics is the generation of the monodisperse emulsions that offer large numbers of identical,

isolated compartments—without the need to build solid wall enclosures for each of the microvolumes[8]. Risk of cross contamination is greatly reduced by the spatial isolation of sample elements by the continuous phase, which also eliminates Taylor-Aris dispersion[62]. Chaotic advection inside the droplets provides fast mixing [63-65]. Using nanoliter droplets instead of hundreds-of-microliter samples allows performing typical laboratory protocols using a fraction of the volume of the reagents. In some applications, mostly operations on single cells and single molecule assays, the run time is shorter when compared to batch methods[66]. Another advantage of droplet microfluidics is the possibility of automation of the protocols, which increases the throughput of procedures to thousands of operations per second (e.g. generation or sorting of droplets in the microfluidic device)[67-70]. In Figure 4 some of the properties and advantages of microfluidics are presented.

A) Presence of the interface
- isolation of the reaction volume
- reactions on the liquid-liquid interface

C) Operations on discrete microvolumes
- splitting
- merging
- sorting
- incubation
......

B) Small volume
- encapsulation of single cells or biomolecules
- stochastic confinement

D) Large number of droplets
- up to several thousands on a chip
- up to several millions during off-chip incubation

Figure 4 Schematic illustration of droplet microfluidic technologies and its properties. Adapted from Kamiński et al[7].

The strength of droplet microfluidics comes from the control over numerous droplet microreactors. Control is exerted by so called unit operations performed on droplets[71]. The unit operations can be divided into categories: generation, transportation, merging, splitting, incubation, detection, sorting[7]. Droplet generation is described extensively in the previous sections. Transportation unit operations are

all procedures that involve droplet change of position. Merging and splitting are operations that reduce or increase the number of droplets by joining them (e.g. by picoinjector[72]) or metering them into smaller ones (e.g. nanoliter droplet libraries made from microliter plug[73]). Other operations are detection of a signal from a droplet (e.g. fluorescent[74]), incubation (giving the confined reaction time to run)[75,76], and sorting – redirection of the droplet to one of distinct destinations, either by active redirection by e.g. by dielectrophoresis[8] or by use of passive external force, such as buoyancy coming from the density difference of the phases[77]. Microfluidic protocols contain variants of those unit operations, arrayed in desired order. Moreover, the unit operations can be carried out in the dedicated module, which is a building block of the integrated microfluidic system. Such modules can be arranged to form complex integrated microfluidic systems integrating multiple functionalities into a single microfluidic chip[78,79].

2.2. Fabrication of the microfluidic devices for production of microdroplets

Droplet microfluidic chips are not necessarily monolithic when it comes to the material used for their fabrication. Many materials can be used for that purpose, ranging from glass and silicone, through polymers to metals, and hybrids of the various materials[9]. Intended functionality, number of the chips, budget and the infrastructure of the research facility play major role in the choice of the material of the chip. Here I will describe the most widespread techniques of the microchip fabrication, namely prototyping in glass and polymers[80].

2.2.1. Prototyping methods

Classic technique for microchannel fabrication is etching silicone or glass pieces, e.g. by deep reactive ion etching (DRIE)[81]. Etching-based chip fabrication yields microchips of really small features, however is labor intensive and technically challenging[52,82]. More widespread technique is use of glass capillaries[83]. Glass capillary-based systems share some drawbacks with glass plates (fragility, complicated and labor intensive process), however they come in form of ready microchannels, eliminating need for potentially dangerous etching. Nesting capillaries within one another requires manual skills, and this is why the

workarounds are being introduced – e.g. placing the capillaries in Lego®-like connectable blocks[84].

Polymer-based microfluidics are a majority of all the chips, as they are e.g. easier to work with, often much cheaper, and prototyping might be significantly faster than in glass[49]. The most commonly used material is PDMS, poly(dimethylsiloxane). This elastomer can be quickly polymerized by increasing the temperature, producing solid blocks of material from the liquid. Solid PDMS is clear, transparent to visible light, gas-permeable, non-toxic and biocompatible material, with rich surface chemistry offered by the siloxane groups[85–87]. Ease of using liquid pre-polymer to fill molds and ease of detachment of the solidified PDMS blocks from many surfaces make PDMS perfect for casting replicas.

Polystyrene is the main competition for PDMS in biological applications. Polystyrene is used for most of the lab plastics in which all of the traditional protocols are carried out[49]. Even though PDMS is suitable for many applications, it also has limitation – it is not chemically compatible with many organic solvents[88], and its surface can get contaminated easily e.g. by proteins from the sample if it is not modified[89,90]. Some residual uncured oligomers of PDMS might be present in the bulk of the microfluidic device, and potentially interact with cells[89]. The last issue is the cost and availability of the PDMS – it is more expensive and not suitable for cheap, mass production schemes (such as injection molding)[49]. For those reasons, PDMS-devices-based assays so far remain complementary to experiment traditionally carried out in bulk in polystyrene dishes, bottles, and plates.

PDMS naturally completes the traditional lithographic techniques (used e.g. to make silicone processors). As solid PDMS is quite soft, such combination is called soft lithography, introduced by Xia and Whitesides, and presented in Figure 5[91]. Soft lithography enables fabrication of fluidic components (channels, valves, hydrodynamic traps etc.) within a single piece of PDMS. Large scale integration of the microfluidic circuits made them more versatile and useful for researchers, allowing microfluidics to bloom ever since[57,82] Soft lithography protocol involves replication of the microsystem from the prepared master. Master can be produced using traditional photolithographic techniques, e.q. spincoating photosensitive resin (e.g. SU-8 or AZ photoresists) on the solid substrate. Resin is solidified locally by exposition to

ultraviolet light through the lithographic mask containing pattern of the microfluidic device. Resin that did not harden is washed away, leaving perfectly defined structure of the future microchip, adhered to the solid substrate – so-called master. After chemical protection of the microstructures, the liquid PDMS with the curing agent is mixed properly, degassed, then poured over the master, and subsequently baked. PDMS solidifies faster at elevated temperatures and replicates the pattern of the hardened resin, producing a negative of the master. Such mold, after chemical protection to reduce adhesion of PDMS, can be used to cast positive PDMS replicas of the microchannels. If negative of the master is needed, procedure with producing the PDMS mold is iterated, using the negative mold as the template, and resulting in positive PDMS-mold. Prepared PDMS microfluidic devices are chemically bonded to a flat substrate, either PDMS or glass, after the surface activation by low-temperature plasma[91,92]. Such prepared chips can be then used, with or without additional chemical treatment of the surface. Worth underlining is that the master (positive or negative) does not need to be manufactured only by lithographic techniques. More and more common are CNC-milled thermoplastic masters, e.g. in polycarbonate[9,93,94].

1.Perform photolitography   2.Pour PDMS over master and cure   3.Peel PDMS from the master

4.Seal against a flat surface   5. Microchannel is complete   6. Channels may be chemically modified
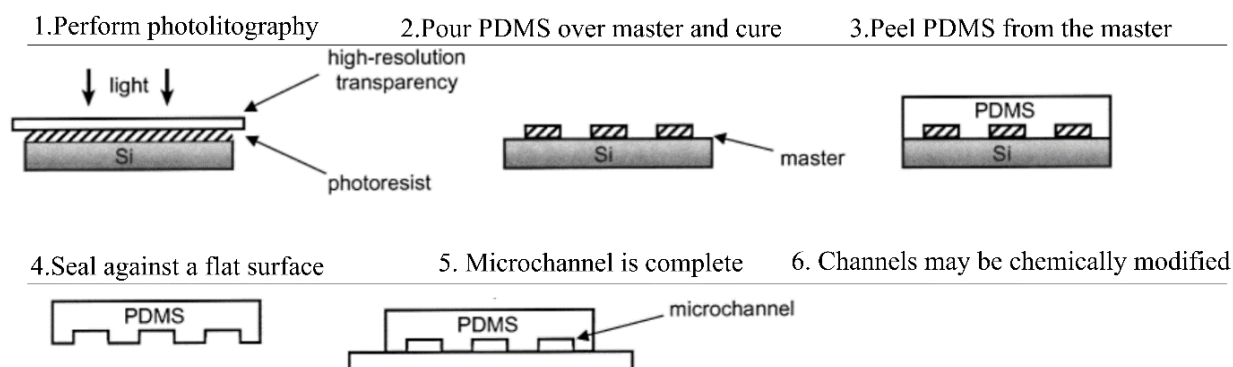
Figure 5 Schematics presenting consecutive steps in common soft lithography procedure. Adapted from[9].

As mentioned, PDMS is not the primary choice for every application. Wide variety of polymers offers numerous materials more suitable for organic solvents, mass production, biological experiments or simply cheaper. A class of thermoplastics is a middle ground between PDMS and glass as it features moderate chemical and thermal compatibility properties, good enough for many applications[80]. To list a few thermoplastics used for microfluidics chips: polycarbonate (PC)[95],

polymethylmethacrylate (PMMA)[96], cyclic-olefin copolymers (COC)[97], polystyrene(PS)[98]. Also relatively expensive and chemically inert fluorinated polymers are used for chip fabrication: polytetrafluoroethylene (PTFE, known under brand name Teflon®) or fluorinated ethylene propylene (FEP).).[74] Thermoplastic chips usually comprise micromachined plate with the network of fluidic elements and the substrate to which they are thermally or chemically bonded[95].

Two of the common prototyping methods for thermoplastics are CNC-milling and 3D printing. In CNC milling, a computer-controlled sharp drill mills the microchannels in the hard polymer plate[95]. Milling in metal is also possible, but more laborious and expensive. The resolution of such channels depends on the tool and the CNC-milling machine, but generally the minimal sizes of the channels are tens of micrometers, as compared to single micrometer to nanometer resolution of soft lithography. The advantage of CNC milling is the ease of prototyping, especially of simple designs. Complex systems with multiple elements (e.g. large arrays of microwells) can take up to 20 hours to be milled. On the other hand, there is a very trendy solution, 3D printing[99]. The fabrication of the microfluidic chip is realized by printing layer-by-layer of the appropriate material, such as e.g. methacrylate based photoresists. However, so far the attainable resolution is the order of tens to hundreds of micrometers and the upscaling of production is not easy[99,100] This is why 3D printing is very versatile and fast prototyping method that can cut time and cost of fabrication of single chips, but it is not suitable for preparation of large number of chips[101]. Mass production of the microfluidic chips differs from prototyping – instead of multiple designs in small quantities, a single design is delivered in vast number. Injection molding and hot embossing are the popular, but not the only choices for mass production[80].

2.2.2. Surface chemistry in droplet microfluidics

Control over the multiphase liquid system is possible when droplets do not wet the walls of the microchannels, while the continuous phase wets them[26]. This can be achieved by choice of the material of the microchannel and set of liquids – e.g. glass is intrinsically hydrophilic, and PDMS is hydrophobic. This means that O/W emulsions can be produced in glass microchips, and W/O emulsions can be produced in hydrophobic polymeric devices. However, not always there is such a possibility and

39

a need to chemically modify the surface of the microchannels is required (e.g. to produce W/O emulsions in glass devices).

Surface modification of the microchannel walls is performed mostly to increase/decrease the contact angle between the fluid and wall[27] to avoid wetting and cross-contamination between droplets[88,102,103]. Not all of the areas of a device must feature identical surface properties – the channels can be locally modified (patterned) in order to e.g. produce multiple emulsions[104,105] or to increase adherence of the cells to the solid substrate[90]. Numerous modifications methods are available for PDMS or hybrid PDMS-glass devices. The modification schemes are either hydrophilic, hydrophobic. Distinct kind of modification, namely increasing affinity of the walls to the fluorinated compounds, is technically called fluorophilic, but is usually referred to as hydrophobic.

Hydrophilic surface treatment of the PDMS occurs naturally during fabrication of the microfluidic devices. The surface activation by oxygen plasma required for bonding of the devices renders the surface hydrophilic[92,106]. The surface remains hydrophilic if in contact with water, exposition to air and time reduces the hydrophilicity. To increase the time the surface is hydrophilic, the chemical treatment is necessary. Usually polymers such as PVA, PVP or PEG-containing co-block polymers are employed –deposited to the still activated surface[102,107–110].

Contact angle between water and native PDMS is >110°, as PDMS is hydrophobic[111]. While this is good enough to produce W/O emulsion, the surface is usually modified to increase the contact angle even higher, up to super-hydrophobic surfaces[112]. A sol-gel method is one the available methods - PDMS and glass channels are coated with a glass-like silane layer with tunable properties[103]. Just like in case of hydrophilic channels, deposition of hydrophobic (or fluorophilic) compound on the surface of the channels is an option to modify the surface. Usually fluorinated silanes are injected into the microchannels, and baked after solvent evaporation[113]. Stabilities of coatings vary from very robust (sol-gel method) to short-lived (fluorosilanes, especially on thermoplastics). The reason for discrepancy is that sol-gel substrates are covalently bonded to the walls, while fluorosilanes (if not injected to surface activated chip) adhere and can be washed away.

To pattern the devices with areas of different surface properties, two main paths are used. In the first the surface is selectively treated by the surface-activating agent, e.g. oxygen plasma treatment of non-covered areas of the hydrophobic chip[105,114]. Exposed areas are oxidized by the ionized oxygen species, and subsequently rendered hydrophilic. The other method involves flowing the surface-modifying chemicals only in the areas that are to be modified. This requires careful designing of the system and flow control, but yields good results[103,107,115].

As mentioned, a variety of materials can be used for microfluidic device fabrication. Methods to modify thermoplastics were developed – PC, PMMA or COC can have their surface properties changed with modified protocols for PDMS modification. For example, plasma treatment, even though not as successful as in case of PDMS, can be used to make the chips hydrophilic[120]. The modification is temporary and the surface regains original properties with time. Permanent modification schemes involve chemical reactions, such as grafting the polymer to the surface of the thermoplastic[97], deposition of silica nanoparticles[116] or layers of polycations and poly-anions[26], as well as micromachining the surface to feature nano-pillars that render the thermoplastics superhydrophobic[117].

2.3. Methods of droplet formation in microfluidic systems

In 19th century Rayleigh and Plateau investigated the capillary-driven breakup of a liquid jet in air, a two-phase fluid system[118,119]. They discovered that perturbations of the shape of the viscous jet lead to collapse of the interface and formation of the separate entities, droplets. This phenomenon of dominance of surface forces over viscous forces was called Rayleigh-Plateau instability. Observation that change of the shape of interface is sufficient to drive the droplet formation is widely used in the emulsification processes[120]. Especially droplet microfluidic techniques thrive at exploiting Rayleigh-Platea instability for droplet formation, due to the high degree of control over fluid flows at the microscale[121].

Droplet microfluidic techniques can be divided into two categories based on the method of droplet production:

i) active shearing of droplets from the stream of the to-be-dispersed phase (thread),

ii) passive droplet microfluidics, relying on surface forces to break off the droplets from the thread.

Active techniques were favored over the passive ones for a long time due to the offered higher throughput and flexibility in setting the parameters of the flows of fluids. However, active techniques also require more sophisticated actuation and are more challenging to upscale in comparison to passive techniques. Advantages of passive droplet microfluidics originate in geometry-based droplet formation. Droplet volume is determined by the device geometry and may exhibit low sensitivity to the change of flow rates, step emulsification junctions are relatively ease to upscaling and easy to operate. Thus, by designing the geometry of microchannels, user is able to control the process which results at the level of design of the microsystems. Little actuation and knowledge is necessary to operate such devices. This is why passive microfluidics, especially step emulsification, is in focus of microfluidic community[9,100].

It is worth stressing that passive droplet microfluidics is not limited to droplet formation. Operations can be carried out on droplets without external actuation in passive microfluidic modules, such as hydrodynamic traps or rails[122,123]. Passive modules allow for droplet metering, merging and locking in position as well as for guiding the droplets by the rail[124], or anchoring droplets in predefined position for performing biochemical assay[123,125].

2.3.1. **Active droplet formation**

Currently, to produce droplets within a microfluidic device active microfluidic methods are usually employed. Active droplet formation is a process during which the droplets are sheared from the liquid thread by a stream of continuous phase[100]. Dedicated geometries for droplet formation are

i) T-junction[42] depicted in Figure 6A,

ii) flow-focusing junction[126] shown in Figure 6B,

iii) co-flowing junction[83,127] presented in Figure 6C.

42

Presented microchannel geometries require maintaining control over the flow of all the fluids. Active generation of droplets requires excess amounts of outer phase liquid over the to-be-dispersed phase. Use of large amounts of some liquids may be costly (e.g. fluorinated oils). However, the produced emulsions are monodisperse, and the throughput is easily tunable from single droplets up to tens of thousands of droplets per second (so called high-throughput)[100,128].
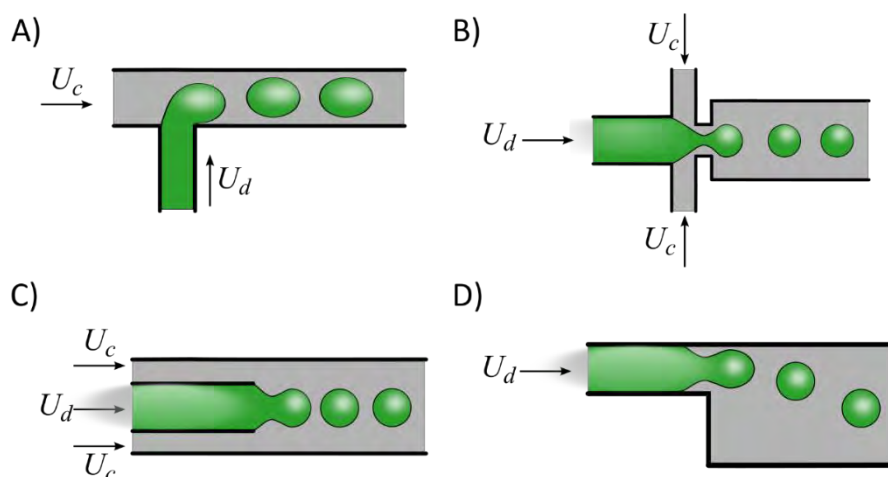
Figure 6 Depictions of microchannel geometries for droplets formation: A) T-junction, B) flow-focusing junction, C) co-axial capillaries, D) step-emulsification module. Size and frequency of produced droplets depend on several factors, including dimensions and architecture of microfluidic junction and flow velocities of fluids (dispersed phase (U_d), continuous phase (U_c)). Adapted from [9].

The aforementioned capillary number is a good measure to describe qualitatively the droplet formation process, described here on example of T-junction. For low Ca values (Ca<0.01), droplet formation is driven by interfacial forces, and such situation is called the squeezing regime of droplet formation[43,121]. The tip of the droplet phase advances to the microfluidic junction, where outer phase is flowing. The shear exerted by the flow of the outer phase is not strong enough to detach the growing droplet. The droplet grows until obstructing the flow of the outer phase through the junction and leads to the build-up of the pressure upstream of the junction. The pressure squeezes the neck connecting the growing droplet with the inflow of the droplet phase. Eventually, the neck collapses and a droplet is released. Within the squeezing regime the volume of the droplet depends predominantly on the ratio of flow velocities of

43

both immiscible phases and does not significantly depend on the viscosities of the liquids or the interfacial tension between them[44,129,130].

Higher values of Ca (Ca>0.02) indicate that the surface forces prevail, but are not the only factor important for droplet formation. For such conditions, called dripping regime, viscous shear stress causes the detachment of growing droplet of droplet phase before it blocks the lumen of the channel. Since formed droplets are sheared off faster than in the squeezing regime, the sizes of produced droplets are smaller and droplet formation rates are higher[44].

At very high flow rates of fluids, high shear forces enable the transition from dripping to jetting regime. In it droplet forms from an unstable jet of fluid that is formed downstream of the microfluidic junction. The droplets are pinched-off far from the junction, often very small and at very high-throughput[45,100]. The exact moment of dripping-jetting transition depends not only on capillary number, however value of Ca>0.1 is treated as the border between regimes[131]. For co-flowing fluid geometry Weber number of the dispersed phase must be taken into consideration[45]. However, in other geometries, e.g. flow-focusing junction, the Weber number was shown to be of no such significance[132].

2.3.2. **Passive droplet formation**

In order to overcome some of the drawbacks of the active droplet formation methods, such as e.g. excessive use of continuous phase, passive methods are used. Passive microfluidic techniques base on surface forces rather than shear forces[100]. Passive methods produce highly monodisperse droplets without the need for actuation of the outer phase[100,133]. However, some cross flow is often applied to remove the newly formed droplet from the junction which does not influence the mechanism of droplet formation[134].

Membrane emulsification is a first passive droplet formation scheme, developed around 1990s in Japan[135] and depicted in Figure 7. Key element of membrane emulsification is the membrane with uniformly sized pores, such as porous Shirasu glass. To-be-dispersed phase is pushed by applied pressure through the pores of membrane into the reservoir filled with moving and immiscible outer phase. Droplet formation occurs when to-be-dispersed phase crosses the pores of membrane and is

subjected to high surface forces due to the thread deformation. Droplet size scales with the size of the pore and produced droplets and particles are significantly more uniform than those obtained from conventional homogenizers. However, produced emulsions are not monodisperse – their CV is around 10%[136].
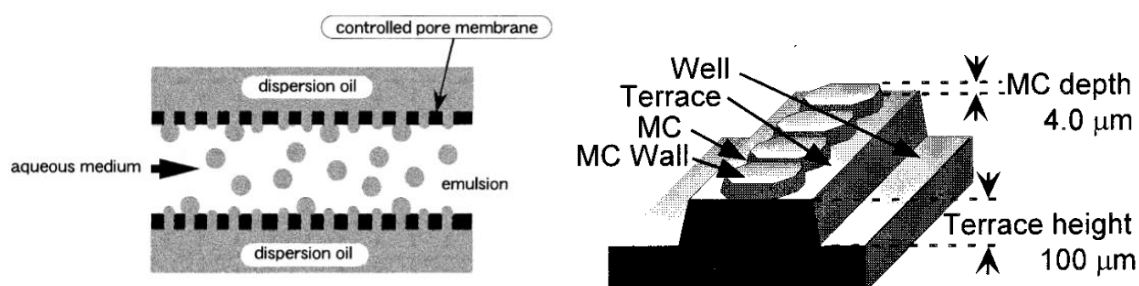
Figure 7 First passive droplet production methods. Left: membrane emulsification[135]. Right: microchannel emulsification[136]. MC stands for microchannel.

Production of porous membranes is technically challenging which stimulated Nakajima and coworkers to fabricate the analogue of the porous membrane with well-defined features. The new system, called microchannel emulsification system, comprised multiple microchannels (pore analogues) etched in silicone plate sealed with glass plate[136–138]. Example of microchannel emulsificator is depicted in Figure 7. Principle of operation is the same as in membrane emulsification, the to-be-dispersed phase is pushed through the microchannels into reservoir filled with cross-flowing continuous phase. Microchannels end with a terrace, an expansion of the channel in the horizontal direction, allowing the to-be-dispersed phase to start expanding before reaching the sharp height change (well, reservoir). Elongated threads of to-be-dispersed phase are unstable and snap-off easily and reproducibly when entering the reservoir filled with immiscible outer phase. Produced emulsions are more uniform than in membrane emulsification, with CV around 5%, due to the control over the microchannel dimensions[136].

Complex fabrication schemes of membrane and microchannel emulsifications inhibited upscaling and spreading of the methods. Next development in the world of passive droplet formation techniques was tied to fabrication of microfluidic devices with microchannels using standard soft lithography techniques. The microfluidic devices contained smaller number of step emulsification junctions, but offered greater degree of control over microchannel dimensions and shapes. As in passive

45

droplet production droplet sizes scale with the size of the emulsifying nozzle, the microfluidic devices offer production of very uniform droplet population, often with CV~1%. Numerous variants of microfabricated microfluidic devices were introduced, differing in number of droplet forming junctions (from single to thousands) and their geometries (from straight microchannels, to carefully designed and executed 3D structures) [20,133,139,140]. As the microfluidic devices microfabricated in glass, PDMS and thermoplastics rely on the change of the height of the microchannel on the droplet production, they are collectively referred to as step emulsification systems, or step emulsificators.

2.4. **Step emulsification**

The primary concept of the step emulsification systems is to take advantage of the pressure drop in the thread of the to-be-dispersed phase as it encounters a sharp expansion of the microchannel (called the 'step')[139,141]. Release of the to-be-dispersed phase from the spatial confinement results in increased radius of curvature, and subsequently, lowered Laplace pressure in the region downstream of the step[139]. The difference in pressures between the growing front of the thread and the still confined thread causes the more rapid inflow of more to-be-dispersed to the bulb. When the rate of inflow of the to-be-dispersed phase into the growing bulb exceeds the provided flowrate (by e.g. syringe pump), the thread starts thinning (see Figure 8C). This process is called 'necking', and lasts until the thread thickness (in the area with smallest cross section, the 'neck') is smaller than the dimension of the microchannel. At this point the thread becomes locally unstable and is ruptured by the Rayleigh-Plateau instability, releasing a droplet[139]. The process repeats when the head of the interface crosses the step again. Location of the neck depends on the regime of the droplet formation – for dripping the neck is upstream of the step, while for jetting it is exactly on the step or beyond[142] (see Figure 8E-F).
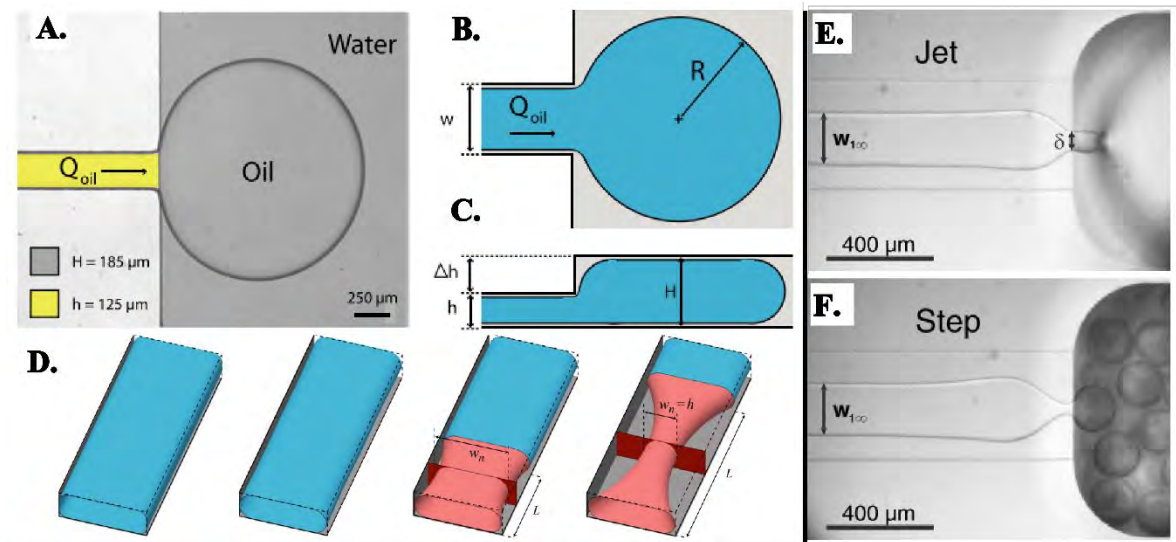
Figure 8 Mechanism of step emulsification. A. Top view of the oil phase coming from the microchannel into the bigger channel (reservoir). B-C. Top (B) and side (C) view on the formed bulb at the tip of the to-be-dispersed phase thread. $Q_{oi\ l}$- flow of the to-be-dispersed phase, w – width of the microchannel, R -radius of curvature of the bulb, h – height of the microchannel, Δh – change in the height of the microchannel at the step, H - height of the bulb. D -necking of the to-be-dispersed phase. E-F. Location of the neck for the jetting (E) and dripping (F). Adapted from[139,142].

Size of the growing droplet depends on geometry of the step emulsificator, necking time of the to-be-dispersed phase thread, and the flow rate of the to-be-dispersed phase[143,144]. Necking time is a quantity that describes the time between two moments: when the head of the to-be-dispersed phase reaches the step, and when the newly-formed droplet breaks off. Necking time depends linearly on viscosity of the outer phase – this characteristic time scale increases with the increase of viscosity of the outer phase[134]. Necking time governs the formed droplet size as the longer the bulb can grow, the more liquid can be accumulated in the bulb. Increase of flow rate of to-be-dispersed phase also increases droplet size for the same reason – more liquid can fit in the droplet during necking time in comparison to the lower flow rate[134].

2.4.1. **Parallelization of the passive emulsifying junctions**

A crucial element of the step emulsificator is the nozzle of the microchannel feeding the to-be-dispersed phase to the reservoir filled with outer phase. The nozzle can be also called Droplet Forming Unit (DFU). Different kinds of step emulsification systems differ mostly in the nozzle geometry, and in the number of DFUs. The geometry of the nozzle is the most important parameter of the step emulsificator, as the features of the nozzle (hard-wired into geometry) determine the drop of Laplace pressure, neck location and the access of the continuous phase to the neck[133,145,146]. Various geometries of the nozzle were introduced, from straight microchannel[139] (seen in Figure 6D), through gradually expanding nozzle[124], to complex 3D structures (see Figure 9)[133,146].
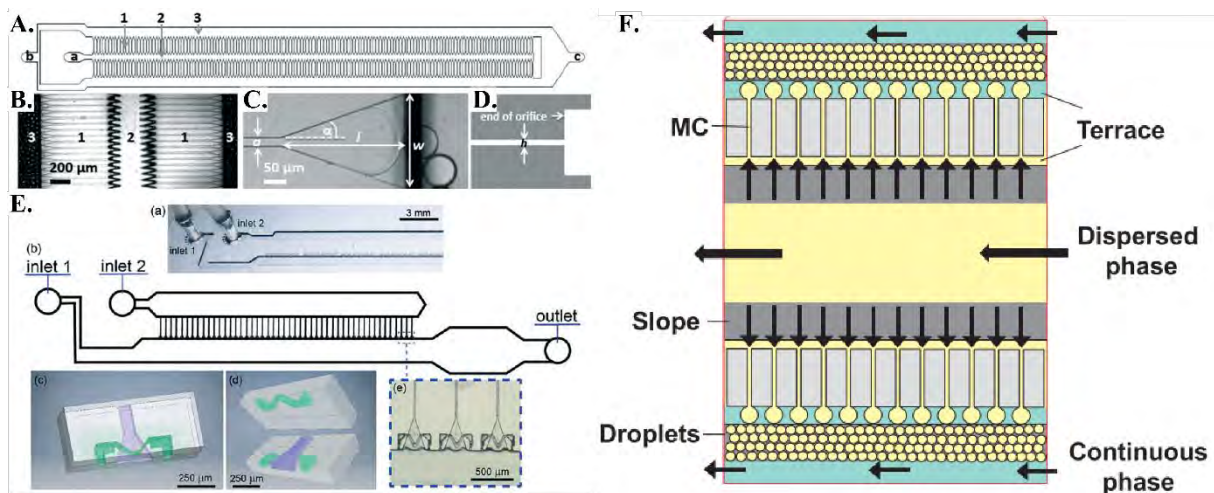
Figure 9 Upscaled step emulsifying nozzles of complex geometry. A-B. Top view of the parallelized step emulsificators with inlets of dispersed and continuous phases (a,b, respectively), outlet for the emulsion (c). 1 denotes the side channel for the dispersed phase, 2 denotes the channel feeding the side channels, and 3 denotes the location of the nozzle – as can be seen in B. C-D. View of the nozzle (top C, side D). E. Modification of the system shown in A-D by adding bypasses allowing continuous phase free access to the neck location. F. Upscaling of the nozzles in MCE device. Adapted from [145–147].

Two of the well-known upscaled step emulsificator variants are: microchannel emulsification (MCE, see Figure 10A) [138,148], and Edge-based Droplet Generation (EDGE, see Figure 10B)[149]. MCE (mentioned in section 2.3.2 Passive droplet formation) employs from thousands of independent DFUs. They are microchannels of

circular or rectangular cross-section holes etched through the silicon plate, entering the outer phase reservoir[133,144,147,150,151]. Aspect ratio of the channel is relatively small, with width being ~1-10 times larger than the height[147]. DFUs positions are fixed, as microchannels are separated by solid walls. Each DFU operates independently and the process is highly reproducible. Geometry of the MCE DFUs includes a terrace (see Figure 10A), a structure on which a to-be-dispersed phase assumes disc shape. Change of curvatures induces change in Laplace pressure and leads to generation of highly monodisperse emulsions. When a critical flowrate is reached, determined by critical capillary number, droplet size and dispersion sharply rise[150,152,153].

In EDGE emulsification takes place along a single, wide and shallow slit that enters the deep reservoir filled with continuous phase. The slit aspect ratio (width to height) can exceed one hundred. On a wide channel-reservoir junction there are multiple places where droplets can form, unlike in MCE where the DFUs positions are predetermined by the chip geometry. An EDGE system self-tunes the number and position of the DFUs, which allows for emulsion production at higher flowrates than MCE systems[154]. Continuous self-adjusting of the DFUs positions dynamically changes conditions of emulsification process, increasing polydispersity of produced droplet populations, as when compared to MCE devices[100].
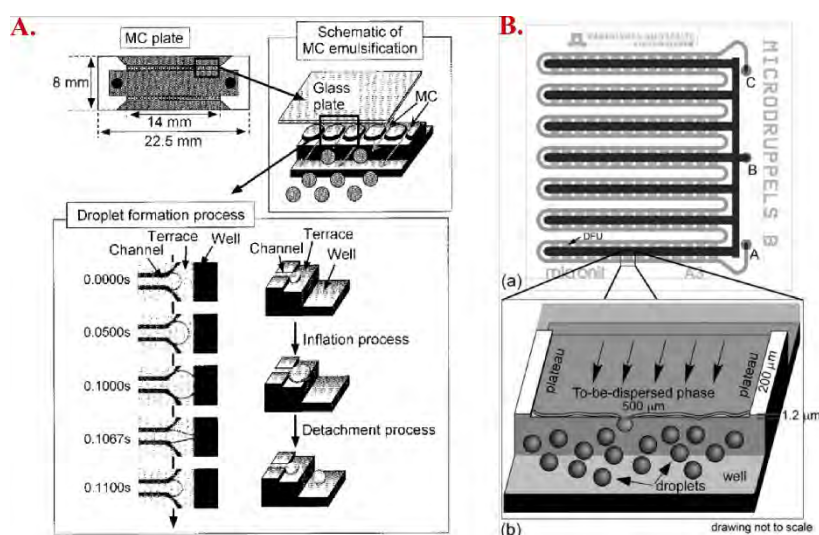

Figure 10 Passive droplet generating systems: A) MCE[152] and B) EDGE[155]. Adapted from [152,155].

2.5.   **Production of double emulsions**

Multiple emulsion, droplets nested in droplets and suspended in continuous phase, can be produced by means of microfluidic techniques, allowing degree of control over the population dispersion and the emulsion content unrivalled by traditional shake-based methods[100,156,157]. The most widespread multiple emulsions are double emulsions (DE) with two aqueous phases: core (innermost droplet) and continuous phase (environment), separated by the oil shell phase. Such double emulsion is denoted water-in-oil-in-water double emulsion or W/O/W DE. Notably, DE of various compositions, including emulsions of higher orders, can be generated in microfluidic systems[158,159]. Ideally, the volume of the middle phase of DE should be as low as possible – the thinner the shell between the other fluid phases, the more stable against rupture the droplet is[88]. It is because the rupture of the multiple emulsion occurs when the inner droplet moves towards the outer interface of the shell and breaks it, merging with the outer phase. The hydrodynamic resistance that impedes the movement of the inner droplet increases with reduction in shell thickness as it is harder to displace the shell phase volume somewhere else for the core droplet to move. For sufficiently thin shells the hydrodynamic resistance allows only marginal fluid flows[160,161]. One of the most advanced direct method of single core DE production yields 5% shell thickness for 50-µm DE. It is important to note that shell can be reduced further (down to <1µm) by post-processing like squeezing the DE through the slit [161–163] or by dewetting of the shell phase from the multiple emulsion[164–166]. Microfluidic devices for multiple emulsion generation are similar to those used for formation of single emulsions. Often they are even the same device with adjusted wettability of the channel walls and single emulsion used as to-be-dispersed phase[46]. Actively controlled DE production methods allow high degree of control over the process of formation and structure of double-emulsions (e.g. whether DE comprises single or multiple core droplets). Usually an aqueous droplet is generated in oil in a hydrophobic junction and then transported within an oil thread to another junction of different wetting properties (hydrophilic) where second aqueous phase shears off the W/O single droplet to form a double (W/O/W) droplet (see Figure 11AB)[108,167]. For co-axial glass capillary system (see Figure 11C) DE formation occurs in a single step - all fluids are hydrodynamically focused into a co-axial thread that eventually ruptures to Rayleigh-Plateau instability to form multiple droplets[83,118,168].

50
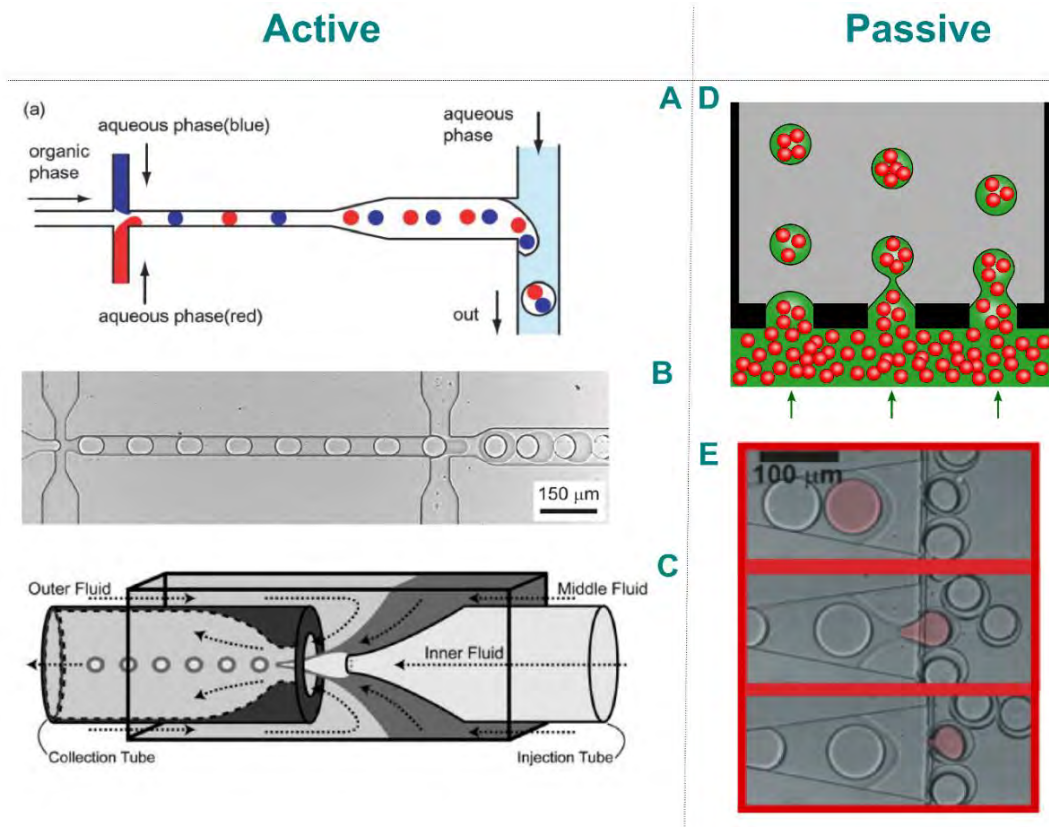
Figure 11 Double emulsion microfluidic technologies. Left-hand side depicts active methods, right-hand side shows passive methods. A- two consecutive T-junctions; B – two consecutive flow-focusing junctions; C – co-axial capillary device; D – microchannel emulsification of single emulsion into double emulsion. E – a single emulsion fed into step-emulsification module to produce double emulsion. Adapted from[9].

Double emulsion production techniques are considered passive if just the final emulsification step is passive. Whether the single emulsion is produced in another chip or at junction upstream of the passive junction does not matter for the process of turning single emulsions into double emulsions. Operation of second emulsification is hard-wired into the geometries of the passive devices, limiting the degree of control of the user, but also requirement for actuation. Droplet formation also depends on parameters of fluids used, however to smaller degree than on the geometry[156,169].

Passive transformation of single emulsion into double emulsion was introduced by Sugiura et al[170], using microchannel emulsification. Single emulsion is extruded from the microchannel through the orifices in the silicone membrane to the outer phase (see Figure 11D). The core droplets were significantly smaller than the formed DE, and there was no direct control over the number of cores with the DE. Improvement

51

in this field came from Eggersdorfer, Ofner, and coworkers who proposed[171] and then improved[172] tandem system for DE production. In short, they used two 'millipede' devices with multiple step emulsification junctions operating in parallel. First device, hydrophobic, produced feed W/O emulsion that was directly transported to identical, but hydrophilic, device and there passively emulsified into W/O/W emulsion (Figure 11E and Figure 12).
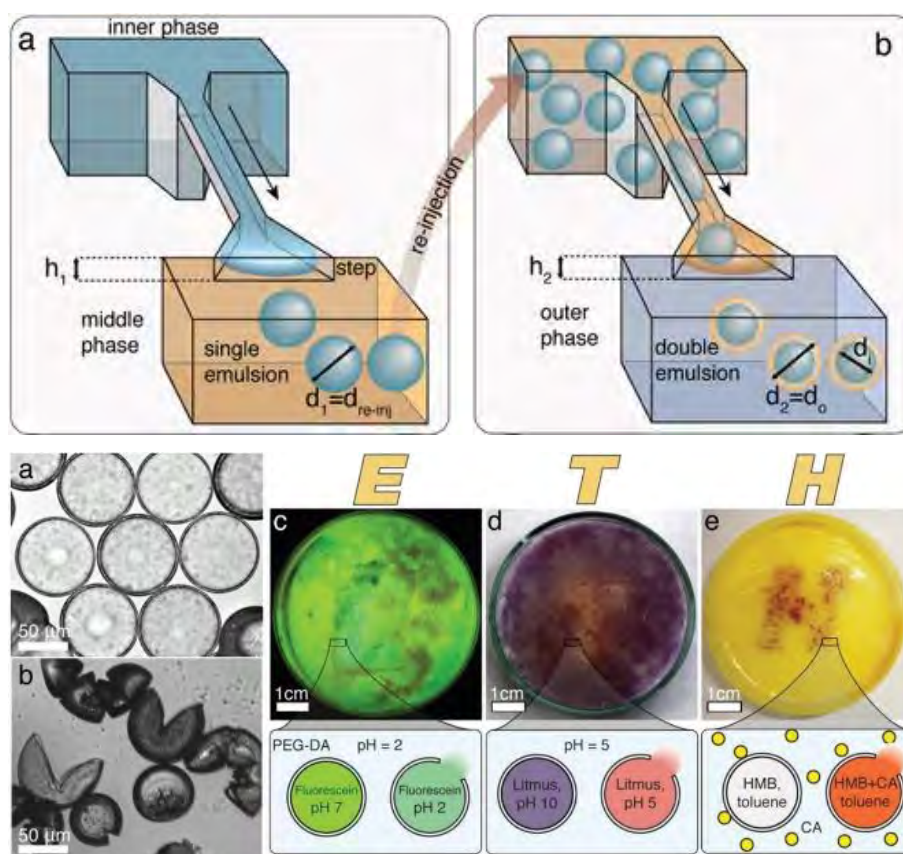
*Figure 12 **Top:** Scheme of tandem step emulsification. Monodisperse DE are formed in multiple parallel passive junctions (hydrophobic, a, and hydrophilic, b). **Bottom:** Produced monodisperse and thin-shelled polymerosomes before (a) and after (b) polymerization. Such particles can be mechanoresponsive – c-e show different types of reaction that happen after stamping the particle layer with letters E, T and H. Adapted from [172].*

Automated droplet microfluidic systems can improve the double droplet production and enable custom tailoring of multiple droplets one by one[173]. Custom tailored multiple emulsions can have many parameters tuned – number of cores, ratio of core to total volume (volume fractions), shape, and throughput of the DE[38,173,174]. Guzowski

et al. reported an automated microfluidic systems in which user, by controlling the valves, encode a protocol to be executed. For example, single emulsion droplets of controlled, but varying sizes are produced at the first junction (T-junction, active droplet formation) and transported to the second junction (step emulsification, passive method). There the feed emulsion gets transformed into double emulsion[38,173,174]. Automated DE producing systems offer interesting advantages as. E.g. the possibility to tune the composition and size of DE droplets one by one – see Figure 13. Various emulsion shapes can be obtained, from round single-core double emulsions to multi-cored 'chains' (see Figure 13D, inset c). Packing of the inner cores depends on the number of cores and the volume fraction of cores in DE[174].
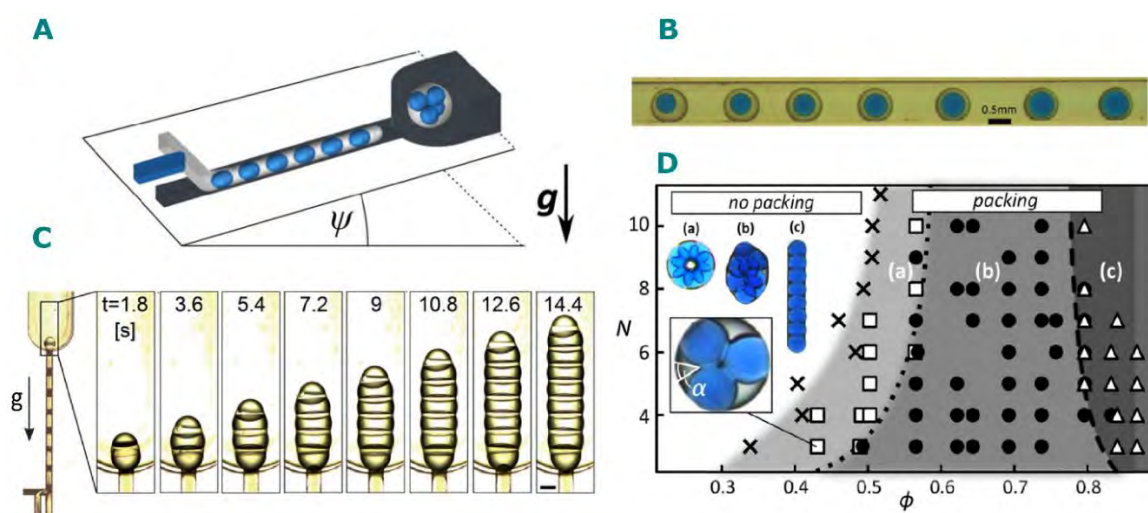
*Figure 13 Automated microfluidic systems for production of multiple droplets developed by Guzowski et al allow for production [71]of tailored double emulsions[38,173,174]. **A** – schematic representation of an automated microfluidic device for production of tailored multiple emulsions; **B** – exemplary tailored double emulsions, with varying core size, produced in system from **A**; **C** – example of multiple droplet in form of a chain with increasing number of segments in time; **D** – stability diagram for tailored double emulsions with multiple cores (N) as a function of volume fractions of the cores (φ). Different packing regimes of the cores are a) negligible deformation of the shell, b) strong deformation of the shell, and c) linear chains of droplets (like in **C**). Inset shows the equilibrium contact angle between the drops, 45°± 5°. Adapted from [9].*

2.6.   Analytical assays employing droplet microfluidic systems

Numerous analytical assays can be performed in traditional bulk format, as well as in adapted digital format. Here, I will show on example of the staple digital assay - polymerase chain reaction (PCR) - the idea and advantages of the digitalized assays.

2.6.1.   Droplet digital analytical assays

First report on the PCR assay, from 1985[175], described a method to amplify genetic material. In short, in the PCR method short oligonucleotides called primers, single nucleotides, and enzyme polymerase are added to the target DNA in order to *in vitro* exponentially amplify the region of DNA flanked by the primer-complementary regions. If multiple molecules of DNA are present in solution during the process, each of them undergoes the amplification provided it is complementary to the primers. To gather quantitative information on the product, a modification of PCR, namely quantitative PCR or real-time (qPCR, RT-PCR) can be used[176]. Still, the process occurs in the whole reaction volume (in bulk), and single DNA molecules cannot be identified.

Droplet digital PCR is a digital version of the PCR, conducted in droplets[177] or microchambers[178]. The chemistry of the PCR reaction is the same, but more information is obtained from the experiment. A sample is split into numerous compartments and the PCR reaction occurs in each compartment independently, resulting in a collection of two types of droplets – with no DNA, and full of DNA (see Figure 14). Discrimination between two populations by measurement of the fluorescence intensity allows to enumerate the DNA-laden droplets, number of which corresponds to absolute number of copies of DNA in the initial sample. The ddPCR provides orders of magnitude more precision and sensitivity than traditional real-time PCR. Throughput of ddPCR is higher than of the qPCR, and the consumption of reagents is lower. 20 microliters of sample - a fraction of sample required for real-time PCR - yields 20 thousand 1nL droplets in ddPCR, which allows for simultaneous execution of several assays. However, the number of the possible compartments can be much higher, e.g. 1 million[179]. Possibility to execute PCR on single copies of DNA allows profiling and analysis of heterogeneous tissues[6].
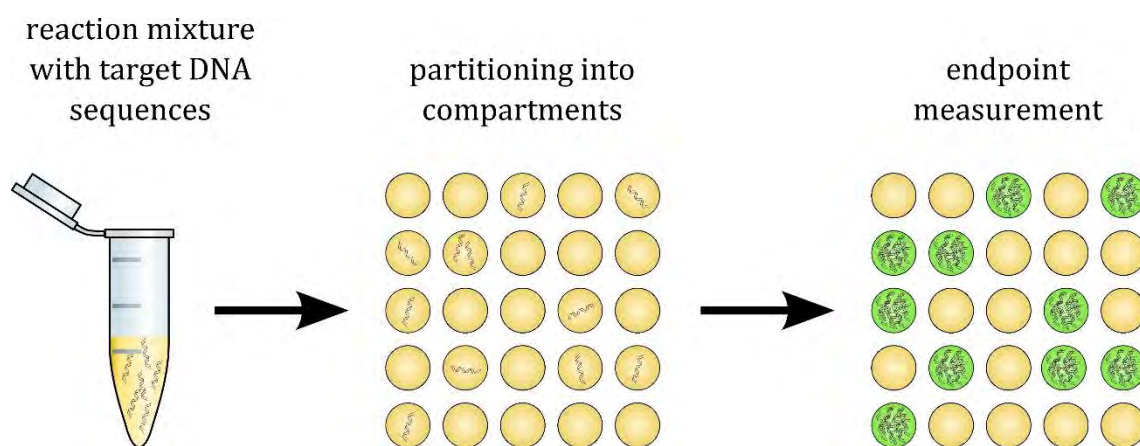
Figure 14 Droplet digital PCR. Reprinted from[180].

Principle of digital assay can be applied to other biochemical and microbiological assays. Examples of such assays are:

i) directed evolution of enzymes[128],

ii) screening microbial communities[181],

iii) assessment of bacteria susceptibility to antibiotics[182]

iv) bacteria enumeration[123],

v) drug screening [182–184],

vi) enzyme properties screening[79],

vii) protein crystallization[60],

viii) studies of single cell genomes[5,185] and proteomes[186].

2.6.2. Passive microfluidic systems in analytical assays

The main element of the digital droplet systems are naturally droplets. Success of the digital assay relies on their quality (size, dispersion, stability, biocompatibility etc.). Passive microfluidic devices, easy to upscale systems yielding perfectly monodisperse emulsions that can use very little continuous phase[187], are a perfect tool to supply the analytical assays with emulsions. Multiple operations are reported to run on passive single and double emulsion producing systems, e.g. nucleic acid amplification[78], microgel cell scaffolds production[188], polymerosome production[172], artificial cell membrane investigation[125], or nanoparticle production[147]. Combining the operations into fully functional assays are a matter of time, for example ddPCR system based on step emulsified sample is being commercialized by a French start-up company Stilla[189].

3. **Research objectives**

Droplet production is essential for many digital assays that benefit from the use of monodisperse and stable emulsions. Production of perfectly monodisperse emulsions is a trademark of passive droplet microfluidic systems. Thus, use of passive schemes of droplet generation would be beneficial for the development of analytical assays.

Despite their advantages, passive step emulsificators have three major drawbacks:

i) dependence of the droplet size on the flow rate of droplet phase,

ii) low throughputs of monodisperse emulsion production,

iii) process of multiple emulsion formation on the step has not yet been understood.

In this dissertation, I investigate how to overcome those limitations of state of art passive emulsificators. My first research objective was to minimize the influence of the flow rate of to-be-dispersed phase on the size of the resulting droplet. Since step emulsification relies on the geometry of the nozzle, I focused on the nozzle architecture optimization. By modifying the structure of the step emulsification junction I aimed to insensitize the size of the formed emulsion from the flow rate of the droplet phase.

The second objective was motivated by the need for multiple droplets in order to perform sophisticated analytical assays. In order to prepare a system producing emulsions suitable for analytical assays I needed to increase the throughput of the step emulsificator. Thus, the second goal set in this dissertation was to further optimize the step emulsificator system to increase its throughput without sacrificing small droplet size and its uniformity.

The third objective is tied to the need of some assays to use double emulsions, preferably with thin oil shells. Such droplets can be produced by existing passive methods using two connected microfluidic devices. However, description of influence of the parameters of the feed emulsion upon droplet properties is missing. Since viscosities of fluids are crucial parameters in the process of emulsification I set out to investigate the influence of the core droplet viscosity on the characteristics of passively produced double emulsion and its shell thickness.

4. Materials and methods

In this chapter I present the used materials and methods for fabrication of the microfluidic devices and for conducting experiments.

4.1. Materials

4.1.1. Chip fabrication

Poly(dimethyl siloxane), PDMS Sylgard 184, Dow Corning, USA

Polycarbonate, Macrolon® GP, Covestro, Germany

Poly(methyl methacrylate), Bayer, Germany

1mm thick Glass slides, SP Przełom, Poland

Aluminium foil, Jan Niezbędny, Poland

4.1.2. Surface modification and surfactants

Dichloromethane, POCH, Poland

(Tridecafluoro-1,1,2,2,-tetrahydrooctyl)-1-trichlorosilane Alfa Aesar, Germany

Novec 1720, 3M, USA

Aculon E, Aculon Inc., USA

1H,1H,2H,2H-Perfluoro-1-octanol, Sigma Aldich, Germany

Perfluoropolyether-poly(ethylene glycol)-perfluoropolyether (PFPE-PEG-PFPE), custom made, Poland[35]

Poly(vinyl alcohol) 13-23 kDa,87 89% hydrolyzed, Sigma Aldrich, USA

4.1.3. Aqueous phases

Deionized water,

Glycerol, POCH, Poland

Solution (0.02 mg/L) of Congo Red dye, POCH, Poland

Solution (2%wt.) of low-melting agarose, Sigma Aldrich, USA

Solution (2-10%wt.) of poly(vinyl alcohol) 13-23 kDa,87 89% hydrolyzed, Sigma Aldrich, USA

4.1.4. Fluorinated oils

Novec HFE 7500, 3M, USA

FC-40, 3M, USA

4.1.5. Small laboratory equipment

Single use steel needles, gauge 21, Terumo, Japan

1-20mL plastic syringes, BD, USA

PTFE tubings, inner diameter 0.5 mm, outer diameter 1 mm, Bola, Germany

PE tubings, inner diameter 0.76 mm, outer diameter 1.22 mm, BD, USA

1mm Biopsy punch, Ted Pella, USA

Scalpel, Bionovo, Poland

Glass syringes with removable needles, 0.1-5 mL, Hamilton, USA

4.1.6. Hardware

Low-pressure syringe pumps NemeSys, Cetoni Gmbh, Germany

Syringe pumps, model PHD 2000, Harvard apparatus, USA

Electronic pipette VIAFLO II, Integra Biosciences AS, Switzerland

uEye USB camera, UI3180CP-HQ-R2, IDS Imaging, Germany

Fast camera, FASTCAM 1024 PCI K100, Photron, Japan

Optical profilometer, ContourGT-K, Brücker, USA

Plasma generator, Harrick Plasma, USA

LCD diode, TME, Poland

Stereoscope, model SMZ 1000, Nikon, Japan

Objectives 0.5x and 1.0x, Nikon, Japan

CNC-milling machine, MSG4025, Ergwind, Poland

Laboratory oven, Binder, Germany

4.1.7. **Software**

MATLAB 2016-2018, Mathworks, USA

OriginPro 8, OriginLabs, USA

MS Office, Microsoft, United States

Automated Droplet Measurement[190]

ImageJ2[191]and Fiji[192]

Mastercam, CNC Software, USA

4.2. **Methods**
4.2.1. **PC chip fabrication**

Microchannel architecture was designed in Mastercam by the milling machine operators and milled by CNC-milling machine in PC or PMMA plate. Polymeric plates were inspected with optical profilometer to measure the actual dimensions of microchannel features. Prepared milled PC plates were bonded to clean plate of native polycarbonate either by high-temperature bonding in the press (30 minutes, 2 bar, 135^0C)[95], or by tightly screwing two plates with sets of screws, gaskets and nuts.

For polycarbonate surface polishing, vapors of the dichloromethane (DCM) were used[193]. A few milliliters of DCM were put in the tightly flask and sealed with pierced stopper. The orifice in the stopper was tightly sealed with hollow copper tube. End of the tube was bent to form a dispensing nozzle. Flask was heated to 55^0C on a hotplate, and the metal tube was heated by applying 2A, 4V current to it. Boiling DCM turned into vapors that entered the tube. By moving the nozzle of the tube over the polycarbonate, the vapors were locally applied to the PC surface. DCM dissolved the top layer of PC, rendering it smooth. Caution was paid to treat the devices no longer than until the milled surface changed color from cloudy to transparent.

4.2.2. **PDMS chip fabrication**

Positive master of microfluidic chip was prepared like the PC chip and placed in container self-made of aluminum foil. Mixture of PDMS with curing agent (10:1 ratio) was poured over the plate, degassed and baked at 75^0C for 2 to12 hours. PDMS negative master was peeled off, and its surface was activated by oxygen plasma and

protected by vapor of tridecafluoro-1,1,2,2,-tetrahydrooctyl)-1-trichlorosilane (30-90 minutes, 10 mbar). After baking the negative master (130^0C for at least 30 minutes), and cleaning it (rinsing with water and isopropanol, drying with compressed air), it was filled with the same PDMS-curing agent mixture, and baked again (75^0C for 2-12 hours). After cooling down, the PDMS positive-cast was peeled from the negative master. The PDMS cast was punched in the inlet and outlet positions. Both the prepared PDMS device and glass substrate were cleaned (rinsing with water and isopropanol, drying with compressed air followed with scotch tape dust removal), treated with oxygen plasma (30 seconds, high intensity) and gently brought in contact. To strengthen the bonding the chip was place in the oven (75^0C for 10 minutes).

4.2.3. Microchannel surface modification

To modify the channels fluorophilically, PC or PDMS-glass devices were filled with Novec1720 or Aculon E. After solvent evaporation, the chip was baked (PC 1 h, 75^0C; PDMS-glass 30 minutes, 130^0C) to ensure good coating with fluorosilanes. For PC the process was repeated three times.

To modify the PDMS-glass channels hydrophilically, the channels were filled with 2% w/w PVA solution around 4 hours after the plasma bonding. The microchannels were three times: filled with PVA solution, incubated at room temperature for 10 minutes, flushed clean with compressed air, and baked at 120^0C for 10 minutes[110].

4.2.4. Fluid handling

Fluids were supplied to the microsystems using inert PTFE tubings connected to delivery system. The delivery system comprised precise glass syringes with removable needles (varying volumes from 0.1 to 5 mL) mounted in computer controlled syringe pumps. The pumps allow dispensing fluids in wide range of volumes and flow rates. However very low flow rates were not used to minimize the unsteadiness of the supplied flow rate, as described in literature..[194] As opposed to pressure-driven systems the pump systems control the volumetric flowrate well, despite the varying resistances of the different microfluidic channels. In case of use of the electronic pipette as the source of flow, the fluids were aspirated from the pipette tip inserted directly into the microchannel inlet.

61

Processes happening inside the microfluidic devices were observed when chips were placed vertically to the ground to utilize gravity for droplet transportation. In order to capture images the chip was mounted in the holder in front of the stereoscope, fixed horizontally by the custom restraints. The chip-holder pair was attached to three-dimensional micrometer stage that allowed for safe and controlled movement of the chip in front of the camera. The stereoscope features the 0.75-11.25 magnification, which can be further modified by use of objectives (0.5x and 1x).

4.2.5. **Data acquisition**

Light of desired intensity was provided by custom LCD-diode lamp with intensity regulation, and diffused by set of two sheets of glass optical diffusers. To record the images two kinds of cameras were employed. For low-speed processes (below 100 frames per second, fps) the USB camera was used for recording. To capture the fast processes, or details of the slower processes, a fast camera was used. It allows to record movies up to 100 thousand frames per second, however the usual recording was 500-3000 fps, each frame of 256x256 or 512x512 pixels.

4.2.6. **Data processing and analysis**

Data from recorded clips were extracted by ImageJ 2.0 [191,195] its modification (Fiji[192]), and freeware – Automated Droplet Measurement, ADM[190]. In short, images are processed so that borders of the droplets are clearly distinguishable and the area of the cross-section of the droplet is obtained. By simple mathematical transformation the sizes (radii or volumes) of the spherical or plug-like droplets were calculated. Custom MATLAB and ImageJ scripts were used to automate the process of data extraction and processing. Data was further processed and analyzed either in MS Excel (for simple and small datasets) or in more advanced environment that allows automation (MATLAB scripts for data extraction and processing). For clarity and aesthetics, the plots were mostly created in Origin Pro 8.

II. RESULTS

The following part of the dissertation describes the research carried out within the projects for passive formation of droplets suitable for analytical assays. It is divided into two experimental parts, each focusing on a separate projects. Together, the research improves existing passive droplet generating systems by optimizing nozzle geometry in step emulsificators. This section of the dissertation ends with a chapter summing up the research and providing insight on the perspectives of the passive droplet microfluidics for development of analytical assays.

5. **Decoupling droplet volume from flow rate in step emulsificator**

In this chapter I describe the results from the first project carried out within my dissertation. Results were published and the chapter is based on the publication: *Nano-liter droplet libraries from a pipette: step-emulsificator that stabilizes droplet volume against variation in flow rate,* F. Dutka, **A. S. Opalski** and P. Garstecki, *Lab Chip*, 2016, 16, 2044–2049, DOI: 10.1039/C6LC00265J.

5.1. Introduction

5.1.1. Problem statement

To perform digital analytical assays (e.g. ddPCR[177]) a sample (usually microliter sized) is required to be split into a number of small, typically nanoliter, droplets (droplet library). Existing methods allow for splitting plugs into libraries, however at cost of dead volume or excessive use of external phase to shear off the droplets[73]. Step emulsificators, microfluidic devices that produce tightly monodisperse emulsions, are a perfect tool to simplify the analytical procedures. Step emulsificators require control only over the to-be-dispersed phase (i.e. sample), which makes the protocol easier to carry out than controlling both to-be-dispersed and continuous phases. The typical issue with step emulsificators of classical, rectangular microchannel geometry, is that they produce droplets of size depending on the rate at which the sample is injected[124,139].

Step emulsificators, where only sample is injected, eliminate the actuation and need for control over continuous phase. Space of parameters governing the step emulsification process include liquid properties, rate of sample injection and geometry of the step emulsificator.

Sets of liquids are usually predefined, especially in case of diagnostic assays. The sample is usually aqueous phase (Newtonian liquid of viscosity similar to water), dispersed in biocompatible oil with surfactant, of well-known properties[19]. Knowing this, the variation between experiments (of the same or different assays) introduced by the change of the sample is usually negligible.

Rate of sample injection determines whether the droplet formation occurs in dripping or jetting regime and, subsequently, the size of the produced droplet populations as shown by teams led by Sugiura[153] and Dangla[124]. Step emulsification mechanism requires the thread of the to-be-dispersed phase to form a neck, allowing the Rayleigh-Plateau instability to break it. During the necking, time the to-be-dispersed phase flows into the forming droplet. Necking time in the dripping regime is constant for the varying flow rates[134]. Thus, in dripping regime the higher the flowrate, the more liquid can flow into the droplet before the break-off from the thread. Increasing the flowrate of sample inflow over certain threshold (reaching critical capillary

65

number value of dripping to jetting transition) leads to increasing the emulsion size and its variation[196]. Hence, it is important to either control the flow rate of the sample, or design a system in which flow rate variations do not influence the size of the produced droplets. Decoupling the droplet size from sample flow rate was anticipated in 2012 in classic paper describing physical mechanism of step emulsification: '*In order to reduce the impact of the dynamics on the drop size, one may imagine designing the inlet channel with local modulations in width or depth in order to facilitate the breakup*'[139]. As I show in this chapter, it is possible to reduce the influence of the flow rate of sample injection on droplet size by modifying the geometry of the step emulsificator. The 'design space' is thus limited to the architecture of the step emulsificator.

Geometry of the microfluidic junction is the key factor in the functional performance of step emulsificator device[145,146,197,198]. Architecture of the step emulsificator nozzle governs the shape of the forming droplet, influencing its susceptibility to breakup. A common approach to modify the step junction is to introduce a terrace, 2D or 3D structure at the sharp change of the height of step emulsificator. The terrace is a local increase of the channel dimensions that influences the Laplace pressure distribution in the to-be-dispersed phase thread, yielding higher throughput and monodispersity of produced emulsions[145,150,152]. Another structure that could be implemented to perform operations on droplets in passive manners are bypasses, i.e. small channels or parts of a channel that allow the continuous phase to flow around the to-be-dispersed phase[122].

As shown first by Sugiura[150], the terraces of various shapes showed that change in geometry of the step junction might influence positively the range of flow rates allowing monodisperse emulsion formation. Me and collaborators followed that lead and showed that a proper design of the passive structures may improve the stability of the droplet size against the varying flow rate.

Pipettes are the main tools used in biology, chemistry and biochemistry labs, allowing transfer of liquid samples between containers by use of single use cartridges (tips). Because of the low control over flow rate, the use of pipettes in microfluidics usually boils down to off-chip operation such as sample preparation[199]. Electronic pipettes offer better control over flow rates than automatic pipettes, however not as precise

and controllable as syringe pumps. In this chapter, I show first report on employing the electronic pipette as the source of flow for the droplet production in passive microfluidic emulsificator.

In this section, I describe a novel step emulsificator geometry that tackles the problem of varying droplet sizes for different flow rates. This junction stabilizes produced droplet size in regard to the changes of the injection rate of the sample. Step emulsificator featuring the introduced junction allows formation of library of nanoliter droplets from microliter sample, even if an automatic pipette is used as the source of flow. In comparison to pressure controller or a syringe pump, the automatic pipette provides much more varying flowrate, but is also more accessible and popular throughout the laboratories. Use of widespread device to power the microfluidic chip with the junction of novel geometry is a step towards wider use of point-of-care microfluidic devices for analytical assays.

5.1.2. **Materials and methods**

Microfluidic chips were fabricated in polycarbonate, prepared as described in sections 4.2.1 PC chip fabrication. Channels were modified fluorophilically with Aculon E as described in section 4.2.3 Microchannel surface modification. Downscaled microfluidic devices were fabricated in glass/PDMS using standard soft lithography techniques. PDMS chip production was then carried out as described in section 4.1.1.

Continuous phase consisted of i) FC40 with 0.5% wt. perfluorooctanol or ii) HFE 7500 with 0.25% wt. triblock surfactant PFPE-PEG-PFPE. To-be-dispersed phase consisted of i) distilled water with Congo Red dye, or ii) solution of glycerol with water and Congo Red (see

Table 2). Fluid handling in the system was performed as described in section 4.2.4 Fluid handling and imaging as described in section 4.2.5 Data acquisition.

Table 2 Used glycerol solution and their densities and viscosity[200].

Glycerol [%wt]	ρ[kg/m³]	μ[mPa s]
0%	998.0	1.00
10%	1024.7	1.30
20%	1051.3	1.74
25%	1064.6	2.01
30%	1077.9	2.46
40%	1104.1	3.69
50%	1131.1	6.02
60%	1157.7	9.46

5.2. **Results**

5.2.1. **Step emulsificator geometry**

Microfluidic chips usually rely on injection of continuous and to-be-dispersed phases simultaneously. Interaction of the streams of both phases allow droplet formation and moving the droplet away from the junction. In the presented design, the chip is prefilled with the continuous phase (oil), and the to-be-dispersed phase is the only one injected to the system in monitored and controlled fashion. The step emulsification junction is aligned vertically, to utilize gravity field to transport the droplets away from the step using the density difference between them and medium. The droplets are transported from the point of origin passively by buoyancy – less dense aqueous phase rises in the denser continuous phase (density difference ~500-800 kg/m³ depending on the used phases). This was one of the first demonstrations of passive transportation of droplets via nozzle alignment, later investigated thoroughly by Stolovicki et al[201].

Used microfluidic device comprised microfluidic channel with two inlets and an outlet. The inlets connected to the square microchannel and allowed inflow of two liquids: to-be-dispersed and continuous phases, while outlet was for collecting the

produced emulsion. The microchannel featured three regions: the supply channel to the step, step, and the reservoir. The supply channel dimensions were (width, w_c, and height, h_c) $w_c = h_c = 200$ μm, and the reservoir dimensions were (width, w, and height, h) w = h = 1mm. The main element of the step emulsificator, the nozzle of the microchannel feeding the sample, was prepared in three variants, as shown in Figure 15:

i) Standard geometry of a channel with no additional elements (see Figure 15.1),

ii) Standard geometry with a constriction upstream of the step (see Figure 15.2),

iii) Standard geometry with a constriction upstream of the step and a set of bypasses (see Figure 15.3).
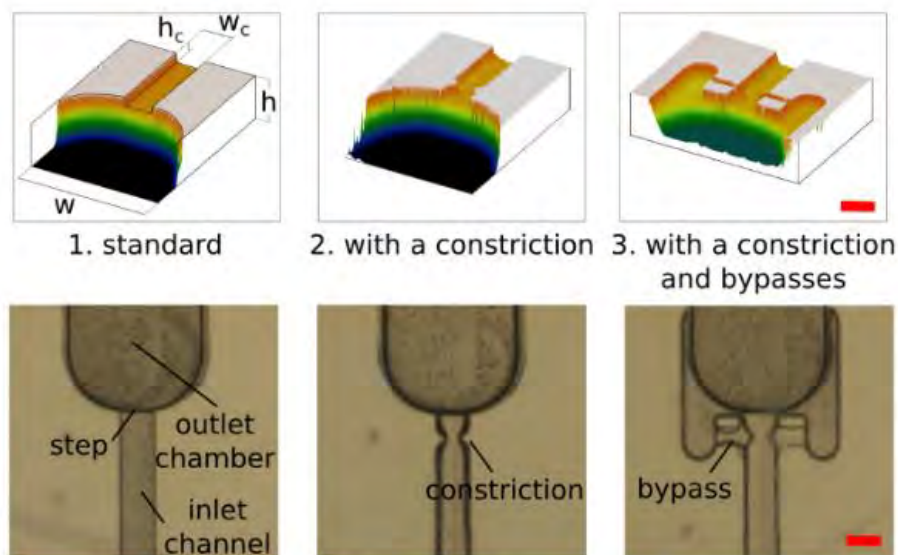
Figure 15 Step emulsificator geometries. 1. Standard nozzle, 2. Geometry (1) with additional constriction, and 3. Geometry (2) with additional bypasses. Top row comprises 3D scans of the devices, bottom row features corresponding microphotographs of the microfluidic devices. Widths and heights of the channels are $w_c = h_c = 200$ μm, w=h=1 mm, scale bar length is 200 μm. Reprinted from [133].

Standard step junction served in our experiments as control. The other two, more complex, solutions were intended to investigate the influence of changing microchannel geometry on the droplet formation process. The targeted element was

the neck of the to-be-dispersed phase thread, described in Dangla et al[139] and section 2.3.2 Passive droplet formation.

As described in the literature, the change of the flow rate of the to-be-dispersed phase is reflected in the change of position of the neck of the thread. The higher the flow rate, the closer to the step the neck forms, and the longer the necking time allowing inflow of the droplet phase[134,143]. Only the position of the neck changes, the shape of the interface is independent on the flowrate, as it depends on the contact angle[196]. The idea behind the constriction is that the necking occurs when the to-be-dispersed phase is drained from the thread of the to-be-dispersed phase to the point when the thread diameter is smaller than the channel height. In the constricted region, of the cross section smaller than the microchannel, the necking should occur faster due to required smaller change in dimension of the thread. Hence, introduction of the constriction should localize the necking in the constricted region. To prove this I observed the position of the breakup in the to-be-dispersed phase for varying flow rates in the tested geometrical variants (see Figure 16).
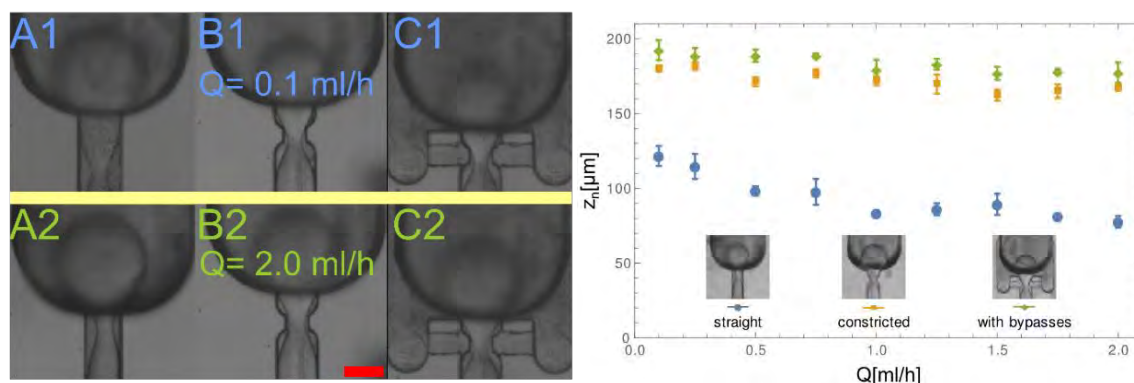
*Figure 16 Neck position for various flowrates and geometries of the nozzle. **Left**: positions of the necks for geometries (A standard, B constricted, C constricted with bypasses) and flow rates (top row – 0.1 ml/h, bottom row 2 mL/h). **Right**: Relationship between the geometry of the nozzle, flow rate of the to-be-dispersed phase (Q) and the upstream position of the narrowest place of the thread (z_n). Adapted from [133].*

The position of the breakup was changing for the standard microchannel, and localized in case of the constricted designs (with and without bypasses, constriction starting at 100 μm and ending at 200 μm upstream of the step, z_n). The experiment

71

confirmed that the neck is confined to the constricted region in the investigated microchannel.

Dimensions of the investigated constriction were 100 µm in each direction – along 100 µm of the microchannel the width and half of the channel were reduced by 50%. The position of the constriction upstream of the step was optimized experimentally. Microfluidic devices differing only in the position of the constriction were fabricated. Start of the constricted region was 0-300 µm upstream of the step edge and the droplet volumes for varying flowrates were measured (see Figure 17). The distance Δz = 100 µm upstream of the step yielded the smallest and most stable droplet volumes against changing flow rates, and was subsequently used in all constricted devices.
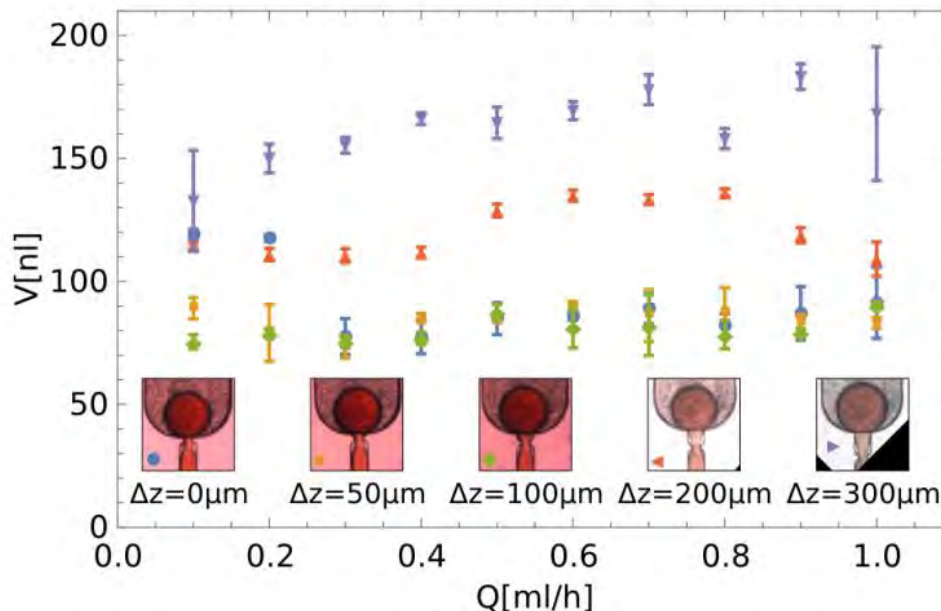
Figure 17 Relationship between produced droplet volumes and constriction location. Droplets of dyed water in FC-40 oil with surfactant. Reprinted from [133].

In the constricted geometry I succeeded in localizing the thread instability in the constricted region of the channel. The next step was to use the fixed location of the necking to increase the speed of the thread breakup. For a neck to break, the thread cross section must decrease below critical value. During necking, the area occupied by the to-be-dispersed phase shrinks, and is filled with continuous phase. In straight microchannel design the continuous phase must come from the only available

location – the reservoir downstream. Continuous phase is forced to invade the microchannel via the gutters of the channel, around the forming droplet. To-be-dispersed phase competes with the continuous phase inflow – the higher the flow rate of the sample, the longer it takes for the continuous phase to reach the neck location. This is what causes previously mentioned change of the neck location downstream with the increase of flow rate of sample.

To avoid competition for the microchannel area at the step, I introduced bypasses, which are shallow side channels connecting the constricted area to the reservoir. Bypasses are significantly smaller than the main microchannel – they are 100 μm wide and 50 μm high. To-be-dispersed phase does not invade bypasses due to hydraulic resistance via this way being much higher than choosing an alternative path to the reservoir, along the main microchannel. Continuous phase, on the other hand, wets the walls of the bypasses and freely penetrates the feed microchannel via bypasses.

5.2.2. Comparison of the nozzle geometries

To measure the influence of the tuning of the geometry of the step nozzle on the droplet size, I measured the droplet volumes from microfluidic devices with different nozzles for varying flow rate. Droplet volumes for the same flow rate was different for each design (see Figure 18).
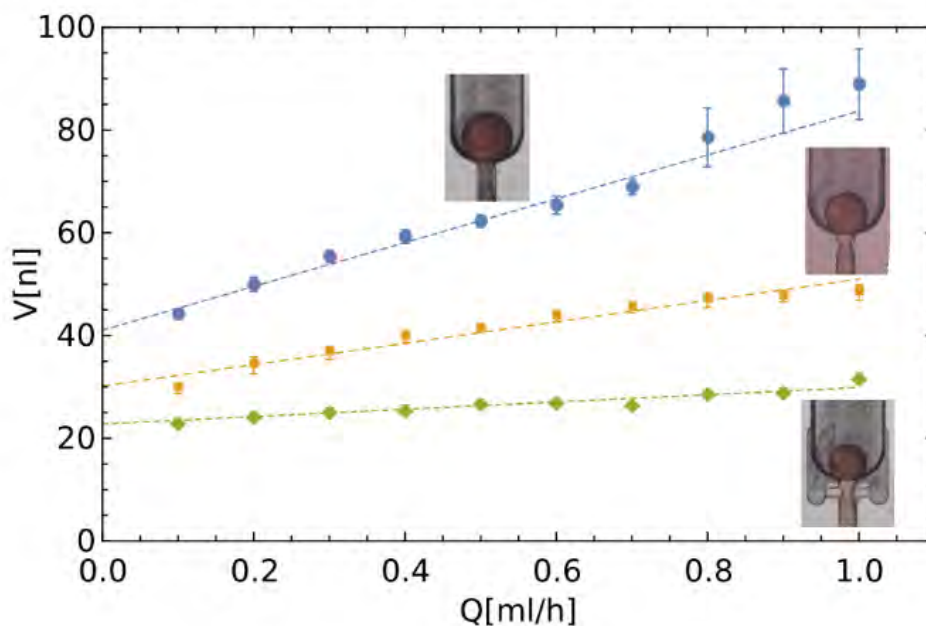
Figure 18 Droplet volumes for different nozzle designs, presented in insets. Blue circles represent straight data points from standard nozzle, yellow squares represent data points from nozzles with constriction, and green diamonds represent data points from the constricted nozzles with bypasses. Linear dependence is fitted to experimental data (dotted line of adequate color). Adapted from [133].

Different nozzle designs yield droplets of different volumes. Standard microchannel yield largest droplets, and bypassed microchannels yield the smallest droplets for each of the tested flow rates. The droplet volumes differed significantly – for example for 0.1 mL/h the nozzles produced droplets: ~25nL (with bypasses), ~30 nL (with constriction), and ~45 nL (standard). Ten-fold increase of the flow rate of the to-be-dispersed phase increased the size of the droplet by 20%, 50% and 100% for bypassed, constricted and standard geometries respectively.

To quantitatively compare the stability of the produced droplet volumes against the changing to-be-dispersed phase flow rate I fitted the linear function in form of y y=ax + b, to the data points, see Equation 11.

$$V = V_0 + V_0 \times \alpha \times Q/Q_0$$

Equation 11 Linear fit of the droplet volume (V) produced in step emulsificator.

Where:

V_0 - characteristic volume of the droplet produced in the system [nL],

α - dimensionless parameter describing slope of the curve,

Q - volumetric flow rate of the to-be-dispersed phase [m^3/s],

Q_0 - characteristic volumetric flow rate of the to-be-dispersed phase [m^3/s].

I defined the volume of the produced droplet, V, as a function of four parameters:

i)   characteristic volume of the droplet formed in quasi-static process, V_0,
ii)   characteristic flow rate of the liquid, Q_0,
iii)   flow rate of the liquid, Q,
iv)   dimensionless coefficient, α,

Characteristic droplet volume is y-intercept parameter (b) of the linear function defined as y = ax +b. This parameter tells about the minimal droplet volume of the given system, assuming the slope of the fit is non-negative.

The variable (argument, x) of the fitted function is the ratio of flow rates: induced by the user (flow rate Q), and the characteristic flow rate of the system (Q_0), x=Q/Q_0. Introduced characteristic flow rate Q_0 is tied to the need for droplets to move away from the step before the next one can be formed. The velocity of the droplet movement away from the step can be characterized by terminal velocity of the droplet flowing upwards by buoyancy in the reservoir [41]:

$$v_0 = \frac{2}{3} \frac{\rho_o - \rho_d}{\mu_o} \frac{\mu_o + \mu_d}{2\mu_o + 3\mu_d} R_0^2 \, g$$

Equation 12 Terminal velocity of droplet of droplet phase in unlimited system filled with continuous phase. For square cross-section, the formed droplets radius is equal to width of the microchannel

Where:

v_0 – terminal velocity of droplet of dispersed phase in an unlimited system filled with outer phase [m/s],

R_0 –radius of the droplet [m],

g – is the gravitational acceleration, 9.81 [m/s^2],

ρ_d – dispersed phase density, 998 [kg/m^3],

μ_d – dispersed phase viscosity, 0.001 [Pa × s],

ρ_c – continuous phase density, 1614 [kg/m^3],

μ_c – continuous phase viscosity, 0.00124 [Pa × s].

Knowing how fast the droplet can move away from the step, I defined the characteristic flow rate as the maximal flow rate of the to-be-dispersed phase for which the subsequent droplets do not collide. To calculate volumetric flow rate I used terminal velocity of the droplet phase flowing through the square microchannel of width *w*:

$$Q_0 = v_0 w^2$$

Equation 13 Characteristic flow rate

Where:

v_0 –terminal velocity of to-be-dispersed phase [m/s],

w – channel width [m].

It is an useful approximation, based on case of unlimited system. In presented system, with finite dimensions, the maximal flow rate is smaller than Q_0. For the presented geometries and sets of fluids, (water in HFE-7500, w = 200 μm), Q_0 = 7.6 ml/h.

For a non-limited ideal system there would be no dependence of the flow rate of to-be-dispersed phase on the droplet volume, and it would be fixed at V_0. However, in the real systems, there is a dependence, which I define by the slope of the fit function, dimensionless parameter α. It is a measure of change of droplet volume (y) in relation

76

to the change of the inflow rate of the sample (x). Values of α for the presented geometries and state of art solutions were calculated and are presented in Table 3.

Table 3 Values of parameter α (Equation 11) for three presented nozzle geometries and state-of-art devices.

Device	*α*
Standard, Figure 15.*1*	7.9
With constriction, Figure 15.*2*	5.2
With bypasses, Figure 15.*3*	2.4
Dangla et al. [139]	~8.0
Dangla et al. [124]	~4.2

Nozzles of standard geometry yield α coefficient around 8 (7.9 in our test and ~8.0 by *Dangla et al.* [139]). Introduction of the geometrical features, such as constriction or a tilted ceiling of the microchannel[124], reduced the slope, and the α coefficient value to 4-5 (4.2 for the tilted ceiling, 5.2 for constricted geometry). A further slope reduction was observed for microsystem where continuous phase had free access to the neck of to-be-dispersed phase via bypasses - the α coefficient value was 2.4. Presented data justifies the claim that factor α is a tool enabling comparison of different systems in terms of sensitivity of droplet volumes to flow rate variations.

5.2.3. **Downscaling the nozzle**

Droplets produced from the square 200 μm microchannels are relatively large. They are from 20 to 90 nL, while most of the biological assays use smaller droplets, of volume of single nanoliters[177]. In step emulsification the droplet size is scaled with the geometry of the microchannel, mainly height[124,145]. That is why in order to produce smaller droplets, I downscaled the bypassed step emulsificator. The microfluidic chip was fabricated in PDMS by soft lithography. The resulting quadratic cross section had width and height of 62.7 μm (see Figure 19), and characteristic flow rate of Q_0 = 0.074 *ml/h*.
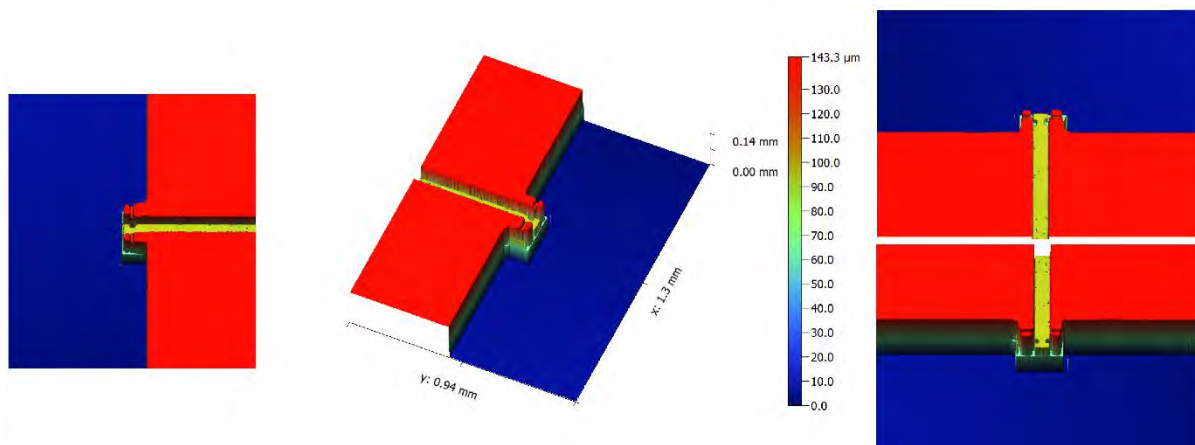
Figure 19 3D scan of the downscaled step emulsificator from different angles. The dimensions and color-coded heights are uniform across all renders..

To test the dependence of droplet volume on the flowrate in the downscaled step emulsificator with constriction and bypasses the emulsions were produced at varying flow rates. The results are presented in Figure 20. Slope coefficient, α = 0.6, meaning that the tested device is very resistant to flow rate variations. 15-fold increase of the flowrate resulted in 10 % increase of the droplet volume (from 0.71 nL to 0.78 nL at 0.001 and 0.015 ml/h, respectively).
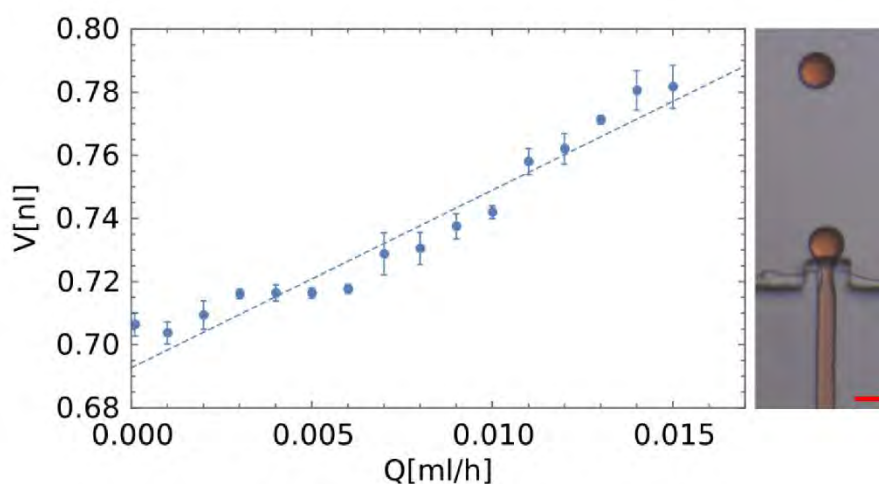

Figure 20 Relationship between the flow rate of to-be-dispersed phase and droplet volumes in the downscaled step emulsificator with constrictions and bypasses. Points represent experimental data points, and dashed line is a linear fit $V=V_0 (1+α Q/Q_0)$. To show the slope of the fit the y-axis ranges only from 0.68 to 0.80 nl. Scalebar is equal to 100 µm. Reprinted from [133].

5.2.4. **Application of the presented step emulsificator for analytical assays**

In analytical assays the sample composition is not always known. Since water is the main component of living matter and environment for biological process, the samples usually are the aqueous solution, such as PCR mix[177] or cell culture medium[5]. Densities of the samples usually do not change much over a high range of concentrations of most agents, especially as very low concentrations are used, usually milimolar to micromolar. The viscosities, of samples, however, can vary significantly between different samples. Presented system aimed at generation of monodisperse libraries of nanoliter droplets from any biological sample, preferably of the same volumes. To mimic different biological samples I injected eight solutions of different viscosity into the bypassed step junction (see Figure 21).
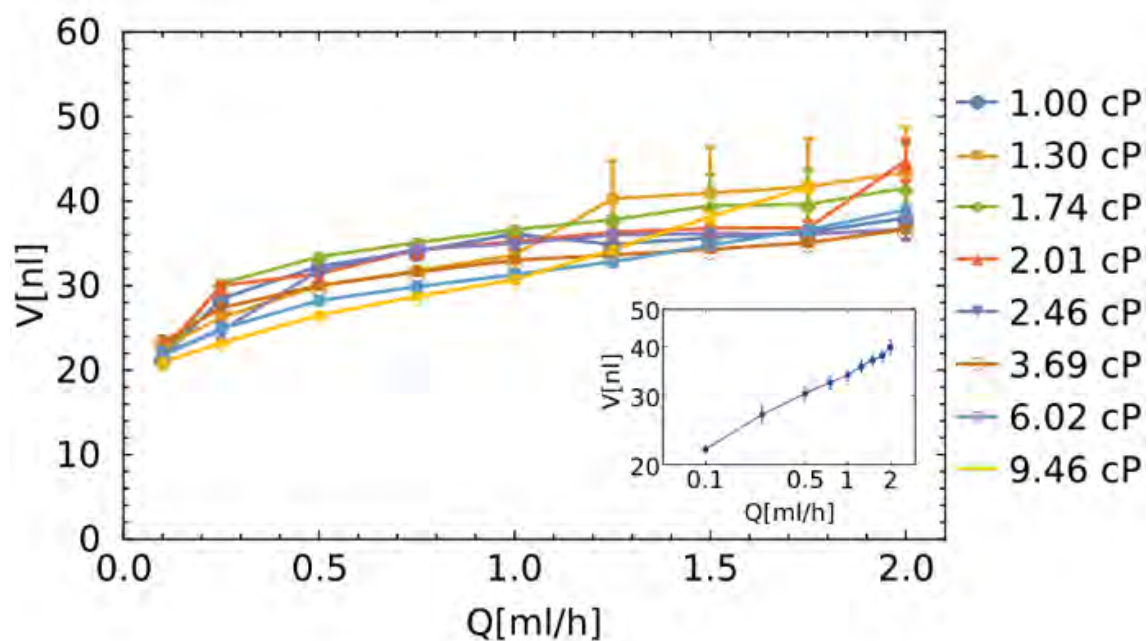
Figure 21 Influence of the to-be-dispersed phase viscosity on the droplet volumes for varying flow rates. Viscosity was tuned by addition of glycerol. Inset shows the averaged values of all the samples for each flowrate, on a logarithmic scale. Reprinted from [133].

The dependence of droplet volume to the flow rate of to-be-dispersed phase in Figure 21 is just like presented previously, in Figure 18. The exact volume values for different viscosities are not identical. There is no systematic change of the volumes of the droplet in relation to the viscosity of the sample, and the deviation of the droplet

volume from the average of all the viscosities is of order of 5% (criterion of monodispersity), as presented in inset of Figure 21. The results indicate that for other parameters fixed, the produced emulsion size should be independent from the sample viscosity. Providing identical microreactor is a very attractive functionality from the point of view of analytical assays.

Key feature of the presented step emulsificator is generation of monodisperse emulsions by injecting only the to-be-dispersed phase to the system. The high tolerance for flow variations allow using sources of pressure less precise than syringe pumps, e.g. electronic pipettes. To validate that claim I used the electronic pipette-powered flow to emulsify microliter sample into nanoliter droplet library (see Figure 22). A pipette tip was sequentially filled with sample, air spacer, and continuous phase. Then the sample was injected into the microfluidic device in a single dispensing operation, using minimal flow rate provided by the pipette, 1.584 mL/h. For this experiment a tailored variant of the microfluidic device was prepared – instead of the straight microchannel it was U-shaped. Shape of the channel allowed injection of the fluids from the top of the device, as well as buoyancy-driven droplet removal from the step. Composition of the pipette tip content was (in order of injection to the chip): 1.5 μl oil, 2 μl air spacer, 4 μl sample, and 5 μl oil (see inset in Figure 22). First portion of oil fills the microchannel and reservoir, air plug prevents to-be-dispersed phase breakup before the step, and the last portion of the oil pushed the to-be-dispersed phase to the reservoir, to remove any dead volume.
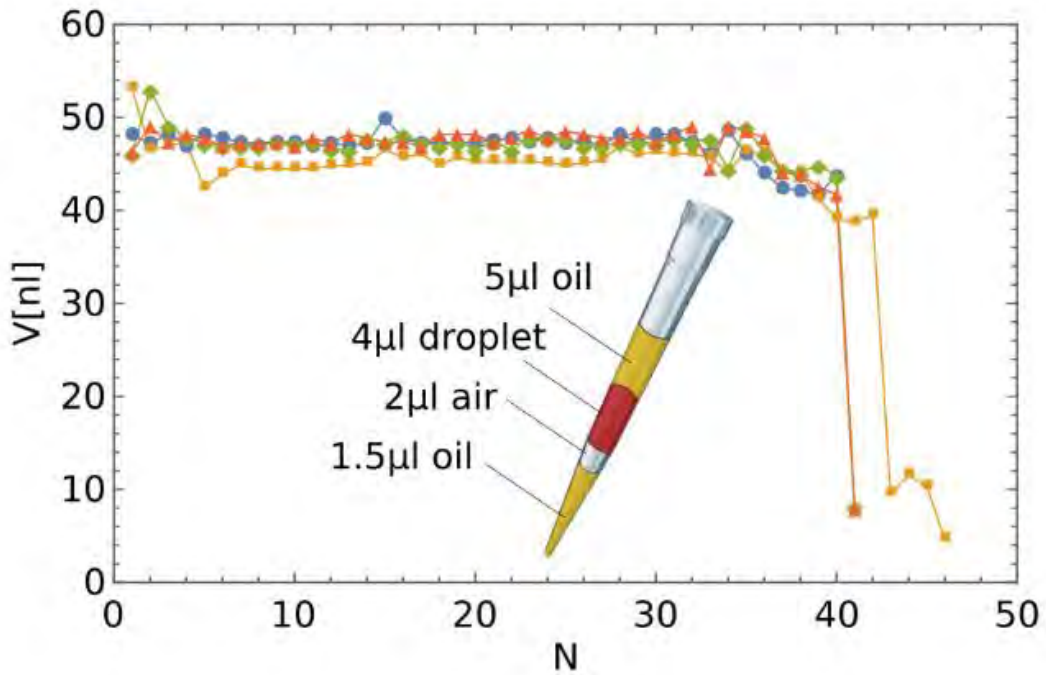
Figure 22 Volumes of droplets produced from the single injections of the oil-spacer-sample combinations. Each color represents one repetition, each point represents a single droplet (not all of the initial droplets were captured). Inset shows composition of the plug injected to the microfluidic device. Reprinted from [133]

I carried out four repetitions of the plug-injection experiment. In each of them the CV of the volume of produced droplets was below 5% (between 0.85% and 4.88%, last five droplets were excluded from the calculation), corresponding to CV of diameter of less than 1.7%. Last droplets are significantly smaller than the rest of the emulsion, due to the fact that the thread of to-be-dispersed phase is shorter than for first droplets. Curvature of the microchannel-confined thread rises, and so does Laplace pressure. Lower Laplace pressure difference between head and tail of the thread results to lower inflow of the to-be-dispersed phase during necking time, and leads to smaller droplets[202]. For large populations of droplets (e.g. commercial ddPCR systems operate on 20 to 30 thousand droplets) influence of few outliers is negligible.

5.3.   **Discussion and conclusions**

In this section, I presented the work on optimization of the step emulsificator nozzle geometry. Together with coworkers I introduced new types of step nozzles:

i)   with constriction upstream of the step,

ii)   with constriction and bypasses upstream of the step.

Operation of the step emulsifying junction was hard-wired into the geometrical features of the nozzle. Constriction allows localization of the neck of the to-be-dispersed phase thread, facilitating the droplet formation. Monodisperse libraries of nanoliter droplets can be produced in a wide range of volumetric flow rates. By prefilling the device with continuous phase, the control can be maintained over only the sample phase. Alternatively, the complete set of fluids needed for emulsification (filling oil, air spacer, sample, pushing oil) can be injected in form of a single plug.

Experimentally I justified claim that introduction of geometrical features such as bypasses and constrictions stabilizes the droplet volume against variations of the sample flow rate. What is more, the size of the produced droplets was reduced, when compared to standard step emulsification geometry. Scaling possibilities of the design were also tested, fabricating downscaled microfluidic chips producing monodisperse sub-nanoliter droplet libraries. The stabilizing effect of the passive junction on the size of the droplet was so large that even an electronic pipette could be used as a source of the flow. Use of tools common in biological laboratories opens a way to introduce presented step emulsificators into biological analytical assays, such as cell enumeration, drug testing or nucleic acid amplification. Ideally, downscaled (in terms of size) nozzles would be incorporated into modified pipette tip in large number to obtain high-throughput of droplet formation.

6. Increasing throughput of step emulsificator

In this chapter I present the second project carried out within my doctoral thesis. The results were published and this section is based on the publication: *Grooved step emulsification systems optimize throughput of passive generation of monodisperse emulsions*, **A. S. Opalski**, K. Makuch, Y.-K. K. Lai, L. Derzsi and P. Garstecki, Lab Chip, 2019, 19, 1183–1192, DOI: 10.1039/C8LC01096J

6.1.   **Introduction**

6.1.1. **Problem statement**

In order to use emulsions industrially, or perform complex analytical assays, a vast number of droplets is needed. Quantity requirement may in some cases even outweigh the monodispersity, and the less accurate, but faster and easier methods for droplet generation are used. For example, accurate quantification of ddPCR is possible using polydisperse droplet system[203], as well as flow cytometry based sorting of polydisperse double emulsions[204]. Still, monodisperse emulsions are preferred to polydisperse ones, especially in the bioanalytical assays. That is why there is currently a trend of upscaling microfluidic geometries, from flow-focusing junctions[81] to step emulsificators[145,147].

However, many upscaled microfluidic systems require either very sophisticated manufacturing process[81], or maintaining control over the flow of two phases[145,147]. Ideally, the microfluidic system should produce monodisperse emulsion at high throughput, and requiring control over just sample injection rate. Such is the system proposed by Stolovicki et al[201], which features parallelized step emulsifying nozzles. The produced droplets are cleared away from the nozzle by buoyancy, straight into external reservoir filled with outer phase –just like in previous chapter of this dissertation.

An approach to upscale a number of step emulsifying nozzles is very attractive, as parallelization of passive junctions is less challenging than upscaling active junctions. The crucial feature is the geometry of the nozzle, which controls the droplet formation mechanism and is reflected in emulsion uniformity. Sadly, Stolovicki et al[201] did not improve the nozzle geometry and upscaled the standard step emulsifying junction, which was shown in the previous chapter to perform worse than my modified step junction geometry.

Two main techniques used for parallelized step emulsification are described in section 2.4.1 Parallelization of the passive emulsifying junctions

    i)   edge-based droplet generation (EDGE),

    ii)   microchannel emulsification (MCE).

In both of them droplets are simultaneously produced in multiple places, called droplet forming unit (DFUs). In MCE the DFUs are located at nozzles of microchannels, separated by full floor-ceiling wall. EDGE, on the other hand, has no partitions on its single, very wide and shallow nozzle and the DFUs are not fixed. These techniques differ in modes of droplet formation that influence the produced emulsions – EDGE yields higher throughput at price of lower uniformity, when compared to MCE. Both techniques require cross-flow of outer phase to remove the droplet from the nozzle vicinity.

In this chapter I investigate how to increase a throughput of step emulsificator to by optimizing geometry of the step emulsification junction. The goal was to combine advantages of existing solutions with a concept of feeding the outer phase to the thread necking location – presented in previous chapter. A result of the project was introduction and systematic study of grooved step emulsifying geometry, a MCE-EDGE hybrid. In this chapter I will characterize the novel geometry, compare it to the state of the art, and describe physical phenomena of the parallelized step emulsification.

6.1.2. **Materials and methods**

Microfluidic chips were fabricated in polycarbonate, prepared as described in sections 4.2.1 PC chip fabrication. Channels were modified fluorophilically with Novec 1720 as described in section 4.2.3 Microchannel surface modification.

Continuous phase consisted of HFE 7500 with 2% wt. triblock surfactant PFPE-PEG-PFPE. To-be-dispersed phase consisted of i) distilled water with Congo Red dye, or ii) solution of glycerol with miliQ water and Congo Red (see

85

Table 2). Fluid handling in the system was performed as described in section 4.2.4 Fluid handling and imaging as described in section 4.2.5 Data acquisition. Information was extracted from the recorded videos using methods described in section 4.2.6 Data processing and analysis, using custom written MATLAB script to automate the processing.

Surface properties of the microchannel play important role in step emulsification process, as the mechanism of droplet formation relies on the contact angle between to-be-dispersed phase and the microchannel walls[196]. In this project, I used polycarbonate chips instead of the PDMS/glass chips, as the elastic PDMS could collapse over wide channels.

The surface of the microchannels was investigated by optical profilometer. Reconstructed 3D image is shown below, in Figure 23. I show there a fragment of the microchannel, as well as the whole device. The surface of the chips is not perfectly flat, but there are no hooks, splinters or any other effects that could disturb the flow of liquids.
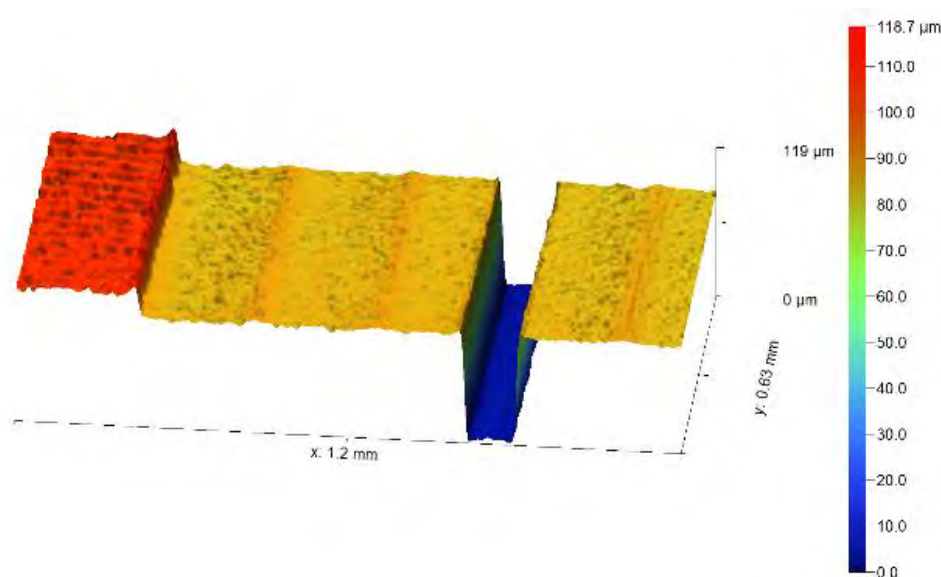
Figure 23 Surface characterization of the milled chips. 3D scan of part of the chip with a single droplet forming unit. Shown device: PGR = 0.2, L_g = 0.5 mm. Adapted from[20].

To characterize the wetting properties I measured the contact angle of water on a milled polycarbonate surface, both native and modified, to choose the right way to fabricate chips. Whole area of four flat polycarbonate plates was milled, and the plates

86

were divided into 2 groups of 2 plates each. First pair of plates was treated with dichloromethane vapor to smoothen the surface, the other was not. One plate from each pair was modified with fluorosilane as described in the section 4.2.3 Microchannel surface modification. Then, contact angles between deionized water and the plates were measured (see Figure 24). Contact angle of the native milled surface was 76^0. Smoothening of the polycarbonate surfaces led to no change in contact angle after silanization, which indicates that the modifying agent did not adhere to the surface. Milled plate, rough after milling, exhibited change of contact angle from 76^0 to 108^0, indicating that fluorosilanes adhere better to slightly rough surface.
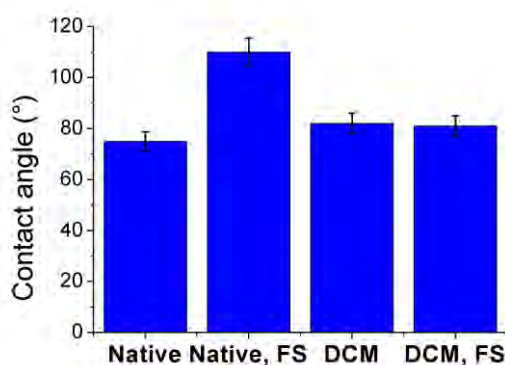

Figure 24 Contact angle between milled polycarbonate (native and modified with fluorosilanes, rough and smoothened by dichloromethane vapor treatment). Adapted from[20].

6.2. **Results**

6.2.1. **Step emulsificator geometry**

In this section I describe the investigation of the transition between two step emulsification techniques: MCE and EDGE. I propose explanation as to why two step emulsifying techniques yield droplets in different modes, identify where the transition point between those modes is, and describe what is the optimal parallelized (wide) step emulsificator architecture. Both MCE and EDGE feature wide emulsifying slit, either with partitions between the DFUs or without. Presented grooved geometry is a hybrid of mentioned geometries – it features elevations (partitions) along the length of the droplet producing step of the wide step emulsificator (see Figure 25).
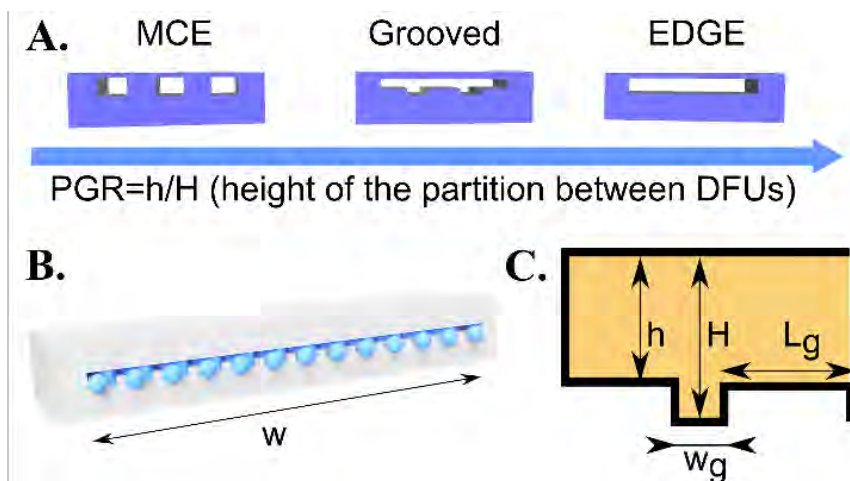
Figure 25 Introduction to grooved step emulsificator. ***A*** *Representation of step emulsificators with partition between DFUs of varying height. From the left to right: MCE, grooved device, EDGE.* ***B****: Render of the front view of the operating grooved device. Aqueous droplets (blue) are produced when extruded from a slit to the reservoir filled with continuous phase (transparent); w – width of the emulsifying slit.* ***C****. Scheme of the geometrical parameters in grooved geometry: h – height of partition, H – height of groove, L_g – width of the partition, w_g –width of the groove, w – width of the device. Reproduced from[20].*

Optimization process consisted of testing devices with partitions of different heights: from no partitions (EDGE) up to full floor-to-ceiling partitions (MCE). The crucial geometrical parameter in such system is the ratio h/H, of height of the partition (h) and channel (H). I called this parameter PGR, which stands for Partition-to-Groove Ratio (PGR), see Figure 25). PGR range is from 0 to 1, from full partition to their absence - MCE and, respectively. I investigated narrow devices (step width w=1.1 mm) that featured one DFU, and wide devices (step width w=15 mm) that contained multiple DFUs. Height (H) and width (w_g) of the grooves were kept at 100 and 120 μm, respectively. Partition height (h) and width (L_g) varied across devices. 3D scan of the grooved device is shown in Figure 26 and Figure 27. I chose two geometrical parameters to scan: partition to groove ratio, PGR=$\frac{h}{H}$, and distance between grooves, L_g. In order to systematically scan over values of both of them would require one order of magnitude more experiments. Thus, the partial scan was performed over L_g for h/H = 0.9 and over h/H for L_g = 0.5 and 0.75 mm. The

parameters offer insight into the influence of partition height and spacing of the grooves on droplet formation.
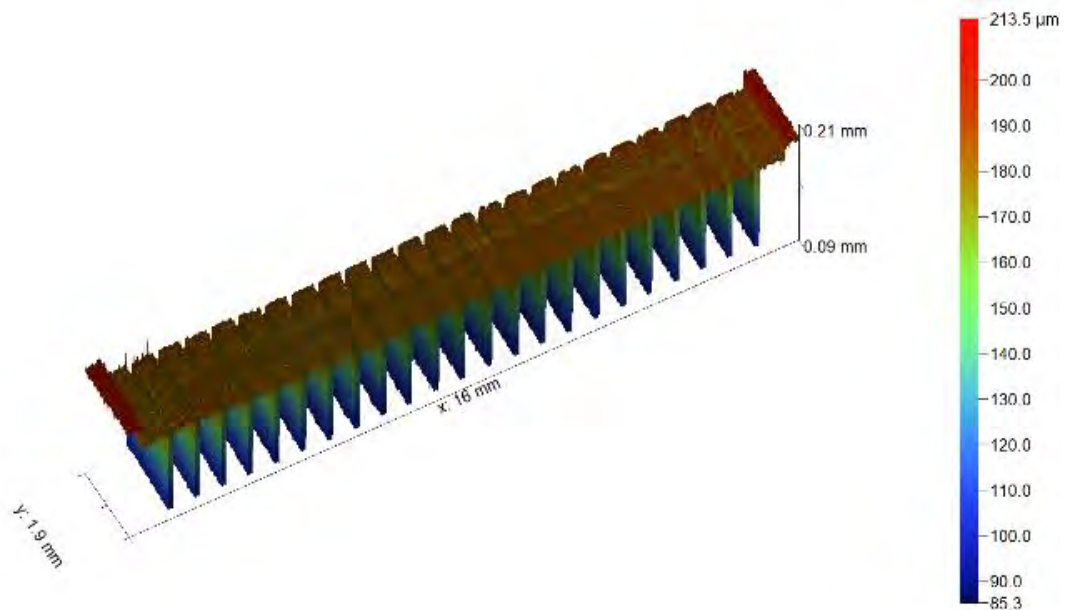
Figure 26 3D scan of the grooved device with 23 DFUs..Adapted from[20].
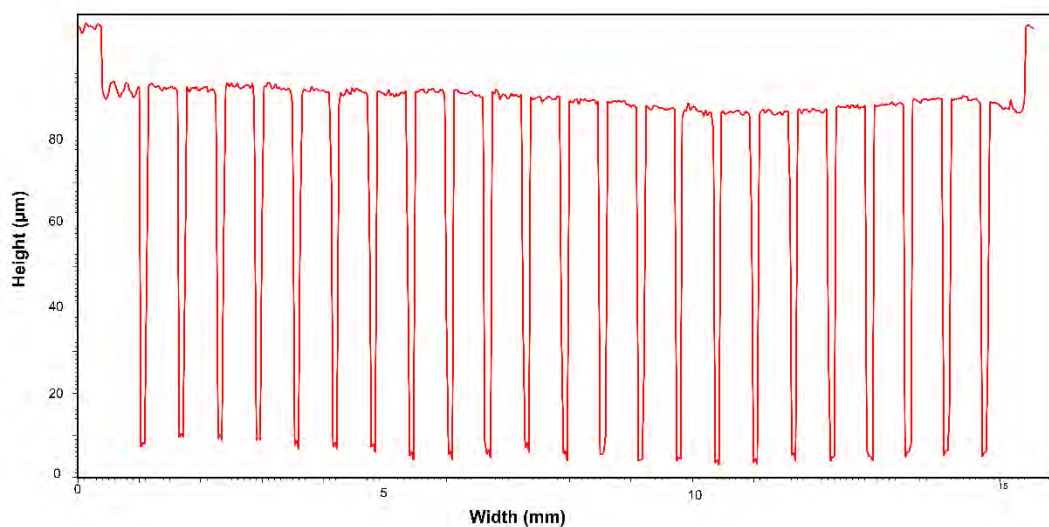
Figure 27 Cross section of the grooved device with 23 DFUs. Adapted from[20].

Fluids that I used in experiments are characterized by viscosities (μ_d, μ_c), densities (ρ_d, ρ_c), interfacial tensions between them (γ), and to-be-dispersed phase flow rate (Q). Independent parameters that could be investigated form multidimensional space that is virtually impossible to fully scan. Instead, four dimensionless independent parameters can be distinguished and investigated: density ratio ρ, viscosity ratio λ,

89

Bond (Eötvös) number *Bo*, capillary number *Ca* (see section 1.6)*.* Fluid densities do not play big role in droplet formation process, as indicated by small Bond number, buoyancy over surface forces ($Bo \approx 0.002$). It indicates that emulsification process is governed by surface tension, not gravity. As a consequence, I did not scan fluids densities. Capillary number defines the ratio of viscous to interfacial forces. Ca combines interfacial tension, viscosity and flow rate, therefore scan over one of parameter is equivalent to scanning all of them. I considered scan of the devices over flow rate of the to-be-dispersed phase as equivalent to scan over interfacial tension and viscosity of continuous phase (for other parameters fixed).

What is important is the value of the critical capillary number, Ca_{cr} ,which determines mode of droplet formation. I performed an experiment aiming to test if changing different parts of capillary number yields different value of Ca_{cr}. I emulsified samples of fluids of different viscosities in HFE-7500 with 2% surfactant (viscosity μ~2 cP). The tested samples were deionized water (μ~1 cP, λ~0.5), 50%wt. glycerol (μ~6 cP, λ~3), and 75% wt. glycerol (μ~35 cP, λ~18), supplied at varying flow rates. Resulting droplet sizes were measured and are presented in in Figure 28. Up to certain flowrate of the to-be-dispersed phase the produced emulsion size was insensitive to the flow rate change of the flow rate. Over crossing the threshold, different for each viscosity of the dispersed phase, size and variation of the droplets sharply increase. For each system the calculated critical capillary number was Ca_{cr}~0.16. The fact that change of both viscosity and flowrate does not change the critical capillary number justifies scanning over only flowrates of the to-be-dispersed phase.
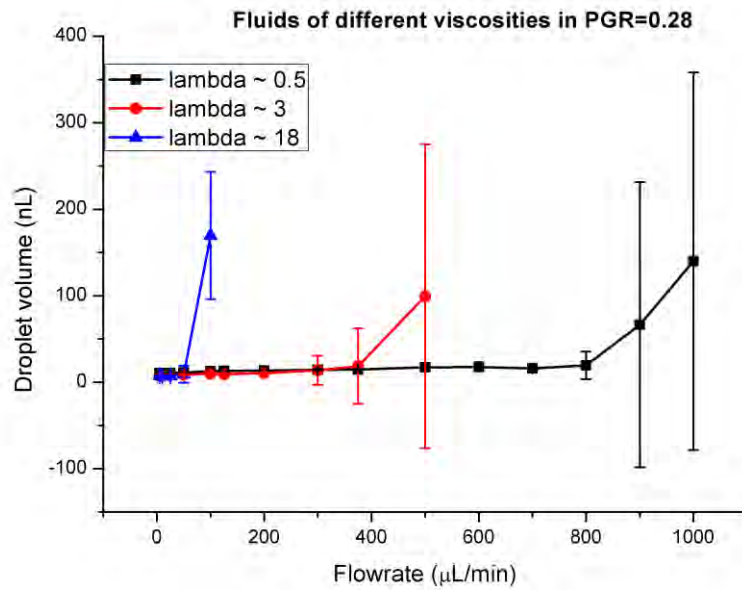
Figure 28 Droplets generated in the grooved devices. Device characteristics: number of grooves=15, groove width = 120 μm, groove height =100 μm, partition height = 28 μm, device width = 15 mm. Adapted from[20].

I started characterization of the devices from narrow devices (w=1.1 mm), with a single groove surrounded by elevated partitions. The only variable between the devices was height of the partition, defined by PGR value changing from 0 to 1. Results are presented in part A of Figure 29.
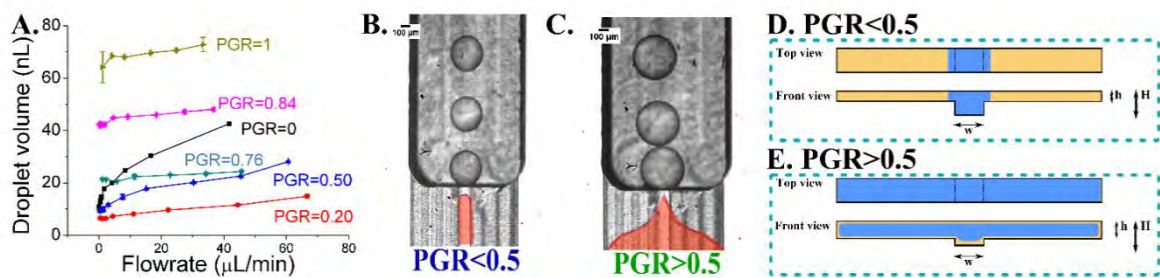
*Figure 29 Characterization of the narrow grooved devices with varying PGR. **A**. Droplet size as a function of the to-be-dispersed phase flow rate. **B, C:** Spreading of the droplet phase over the partition for different PGR values (scale bar 100 μm). **D, E**: Schematic representation of in-groove (D) and spilled (E) droplet phase. Adapted from[20].*

I observed that the volume of emulsion is correlated with the PGR of the device. For example, change of PGR from 0.2 to 1 causes the droplet volume to increase

91

approximately 6 times (see part A of Figure 29). In systems with PGR from 0 to 0.5 I observed that the to-be-dispersed phase remains within the groove, and the droplets are relatively small (see parts B and D of Figure 29). I called this mode of operation of the device an 'in-groove' droplet generation mode, to stress the fact that the droplet phase is confined to the groove only. For PGR larger than 0.5 such confinement is no more – the to-be-dispersed phase spreads over the partition before emulsification. I named this droplet generation mode 'spilt-groove' (see parts C and E of Figure 29). I observed that in the in-groove mode the volume of the generated droplet is more affected by the volumetric flow rate than in the other mode.

In previous chapter I introduced coefficient α as means of comparing various step emulsification systems. To compare the presented devices, I needed to include the cross-section of the microchannel occupied by the droplet phase containing part of the microchannel - whether the to-be-dispersed phase flowed only through the groove (in-groove mode), or spread over the elevation (spilt-groove mode). I calculated the α parameter for presented devices in both cases, using Equation 12 from section 5.2.2. Then I assigned the value basing on observations whether in given device the to-be-dispersed phase spreads on the elevation or not. The data is presented in Table 4 and plotted in Figure 30.

Table 4 Calculated values of coefficient α for single nozzles, including and excluding the partitions into the lumen of the nozzle. Bolded values indicate of α indicate in which mode the device operated and which α value was accepted as correct.

Single groove	In- groove	Spilt- groove	Mode	Assigned
PGR	α	α	-	α
0.00	**2.18**	2.18	In-groove	2.18
0.20	**0.51**	1.33	In-groove	0.51
0.50	**1.00**	5.11	In-groove	1.00
0.76	0.21	**1.50**	Spilt-groove	1.50
0.84	0.35	**2.78**	Spilt-groove	2.78
1.00	0.39	**3.59**	Spilt-groove	3.59

Values of parameter α ranged from 0.5 to 4, which is the same order of magnitude as values reported for constricted and bypassed step emulsificators in previous chapter. The geometry that offered the most stable droplet volumes against flow rate, i.e. lowest α, was one with PGR=0.2. The least resistant was EDGE device with PGR = 1 (see Figure 30).
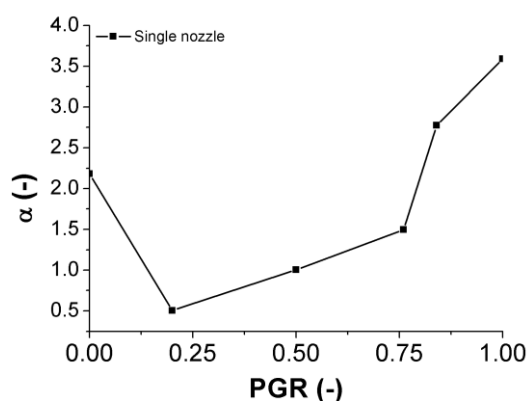
Figure 30 Susceptibility of droplet volume to change with flow rate variation.

Having characterized the operation of single-grooved step emulsificator, I investigated upscaled microfluidic device. Identical grooves were parallelized on 15 mm long emulsifying step. Two series of devices were fabricated: with 23 grooves and L_g = 0.5 mm, and 17 grooves and L_g = 0.75 mm. PGR ranged from 0 to 1. The intended PGR values were: 0, 0.3, 0.5, 0.7, 0.9 and 1, but the real values due to finite precision of fabrication were: 0, 0.28, 0.50 , 0.84, 0.92 for L_g = 0.75 mm, and 0, 0.20, 0.48, 0.68, 0.93 for L_g = 0.5 mm.

The flow rate of the to-be-dispersed phase was changed between 5-1300 μL/min (0.3-78.0 mL/h), unless transition to the jetting mode occurred at a lower flow rate. The results were plotted in a single Figure 31. For easier visualization, the results were split into Figure 32 and Figure 33, for Lg = 0.75 mm and 0.5 mm, respectively. Values of parameter α, including choice of in-groove and spilt-groove mode of operation, are depicted in Figure 34.
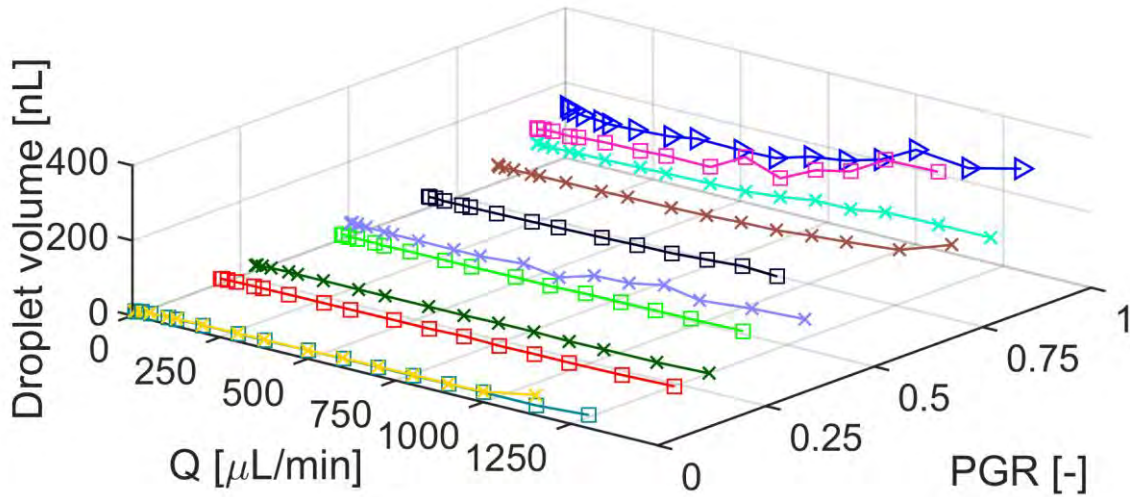
Figure 31 Relationship between droplet volume, the flowrate of dispersed phase and PGR. All of the investigated - devices with grooves spaced by 500 μm (squares) and 750 μm (crosses). Triangles denote EDGE-type device. Adapted from[20].
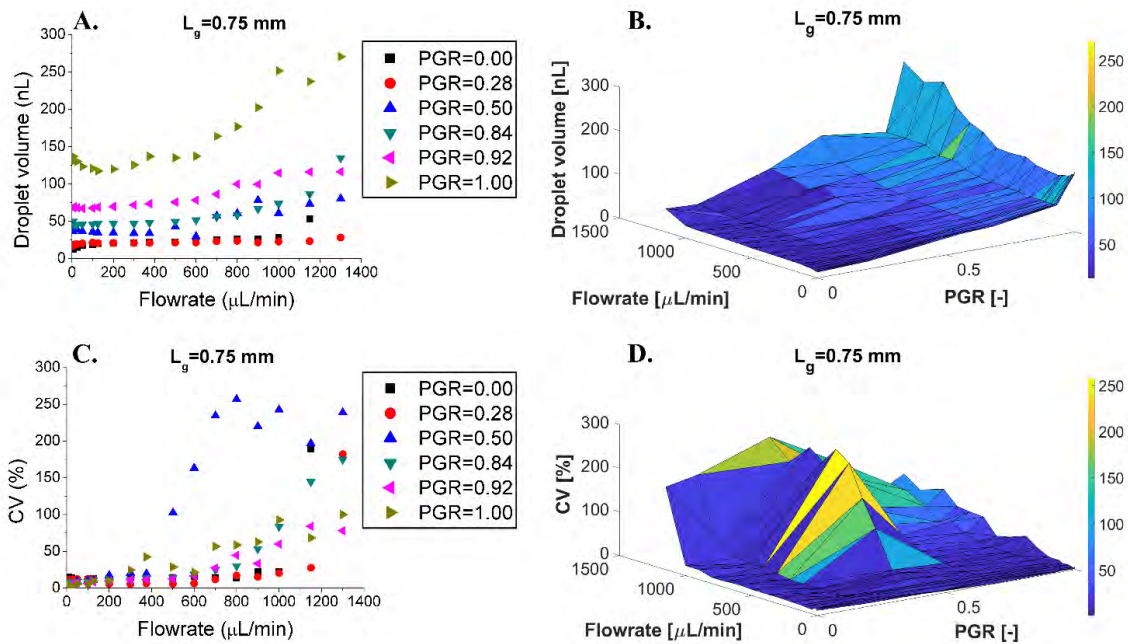

*Figure 32 Droplet sizes (**A, B**) and droplet dispersion reported as CV of droplet volume (**C, D**) as a function of flow rate of the droplet phase for devices with L_g=0.75 mm. Adapted from[20].*
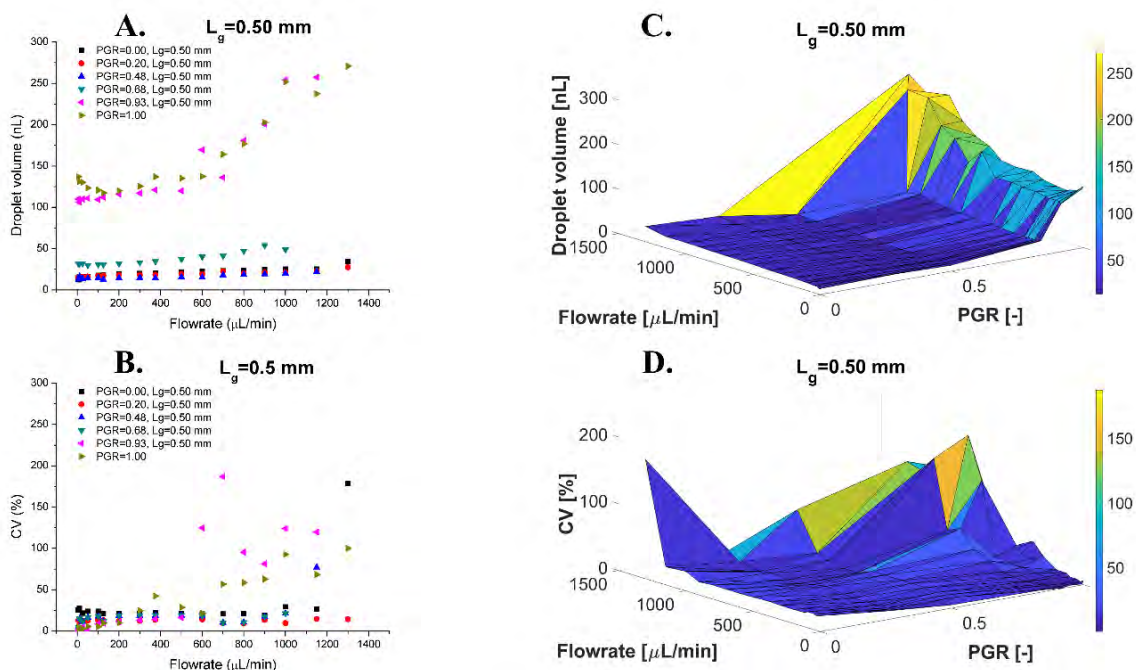
Figure 33 **Top:** *Relationships between: droplet sizes (**A** and **C**) and droplet dispersity reported as CV of droplet volume (**B** and **D**) and the applied flow rate of the droplet phase for devices with L_g=0.50 mm. Adapted from[20].*

Varying PGR and changing flow rates impacted size and monodispersity of emulsions. In the wide microfluidic chips the increase of the PGR translates into the rise of average droplet volume. Rate of droplet generation increase with the flow rate for low PGR values close was very small, and large for PGR over 0.5. PGR reduction from 1 to 0.2 decreases droplet volumes by a factor of 6, exactly like in case of the single-groove devices. I observed that wide devices of the same PGR yield two times larger droplets than the narrow devices, e.g. PGR=0.5, Q= 30 µL/min yields ~20 nL and ~39 nL droplets for narrow and wide devices, respectively. Devices with PGR 0-0.3 exhibited a very wide range of flow rates for which the CV_{volume} was <10% ($CV_{diameter}$ <3.3%), with sudden change to polydisperse droplet formation when reaching certain threshold, around 1000 µL/min. For devices with PGR 0.5-1.0 the monodispersity fell sharply at much smaller flow rates than for small PGR (around 500 µL/min) and for highest tested flow rates reached large values, up to CV_{volume}=300%.

Presence and height of the partitions between DFUs affect the size and CV of the emulsions, as well as their resistance to the flow rate variations (parameter α, see Figure 34). Devices operating in the in-groove mode (PGR≤0.5) were more resistant

to changing droplet volume with the flow rate increase than those operating in spilt-groove mode (PGR>0.5). Devices with PGR=0.2 for L_g=0.50 mm, and PGR=0.28 for Lg=0.75 mm yield the smallest, most tightly monodisperse emulsions, with the smallest α values. Devices operating in the in-groove mode were the most resistant to variation in of the flow rate for almost the whole investigated volumetric flow rate range.
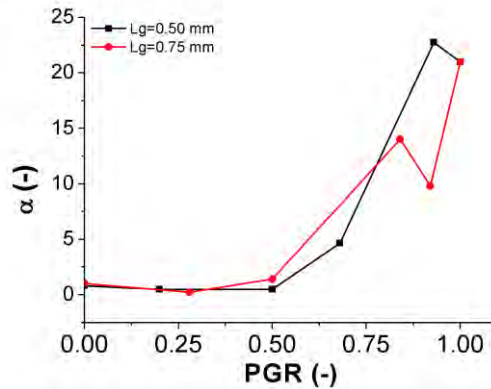
Figure 34 Susceptibility of droplet volume to flow rate variations in wide grooved step emulsificator.

Groove spacing, L_g/H, equivalent to just L_g as H was kept constant, was investigated for a single H value. L_g did not influence much the stability of droplet volumes against flow rates in investigated devices, as presented in Figure 34. The largest variation between two investigated devices was observed for high PGR values. I investigated in detail the influence of L_g parameter on the produced droplet volumes, and stability of the volume against changes in flow rate. Obtained droplet volumes are presented in Figure 35 and calculated α parameter is shown in Figure 36.
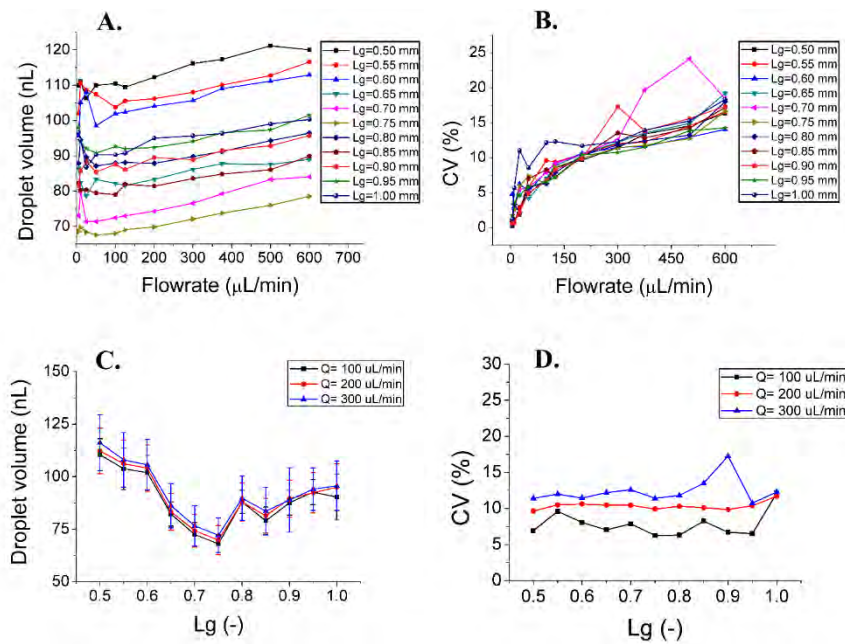
Figure 35 Droplet size (A) and droplet dispersion reported as CV of droplet volume (B) as the function of flow rates for varying DFU spacing, L_g. Droplet size (C) and dispersion of volumes (D) as the function of L_g for chosen flow rates. All experiments for PGR=0.9. Adapted from[20].

Correlation between change of L_g and produced droplet volumes is not monotonic, there is a local minimum for L_g=0.75 mm (L_g/H=6.25). For this value droplets are the smallest for all flowrates (see Fig. 4C). Monodispersity of the droplets for every L_g is almost identical, usually CV_{volume}<15% ($CV_{diameter}$<5%). However, dispersion of the produced emulsion rises with the increase of the flowrate of the droplet phase (see parts B and D of Figure 35). Analysis of stability of step emulsificator against the varying flowrate shows there is no linear correlation of the stability against flowrate fluctuation with and width of partitions. Values of α range varies in a quite narrow

interval from 2.7 to 5.2, suggesting that the distance between the DFUs does not influence the stability of the step emulsification process much.
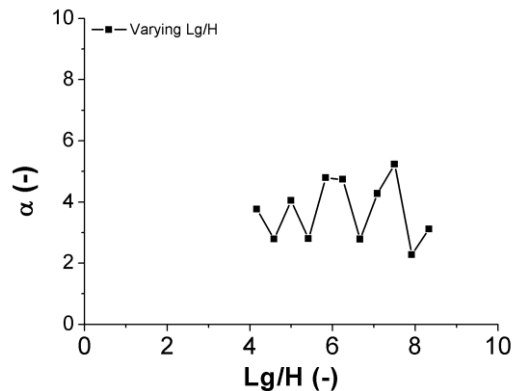
Figure 36 Susceptibility of droplet volumes to flow variations in devices with varying Lg/H parameter.

6.2.2. **Mechanism of step emulsification in grooved microfluidic device**

Step emulsification mechanism is described in detail in section 2.3.2 Passive droplet formation. In this section I focus on the influence of geometry on accessing to the neck by the continuous phase. Change of the geometry junction can increase the access of the continuous phase to the and can be realized by implementing bypasses, as shown in previous chapter. In this chapter I show that partitions of appropriate height may serve as bypasses and that their presence improves performance of step emulsificators, in terms of droplet volumes and their insensitivity to changes of the flow rate. I observed that to-be-dispersed phase either stays in the groove (for PGR 0-0.5) or spills over partitions (for PGR>0.5). The reason for this discrimination and identification of the transition point can be explained by calculating Laplace pressures at the interface in equilibrium configuration[139,143].
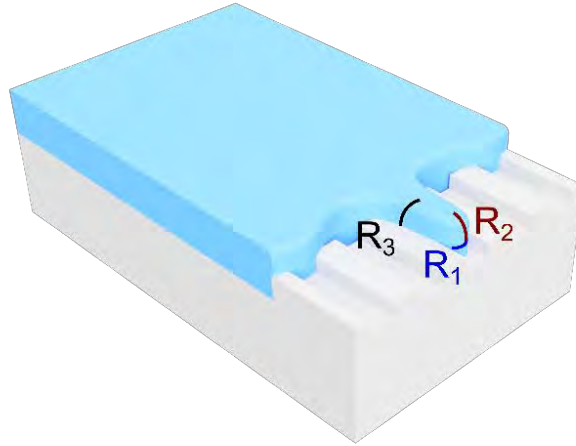
Figure 37 Visualization of the grooved device with three principal radii of curvature of the droplet phase. R_1 and R_2 are principal radii of curvature of the front of the droplet. R_3 is the principal radius of curvature of the side of the plug. There is no other radius of the curvature for the side of the droplet, as the plug lies flat against the ceiling of the device. Adapted from[20].

Laplace pressure at the front tip of the droplet entering the step (ΔP_{front}) is calculated as in the case of a pancake-shape droplet squeezed inside a microchannel (see Figure 37):

$$\Delta P_{front} = \gamma \left(\frac{1}{R_1} + \frac{1}{R_2} \right) = \gamma \left(\frac{2}{H} + \frac{2}{w_g} \right),$$

Equation 14 Laplace pressure in the grooved step emulsificator.

Where:

w_g - width of the droplet (yielding radius of curvature $R_2 = w_g/2$) [m],

H – microchannel height (yielding radius of curvature $R_1 = H/2$) [m],

R_1 and R_2 -

γ – interfacial tension [N/m].

The Laplace pressure at the side of the thread (ΔP_{side}) is calculated as in the case of long and flat droplet invading a gap (partition) (see Figure 37):

99

$$\Delta P_{side} = \gamma \frac{1}{R_3} = \frac{2\gamma}{h},$$

Equation 15 Laplace pressure of the side of the to-be-dispersed thread in the grooved device.

Where:

h –partition height [m],

R_3 –radius of curvature, equal to half the height of partition [m],

γ – interfacial tension [N/m].

From the pressure balance, the droplet phase spreads outside the groove only when the side Laplace pressure is smaller than the pressure at the front of the liquid thread,

$$\Delta P_{side} < \Delta P_{front}$$

Equation 16 Condition of the to-be-dispersed phase spreading defined with pressures.

Thus, the condition of spreading can be defined as

$$\frac{1}{h} + \frac{1}{H} + \frac{1}{w_g}$$

Equation 17 Condition of to-be-dispersed phase spreading defined with geometrical parameters.

For $w_g \approx$ H the condition for the droplet spreading out of the groove becomes

$$h > \frac{H}{2}$$

Equation 18 Condition of to-be-dispersed phase spreading defined with geometrical parameters, simplified.

Calculation that height of the partition must exceed half of the groove height (i.e. PGR>0.5) is in agreement with observations from experiments presented in this chapter. Depending on the PGR partitions of investigated geometries act as i) bypasses constantly supplying outer phase to the necking point for in-groove mode, or ii) storage room for more droplet phase to accumulate before each droplet formation act for spilt mode. In-groove mode produced droplets are smaller than

produced in the spilt-groove mode as the instability breaks off the thinner thread. As the continuous phase has better access to the neck when it is not competing with to-be-dispersed phase on the partition, monodispersity of droplets is better in the in-groove mode than in the spilt-mode.

For a range of tested L_g/H values, droplet volumes and the size stability against variation of the flow rate (parameter α) were of the same order of magnitude. It would be intuitive that in spilt-mode for largest groove spacing the droplets would be the largest, as they should pull the droplet phase from the largest area. However, as presented in panels C and D of Figure 35, the relationship between droplet size and L_g is not monotonous with local minimum (smallest droplets produced) for L_g=0.75 mm. The explanation for the presence of minimum is tied to number and location of the DFUs, which are not constant in EDGE-like devices (high PGR value). Potential DFUs, places where the to-be-dispersed phase is beginning to leave the channel, compete between themselves for the droplet phase. The droplet forms in area with the lowest pressure, withdrawing liquid from the competing low-pressure areas nearby. Optimal groove spacing value for wide step emulsificator was L_g=0.75 mm (6.25 × w_g, 7.5 x H). For systems with Lg<0.75 mm, the DFU strongly compete for the same portion of fluid, which leads to decrease of number of DFUs operating simultaneously. If smaller number of DFUs emulsify the same portion of fluid, the droplets are visibly larger. For Lg>0.75 mm the competition decreases, individual DFU can draw more liquid, which results in increase of the droplet volumes.

6.2.3. Throughput analysis of the presented step emulsificator

In all step emulsifiers throughput of emulsion production is a function of multiple parameters, the most fundamental of which is the geometry of the junctions and the connections between them[139]. I assessed the quality of introduced grooved geometry of the step emulsifier by comparing its performance to the state of the art MCE and EDGE geometries, as presented in Figure 38.
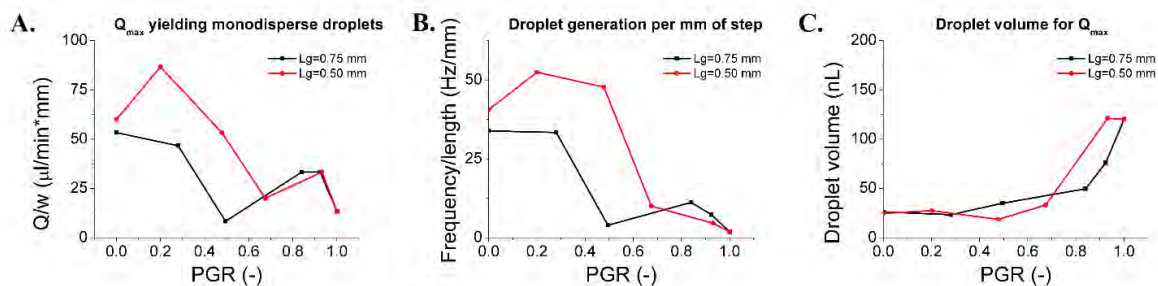
*Figure 38 **A:** Maximum flowrate Q_{max} for which devices produced monodisperse droplets (CV$_{volume}$<15%) per unit length of the step, w. **B:** Frequency of droplet generation for Q_{max} per unit length of the step, w. **C:** Droplet volume for Q_{max} per device Adapted [20] from [24].*

I compared the throughput of droplet production using three parameters:

i)   the maximum volumetric flow rate (Q_{max}, μL/min) per unit length of the step (w, mm) for which devices produce monodisperse droplets (CV of volumes <15%, Figure 38A),

ii)   frequency of droplet production (f, Hz) per unit length of the step (w, mm; see Figure 38B),

iii)   parameter α (see Table 4, Figure 30, Figure 34, and Figure 36).

Microfluidic devices with long droplet-generating edge yielded highest throughput for PGR 0-0.5. Their maximum operational flowrate as well as number of produced droplets production was the highest around PGR 0.2-0.3. Flow rates per unit length were 53 μL/(min × mm) and 87 μL/(min × mm), for devices with L_g=0.75 mm and L_g=0.5 mm, respectively. Droplet production rates per unit length were 30 Hz/mm and 50 Hz/mm, for devices with L_g=0.75 mm and L_g=0.5 mm, respectively. Sharp drop in the system throughput for PGR>0.5 can be attributed to the increase of the average droplet volume with the Q_{max} for PGR>0.5 (see Figure 38C). Droplets produced from systems with PGR<0.5 were roughly 25 nL, while for PGR>0.5 the obtained droplets were roughly 50-100 nL, depending on L_g. To compare, MCE devices (PGR=0) and EDGE devices (PGR=1) yielded droplets up to 25 nL and 120 nL, respectively. They operated up to 50 μL/(min × mm) (MCE) and 13 μL/(min × mm) (EDGE). The frequencies of the droplet production were ~30 Hz/mm (MCE) and 4 Hz/mm (EDGE).

Decrease of sensitivity of the droplet volume to the variation of the flow rate for investigated devices is the greatest for grooved devices (PGR=0.2, Lg=0.5 mm, α=0.5;

PGR=0.28, Lg=0.75 mm, α=0.2 – shown in Figure 34). 75% increase of droplet volume (15.8±1 nL to 27.5±4 nL) was caused by the 260-fold increase of flowrate (from lowest tested Q=5 μL/min to highest Q yielding monodisperse droplets Q_{max}=1300 μL/min per device). In comparison, for MCE the increase in volume was 91% (12.9 ± 3 nL to 24.6 ± 5 nL) for 180-fold increase of flowrate (5 to 900 μL/min). Values of the dimensionless α parameter for MCE devices were α=0.8 and α=1, for MCE with DFUs spaced by 0.5 and 0.75 mm respectively. For EDGE the volume actually decreased by 12% (from 137.2±7 nL to 120.2±12 nL), but the dynamic range of the flow rate allowing production of monodisperse emulsion production was very low. The produced emulsion in EDGE geometry were monodisperse only in the flowrate range of 5 to 200 μL/min.

Range of obtained emulsion sizes and the throughput can be tuned by selecting proper geometrical parameters of step emulsficator. To select the emulsification system user should decide whether they prefer droplets of diameter roughly 3 times larger than DFU height (25 nL for H=100 μm) or 6 times larger than DFU height (>100 nL for H=100 μm). For smaller emulsion, both MCE and grooved emulsificators (e.g. PGR=0.2, Lg=0.5 mm) could be used. Grooved device outperforms MCE in terms of the operational flowrate (87 μL/(min × mm) for grooved, 50 μL/(min × mm)for MCE) and frequency of droplet production (50 Hz/mm for grooved, 30 Hz/mm for MCE). Production of large droplets (~100 nL for H=100 um) can be done by both EDGE and grooved emulsificators (PGR-0.3, Lg=0.75 mm). Grooved device outperforms EDGE in terms of the operational flowrate (53 μL/(min × mm) for grooved, 13 μL/(min × mm)for EDGE) and frequency of droplet production (30 Hz/mm for grooved, 4 Hz/mm for EDGE).

6.2.4. **Application of the presented step emulsificator for analytical assays**

Many assays are performed in solidified hydrogel droplets, beads, e.g. including cell culturing[205]. As a proof-of-concept of grooved step emulsficator I prepared agarose beads in grooved step emulsificator. Solution of low-melting agarose in water was dispersed in HFE-7500 oil with 2% PFPE-PEG-PFPE surfactant using grooved step emulsificator (PGR=0.28, Lg=0.75mm) at 150 μL/min. Then the chip was disconnected from the tubings and placed in -20^{0}C for one hour, to let the agarose solidify. The obtained hydrogel beads are presented in Figure 39. Two large and dark

103

objects visible in the inset of Figure 39 are air bubbles, all the other objects are hydrogel beads. Such stable hydrogel compartments could be further used to perform digital diagnostic assays.
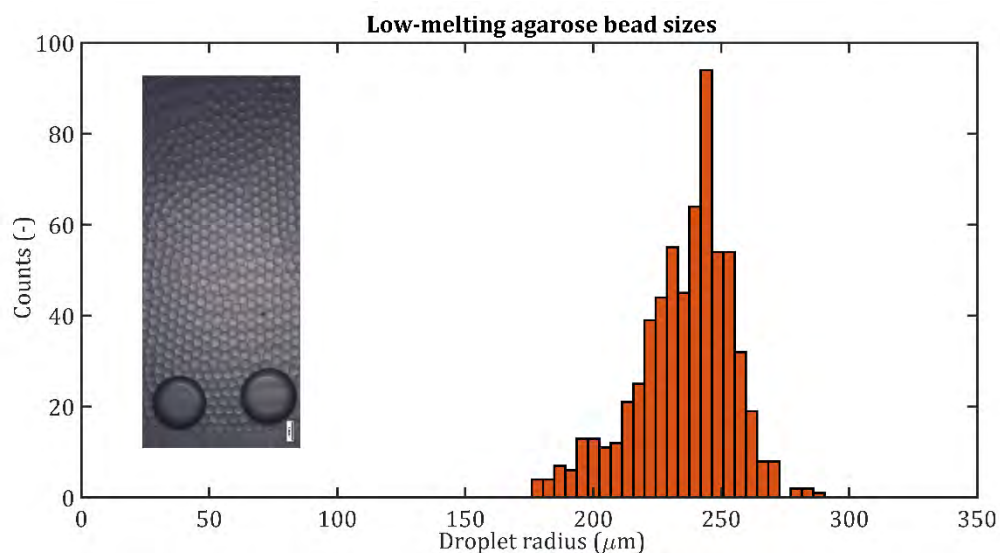
Figure 39 Low-melting agarose hydrogel beads produced in grooved step emulsificator - histogram of the bead sizes. Inset: view of the beads in the reservoir of the microfluidic device. In the bottom of the image two air bubbles are visible.

As mentioned, most analytical assays benefit from using single nanoliter-sized emulsions. In this chapter I presented a method to increase the throughput of the step emulsificator, using fast prototyping technique. Limited resolution of fabrication resulted in relatively large channels, and consequently droplets of tens to hundreds nanoliters. To produce smaller droplets, analytical assay-grade, the optimized grooved geometry should be scaled down and fabricated using method of higher resolution. Thus, manufacturing downscaled grooved system would require employing e.g. glass-etching, or 3D-printing. If the devices were to be upscaled in term of number of produced chips, injection molding is a rational choice. A common method to produce high resolution microfluidic chips, soft lithography, is not suitable to fabricate grooved and EDGE devices due to PDMS collapsing in the wide channels. This is why instead of fabricating the downscaled grooved devices I estimated the parameters of such device.

Droplet volume scales with cube of DFU height,,[145] thus to produce 1 nL droplets (reduce the volume 25 times) the approximate geometrical parameters of the grooved

104

step emulsificator would need to be downscaled $\sim \sqrt[3]{25} \approx 2.9$ times. The suggested dimensions are: h=10 μm, H=30 μm, w_g=40 μm, Lg=0.17 mm. Maximum injection of rate for such system was calculated to be 8 μL/min × mm. Calculation was performed assuming that the Q_{max}/w scales with height squared[145], which leads to:

$$\frac{Q_{max}}{w} = Q * \left(\frac{H_{after}}{H_{before}}\right)^2 = 87 * (\frac{30}{100})^2 = 8 \text{ μL/min} \times \text{mm}.$$

Single DFU width of the downscaled device would be is 0.174 mm (w_g+L_g), yielding 5.71 DFUs per mm. I estimate the throughput of 1 nL droplet production from downscaled grooved device to be around 80 μL/h per DFU.

I compared the theoretical downscaled step emulsificators to state of the art 'milipede' device[145]. It produces droplets at 150 mL/h in 550 DFUs, which is roughly 275 μL/h per single DFU. It is 3 times the rate per DFU in the theoretical grooved step emulsificator. However, the footprint of the grooved step emulsificator would be 3 times smaller than millipede nozzle (approximately 0.06 mm^2 and 0.2 mm^2, respectively). Thus, the two designs offer the similar throughput per surface area of the chip, since the DFUs in grooved system can be placed 3 times denser.

6.3. Discussion and conclusions

In this chapter I presented step emulsification devices with of novel geometry: with a number of grooves on an emulsifying slit, separated by the partitions. As a measure of the geometry I introduced Plateau-to-Groove Ratio defined as PGR=h/H. The devices in limits PGR=0 and PGR=1 are known as MCE and EDGE step emulsification devices, respectively. In the experiments, I fabricated and scanned multiple geometries interpolating between MCE and EDGE. I identified the moment of transition between MCE-like and EDGE-like modes of droplet formation. The transition includes change of the liquid-liquid interface shape, from sharp in-groove (for small h, to-be-dispersed phase is confined to the grooves) to spilt-groove mode (for h>H/2 droplet phase spills outs of the grooves).

A wide range of droplet sizes and operational flow rates are available when using grooved step emulsificators. To choose proper emulsificator one needs to identify the desired size and throughput of produced droplets and hard-wire them in the device geometry. Height of the emulsifying slit and presence and height of the partitions

determines the droplet size. The optimal geometry to produce small and monodisperse emulsions features PGR ~0.2-0.3 for grooves spaced by 4-6.25 times the width of a groove. Presented groove geometry appears to combine advantages of both MCE and EDGE, i.e. spatial localization of DFUs, high-throughput formation of tightly monodisperse droplets from parallel DFUs, and low sensitivity to variation in flow rate.

Grooved step emulsificator is a perfect tool for any application involving production of monodisperse emulsions or [9] The design of the system involves dimensionless parameters and is scalable. In principle, the grooved geometry could be scaled down to produce single nanoliter or even picoliter droplets. I expect theoretical grooved step emulsificator producing single nanoliter droplet to be on par to state of art devices[145]. However, as the grooved system does not require the cross-flow of the continuous phase to collect the produced emulsion it is easier to operate and consequently to integrate into larger analytical schemes. Variants of the grooved step emulsificator would be extremely useful for biological-assay studies, such as single molecule or single cell studies requiring ultra-high throughput of encapsulation and investigation, coupled with need for monodispersity and stability (e.g. single cell genome sequencing[185] or transcriptome profiling[5]).

7. **Passive microfluidic production of multiple emulsions**

In this chapter I present the third project carried out within my doctoral studies, regarding passive production of multiple emulsions in the step emulsificator. The results have not been published as of writing the dissertation.

7.1. **Introduction**

Double emulsions are droplets (called cores) engulfed in larger droplets (called shells) suspended in the outer phase. The most widespread composition of double emulsion is an aqueous core droplet surrounded by an oil shell that is suspended in a continuous aqueous phase (see Figure 40). Ideally, produced double emulsion has very low content of the middle phase - thin shell around the core phase – to increase the droplet stability against rupture (merging of the core droplet with the outer phase). The thinner the shell, the larger the hydrodynamic resistance impeding the flow of the core phase to the shell-outer phase interface. For thin shells the hydrodynamic resistance allows only minimal fluid flows and the core phase cannot reach the outer phase to merge with it and destroy multiple emulsion[160,161]. Double emulsion droplets found use in industrial applications[11,160,206,207], but are also used for analytical assays requiring sorting emulsions by flow cytometry[79,128,208], for preparation of templates for capsules and vesicles[209,210] and in controlled drug-delivery applications[211].
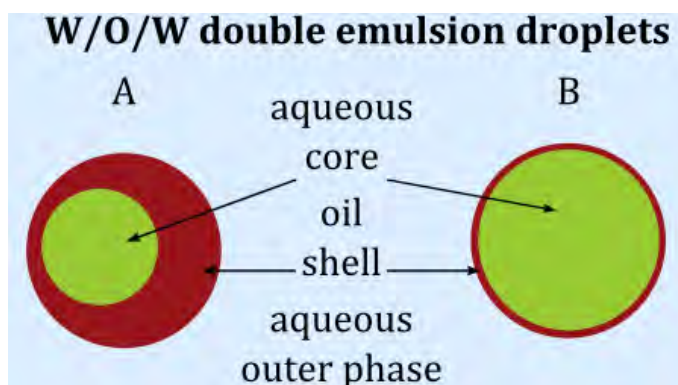
Figure 40 Schematic representation of double emulsion droplets with aqueous core, oil shell, and aqueous outer phase. A. Double emulsion with thick shell in which core can freely move. B. Thin-shelled DE in which core movement is impeded.

7.1.1. **Problem statement**

Microfluidic methods allow production of multiple droplets, with the control over their inner structure, such as the number, type and also arrangement of the core droplets[38,173,174]. Just like with single emulsion droplets, the double emulsions can be produced passively and actively. Generation of double emulsions in microfluidic devices was demonstrated with the use of active methods in various

geometries[157,162,212–214]. Passive microfluidic droplet methods for DE formation have been described only recently, and they are still very challenging[171,172]. However, passive DE production schemes are attractive as they can yield thin-shelled double emulsions without the need for actuation of the outer phase[171,172].

Only very recently Ofner et al[169] investigated possibility to generate double emulsion by the use of two step emulsification devices. In this method, depicted in Figure 12 on p.52, called tandem step emulsification two microfluidic devices are connected by a tube: the first, a fluorophilic device for production of the feed W/O emulsion, and second, hydrophilic, for transforming W/O into W/O/W double emulsions. Such passively produced DE contain pre-defined number of cores, which depends on the ratio of flow rates of the core and shell phases in the first device. Shell thickness of those DE can be tuned by adjusting the size of the droplets fed to the second device.

If in the first device there is no flow of the core phase, only oil phase is fed as the to-be-dispersed phase to the hydrophilic device, yielding O/W emulsion from the tandem step emulsification system. Size of that O/W emulsion is stable for the flow conditions, as the process of droplet formation is geometry-controlled, and can be considered nominal droplet size for emulsification of given fluids under specified flow conditions. The thinnest-shelled double emulsion were produced in hydrophilic device when supplied core droplets were larger than nominal O/W emulsions. The reason for that was that the large core droplet split into smaller droplets during the emulsification at the step of the hydrophilic device, each of the newly formed cores filling subsequent double emulsion droplets.

The publication by Ofner et al[169] demonstrated how to form double emulsions and concentrated on their further use. I am interested in the process of double emulsion formation on a step – why the large core droplets split at the step during emulsification of the single emulsion into DE. Since process of double emulsion production on the step is not yet fully understood, I researched the process to find the range of parameters of the core phase that promotes the slipping of the whole core droplet into the DE droplet. A natural choice of a parameter to test was viscosity, the crucial parameter of fluids in the microfluidic systems.

In this chapter I present my research on the influence of the viscosity of the core droplet on the formed double emulsions. I aimed to test if it is possible to squeeze large core droplets of varying viscosity into double emulsions without the cores splitting into smaller droplets.

7.1.2. **Materials and methods**

Microfluidic chips were fabricated in PDMS, as described in sections 4.2.2 PDMS chip fabrication. Channels were rendered hydrophilic with PVA or fluorophilic with Novec 1720 as described in section 4.2.3 Microchannel surface modification.

Innermost and outermost phases of double emulsions consisted of aqueous PVA solution, 2-10%wt. Middle (shell) phase of the double emulsions consisted of fluorinated oil, either HFE 7500 or FC-40 with 2% wt. triblock surfactant PFPE-PEG-PFPE. Fluid viscosities are presented in Table 5. I described fluid handling and imaging in the system as described in sections 4.2.4 Fluid handling and 4.2.5 Data acquisition. I processed the data as described in section 4.2.6 Data processing and analysis, using custom written scripts to automate the processing.

Table 5 Viscosities of used fluids.

Fluid	Phase	Viscosity [mPa*s= cP]
HFE-7500, 2%wt. surf.	Oil	1.3[32]
FC-40, 2%wt. surf.	Oil	4.2[215]
PVA 2%wt.	Aqueous	2.0
PVA 10%wt.	Aqueous	23.2

7.2. Results

7.2.1. Workflow of double emulsion production

I prepared double emulsions in two-step process, using two connected microfluidics devices (workflow shown in Figure 41). In the first device I produced W/O emulsion that was fed to the second device that transformed emulsion into W/O/W double emulsion.
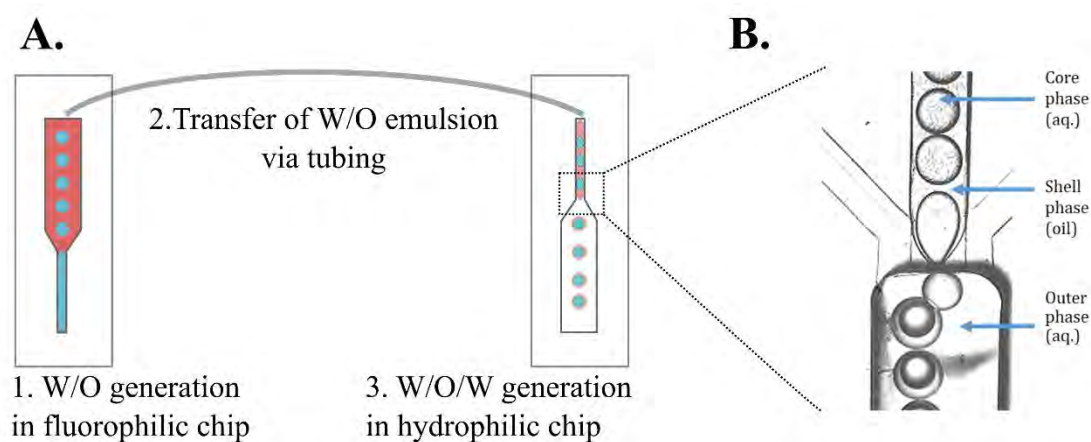
*Figure 41 **A.** Workflow of the double emulsion generation. **B.** View of operational hydrophilic step emulsificator. Emulsion is fed by the channel in the top middle (an aqueous core in oil thread is visible) to the step (expansion of the channel with visible dark edge). After the step there is a deep reservoir filled with outer phase, which can be supplied by side channels.*

The first device was fluorophilic flow-focusing emulsificator, which produced single W/O emulsions. I used active system to produce droplets of wide range of sizes in the same device (see Figure 42).
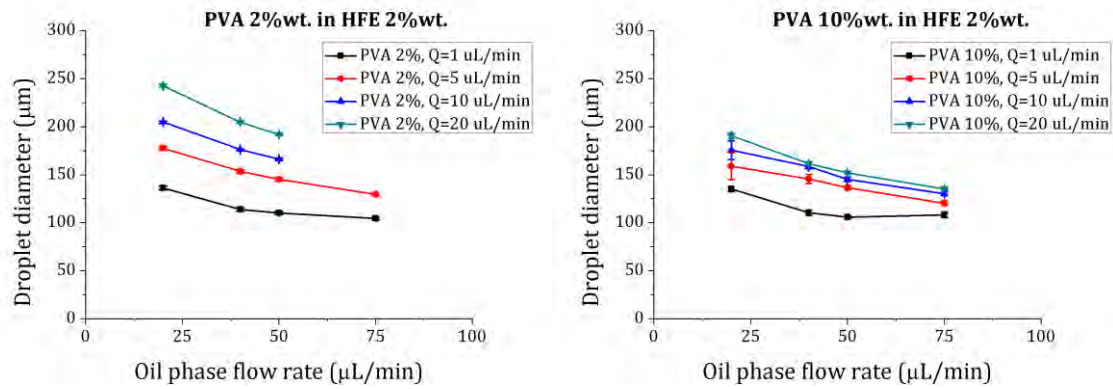
*Figure 42 Examples of water in oil droplets produced in the flow-focusing device. **Left**: PVA 2%wt. in HFE7500 with 2%wt. surfactant. **Right**: PVA 10%wt. in HFE7500 with 2%wt. surfactant.*

I transferred produced W/O emulsion (feed) directly from chip to chip by inert tubing. I prefilled the second microfluidic device, a hydrophilic step emulsificator, with the aqueous outer phase (see Figure 43). There, the single emulsion passively split into double emulsion.
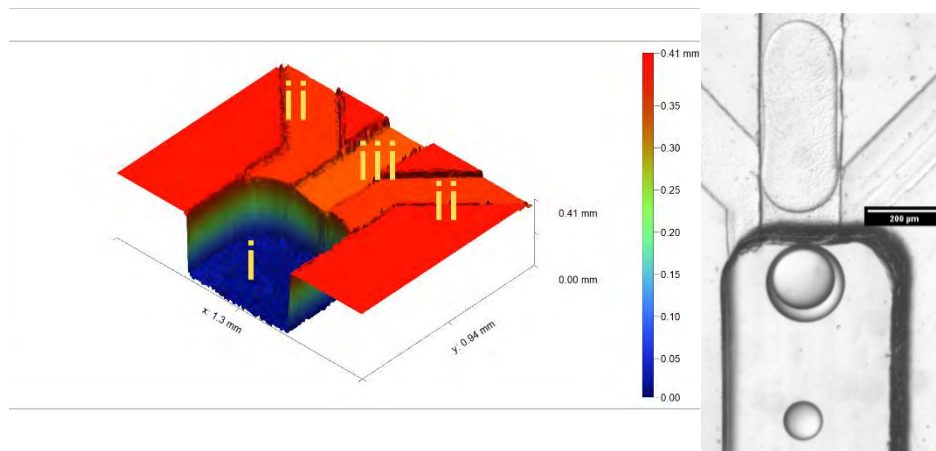
Figure 43 Left: 3D scan of the device used for DE production. i – reservoir, ii – side channels, iii – supply channel. Right: Microphotograph of the emulsification of W/O emulsion into W/O/W double emulsion in the hydrophilic step emulsificator. At the top, in the feeding channel there is a large aqueous plug, carried by the oil phase. In the middle of the image there is a double emulsion, seen just after generation via the step emulsification. At the bottom of the image there is an empty O/W droplet which was generated as the oil phase not carrying aqueous droplet flew over the step.

7.2.2. Geometry of step emulsificator for double emulsion production

Microfluidic device for DE production comprised three main elements, marked in Figure 43: i) large channel (reservoir) prefilled with the outer phase, ii) shallow side channels to prefill the reservoir with outer phase, iii) rectangular main channel supplying to-be-dispersed phase to the reservoir. The main channel was 220 μm wide and 45 μm deep. Side channels served as bypasses that allowed continuous phase to access the neck of the thinning thread during step emulsification process[133]. The side channels (300 μm wide, 20 μm deep) were used to supply the continuous phase prior to the experiments, no flow was induced during the experiments. To prevent the to-be-dispersed phase from entering the side channels their height was kept below half of the main channel height, like in the grooved step emulsificator from Chapter 6. Chip was operated with the junction in horizontal position, to transport the formed emulsion away from the step by means of buoyancy[20,201].

As I have shown in previous chapters, tailored geometry of the step emulsificator stabilizes the droplet size against the flow rate variations. The same principles apply when forming multiple emulsions in the step emulsificator, which is why I designed step emulsificator with side channels acting as bypasses. I compared bypassed geometry with a standard one, without side channels acting as bypasses (see Figure 44). I did not fabricate device with constriction upstream of the step (as presented in Chapter 4), because constriction would introduce additional curvatures of the fluid-fluid interfaces. Presence of the constriction could lock the core droplet in position while shell phase would flow freely to the reservoir (trapping mechanism[122]). The investigated three-phase system was already complex and introduction of additional factors would introduce yet another complexity to the study of the process of double emulsion production.
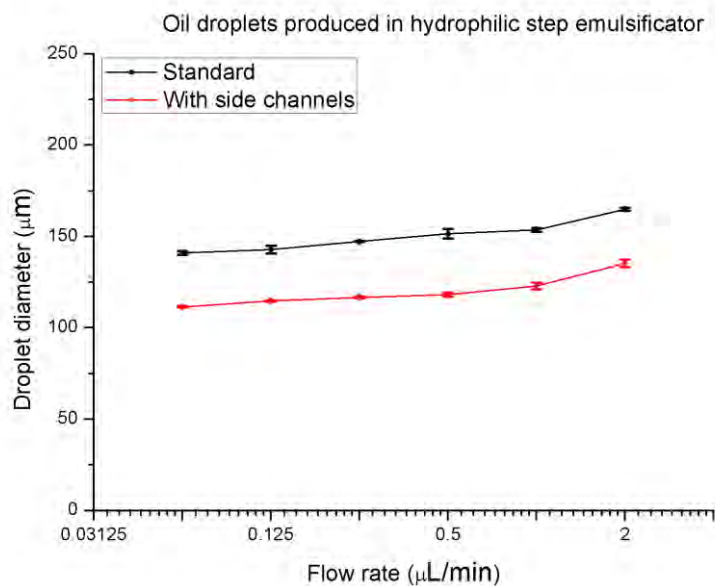
Figure 44 Sizes of droplet produced in hydrophilic chips of different geometries. Dispersed phase is HFE with 2%wt. surfactant, continuous phase is PVA 2%wt.

Both types of devices produced monodisperse emulsions in the range of rates of flow of 0-2 μL/minute. Droplets from the bypassed geometry (with side channels) were smaller than from the standard geometry for each investigated flow rate. I calculated parameter α of the investigated systems using Equation 11 (p. 75) and the values are α=0.56 and α=0.68 for bypassed and standard geometry, respectively. Smaller droplets and higher stability of the droplet sizes to the variations of the flow rate made me decide use devices with side channels acting as bypasses in my experiments.

Operating step emulsificator in the dripping droplet formation mode is beneficial, as generated droplet size is well-defined. I experimentally investigated what is a value of flow rate of the to-be-dispersed phase that would result in dripping droplet generation for all of the pairs of fluids, Q_{drip} (see Figure 45). I measured sizes of droplets formed using our step emulsification system and established nominal droplet size, d_n, for Q_{drip}. Step emulsification of single W/O emulsion to W/O/W double emulsion involves both W/O and O/W emulsions I conducted the experiment for both W/O and O/W systems. Aqueous sample was injected to oil-filled fluorophilic device to obtain W/O emulsion, and oil was supplied to water-filled hydrophilic device of the same geometry to obtain O/W emulsion. To-be-dispersed phase was

114

injected at varying flow rates and the size of the droplets was measured (see Figure 45).
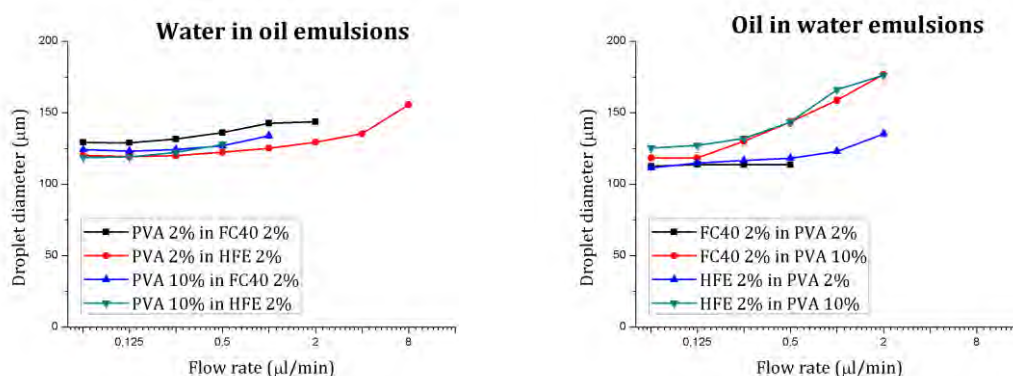
*Figure 45 Single emulsion formation in used devices. **Left**: Size of droplets generated in fluorophilic device (W/O emulsions) as a function of the applied flow rate. **Right**: Size of droplets generated in hydrophilic device (O/W emulsions) as a function of the applied flow rate.*

I established that Q_{drip}=0.5 µL/min is a flowrate that can be used to provide dripping conditions for used W/O and O/W systems (see Figure 45). For such conditions the nominal droplet diameters, d_n are presented in Table 6.

Table 6 Nominal droplet sizes for investigated systems.

Droplet phase	Outer phase	d_n (µm)	SD (µm)
PVA 2%	HFE 7500 2%	122.4	0.5
PVA 2%	FC 40 2%	136.1	0.6
PVA 10%	HFE 7500 2%	127.9	1.0
PVA 10%	FC 40 2%	126.8	0.7
HFE 7500 2%	PVA 2%	118.2	1.0
HFE 7500 2%	PVA 10%	143.4	3.1
FC 40 2%	PVA 2%	113.6	0.6
FC 40 2%	PVA 10%	143.4	2.6

In step emulsification, when the droplet passes over the step there is a pressure difference between the front and tail of the emulsified plugs. For infinitely long droplets (i.e. threads) the curvature of the rear of the droplet is constant, yielding

115

constant tail-pressure, which leads to repeatable droplet formation. In droplets of finite length the curvature of the tail of the plug decreases, increasing tail-Laplace pressure and influencing droplet formation process. I investigated whether W/O droplets could pass over the step without breaking. I established what is the maximum size of the aqueous core in fluorinated oil that can pass over the step without splitting into smaller droplets.

I produced droplets of aqueous PVA solutions of 2%wt. and 10%wt. in HFE 7500 with 2%wt. surfactant, droplet size ranging from 110 to 180 µm. Then I injected the W/O emulsions at Q_{drip} into fluorophilically modified step emulsificator filled with the same oil. Droplet sizes were recorded before and after passing the step (see Figure 46). Nominal droplet sizes, established for the droplets formed from continuous threads of fluids, were $d_{nPVA2\%}$=122 µm for PVA 2% and $d_{nPVA10\%}$=128 µm for PVA 10%wt (see Table 6).
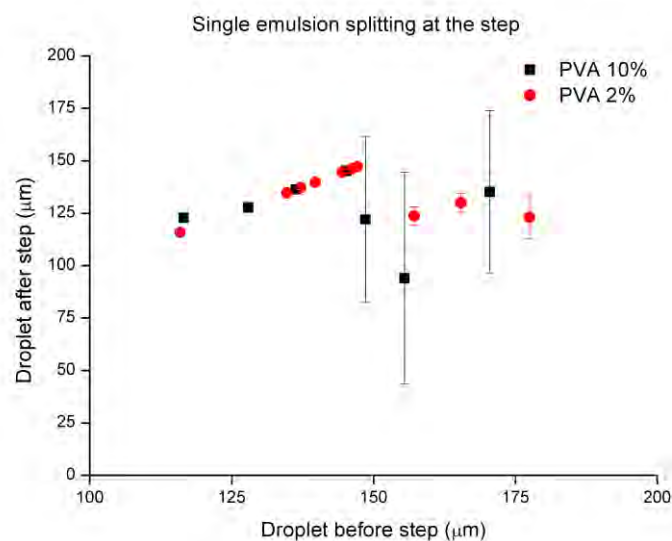
Figure 46 O/W emulsions measured before and after passing the step of fluorophilic step emulsificator.

I observed that the sizes for which W/O droplets started breaking at the step correspond to sharp increase of the standard deviation of the droplet diameter. W/O emulsions split in smaller droplets for around 127% of $d_{nPVA2\%}$ and 115% of $d_{nPVA10\%}$. Worth emphasizing is the fact that the split PVA 2%wt. droplets were still monodisperse until around 145% of $d_{nPVA2\%}$. The results suggest that in step emulsification of emulsions into double emulsions cores larger than ~1.3 d_n should

split into smaller droplets. However, the test was performed in the two-phase environment, without the outer phase. With the third phase present the mechanism of droplet formation could change due to necking of two phases, shell and core, at once.

7.2.3. Core droplet viscosity influence on the passive double emulsion production

Using tandem emulsification system presented in previous section I investigated the influence of the viscosity of the core droplet on the size of the formed double emulsions. First, I produced monodisperse single emulsions (using high flowrates, as presented in Figure 42) and stored them in the tubing connecting fluorophilic and hydrophilic device. After flushing the hydrophilic device with outer phase, the single emulsion was fed to the step emulsificator at Q_{drip}=0.5 µL/min. The process of feed production and subsequent DE production was repeated for multiple sizes of the cores. Two kinds of cores were used, PVA 2%wt. and PVA 10%wt. Shell phase was one of two commonly used fluorinated oils (HFE7500 µ=1.3 mPa*s, FC-40 µ=4.2 mPa*s), and the outer phase was PVA 2%wt.

I observed that core droplets exhibited two behaviors during emulsification into double emulsions: either they split into multiple subsequent smaller droplets (see Figure 47, right) or they slipped whole into DE (see Figure 47, left). In systems with cores of small viscosity (PVA 2%wt) I observed splitting of the core droplets into multiple double emulsion droplets (even for d_{core}<d_{oil}). Droplets that slipped full were made of more viscous PVA 10%wt for both investigated oils and all investigated core sizes.
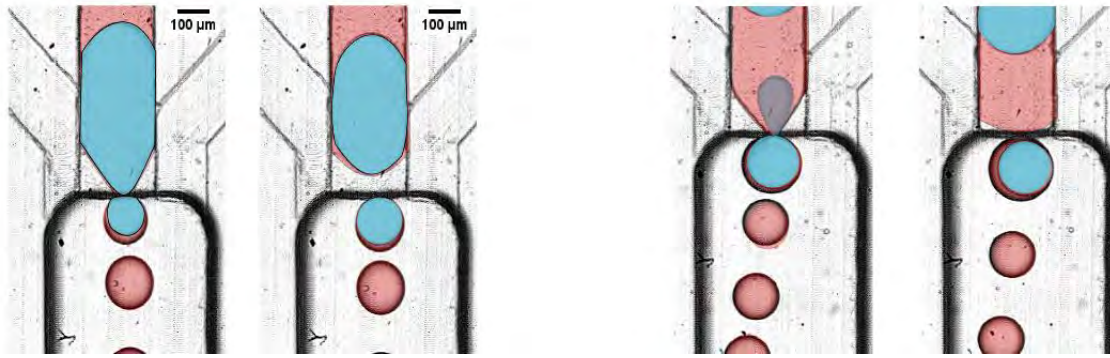
Figure 47 Snapshots from the step emulsification experiments. Two observed behaviors of the core droplets (blue) during DE production on a step. Either the core droplet split into multiple droplets (two panels in the left), or slipped whole to the DE (two panels in the right). Core droplets in the left are made of PVA 2%wt., core droplets in the right are made of PVA 10%wt. Oil was colored red for clarity. Outer phase was transparent.

Three sizes of emulsions were used as the feed phase. In them aqueous cores were either smaller than nominal droplet size (100 μm), similar to the nominal droplet size (120 μm) and larger than the droplet size (150 μm). The resulting double droplet sizes are presented in Figure 48.
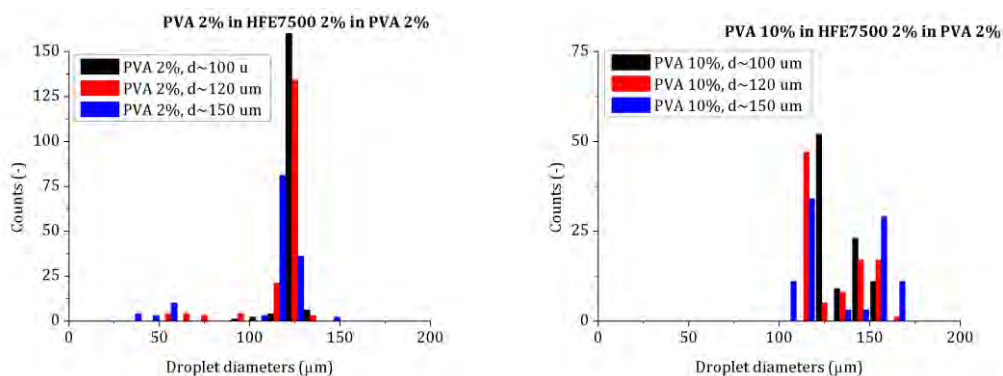
*Figure 48 Histograms of sizes of DE produced using step emulsificator. **Top**: recorded droplet sizes after emulsification of PVA 2%wt. core droplets of varying sizes (diameters 100-150 um) suspended in HFE 7500 2% and dispersed in PVA 2%wt **Bottom**: recorded droplet sizes after emulsification of PVA 10%wt. core droplets of varying sizes (diameters 100-150 um) suspended in HFE 7500 2% and dispersed in PVA 2%wt.*

For double droplets containing PVA 2%wt. cores the sizes of the DE were roughly the nominal droplet size of 122 µm for every investigated core size. Smaller droplets (<100 µm) were a result of DE rupture – core phase merged with the outer phase, and the oil shell formed single emulsion smaller than nominal droplet size. Shell thickness of DE was not measured, but it was observed to vary a lot.

Double droplets containing 10%wt. PVA were significantly larger than the respective nominal droplets of 128 µm for every investigated core size. This is a result of the cores not splitting, but slipping as a whole into the forming double emulsions. Droplets smaller than the nominal droplet size were single O/W emulsions, formed from the oil between subsequent core droplets. Shell thickness of DE was not measured, however, it seemed to be fairly thin.

To investigate the shell thickness of double emulsions with PVA 10%wt. as core phase I produced single emulsions comprising wide range of sizes of the PVA 10%wt. cores and emulsified them in the hydrophilic step emulsificator into DE. I measured the formed DE droplets core diameter, shell thickness and total DE diameter, and presented them in Figure 49 and Figure 50 for HFE 7500 and FC40 as shell phases, respectively. Each core size (blue triangles in the plots) was normalized by division over the nominal droplet size for each system, i.e. if the core size was 118.2 µm and the nominal droplet size was 118.2 µm, the relative core size was 118.2/118.2=1.

W/O emulsion with cores comprising viscous solution of PVA 10%wt. in both fluorinated oils slipped into the double emulsion for whole investigated range of core sizes. DE size rises slightly with the increase of the core size, and shell thickness decreases down to the stable level of 40±5 µm (21±2% of DE diameter) for HFE7500 and 46±9 µm for FC-40 (23±4% of DE diameter). Averaged shell thickness values were measured for DE comprising cores larger than nominal droplet size.

Figure 49 Slipping behavior of PVA 10%wt. core droplets in HFE-7500 with 2%wt. surfactant emulsified in PVA 2%wt. Black squares denote the total DE droplet size, blue triangles denote the relative core size and red circles represent the shell thickness.

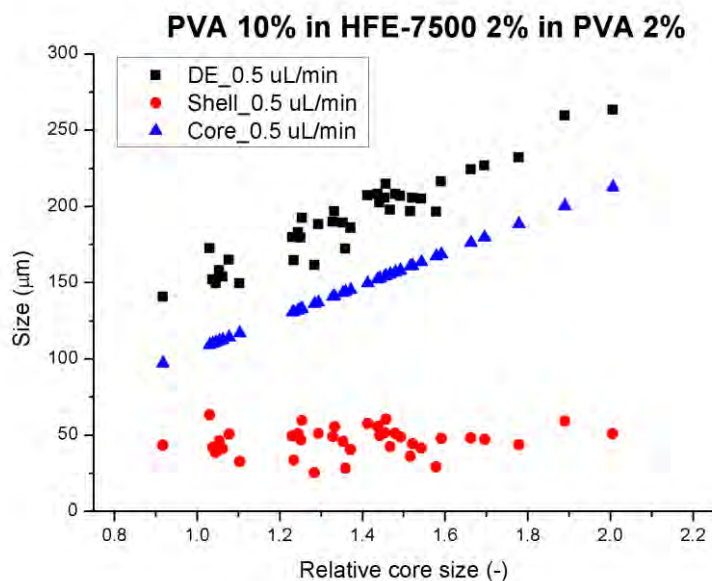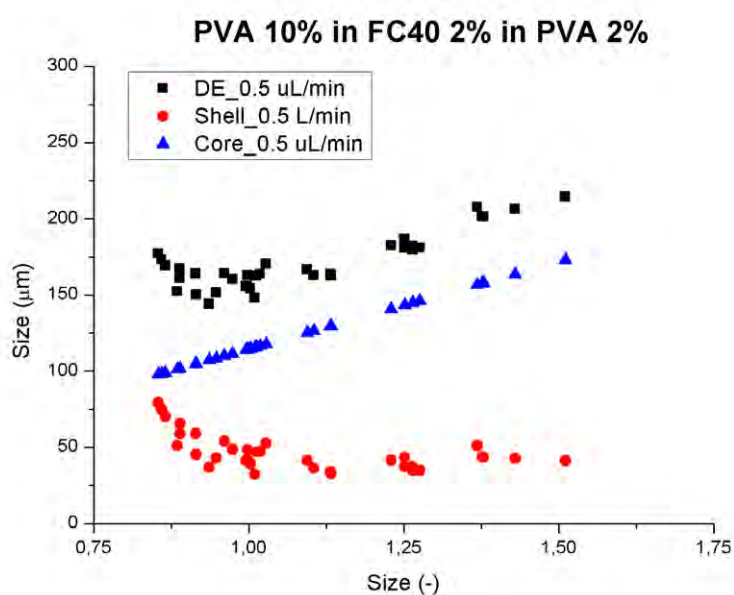*Figure 50 Slipping behavior of PVA 10%wt. core droplets in FC40 with 2%wt. surfactant emulsified in PVA 2%wt. Black squares denote the total DE droplet size, blue triangles denote the relative core size and red circles represent the shell thickness.*

7.3. Discusssion and conclusions

In this chapter I presented passive production of thin-shelled double emulsions. I designed and fabricated microfluidic devices that allowed formation double emulsions on a step. Since the increase of the viscosity of outer phase causes formation of significantly larger droplets than for less viscous phases, I fixed the outer phase in all experiments to be PVA 2%wt., μ=0.002 Pa*s. For single emulsions formed in step emulsificators the droplet size depends weakly on the viscosity of the to-be-dispersed phase (see Figure 21, page 79). The relationship holds also for double emulsion formation if shell phase is considered as the phase being dispersed. I showed this using as shell phase two oils, differing in viscosity - FC40 viscosity is 3 times the viscosity of HFE-7500. As presented in Figure 49 and Figure 50 the produced DE were of similar size for the same flowrate, core size and composition, and outer phase composition, despite oil change.

There was, however, difference in the process of droplet formation and sizes of produced DE if the viscosity of the core was changed. The core viscosity appears to control whether the core splits into multiple smaller droplets on the step during double emulsion formation process. Using highly viscous cores allowed formation of thin-shelled double emulsions in a passive manner. This is in line with previous findings from studies on double emulsion formation in active systems that the core should be viscous in order to fit into double emulsion[216,217].

I presented schematically how the fluids move in the three-phase system during emulsification of W/O emulsion into W/O/W emulsion at the step of the hydrophilic device, see Figure 51. Outer phase invading the necking area comes from both the shallow side channels and big reservoir. Outer phase wets the walls of the microchannel and can freely move through the side channels to get to the necking area. Shell phase does not wet the walls of the microchannels and is confined to the feed channel until it ends in the reservoir. Thus, oil phase and confined within core droplet can only move towards the reservoir, pushed by the syringe pump induced flow and Laplace pressure difference. During necking, the shell phase moves toward the growing head of the thread, thinning the shell-outer phase interface. The core droplet is getting squeezed by the constricting shell-outer phase interface and can yield to that force (i.e. splitting in the necking area). In case the viscous resistance

121

is large enough, the core droplet can withstand the force exerted by the thinning interface until the whole droplet passes through the necking region. In my investigation the sufficient viscosity to withstand splitting was over 20 mPa*s. However, establishing exact value of the core viscosity to provide slipping core conditions requires further studies.
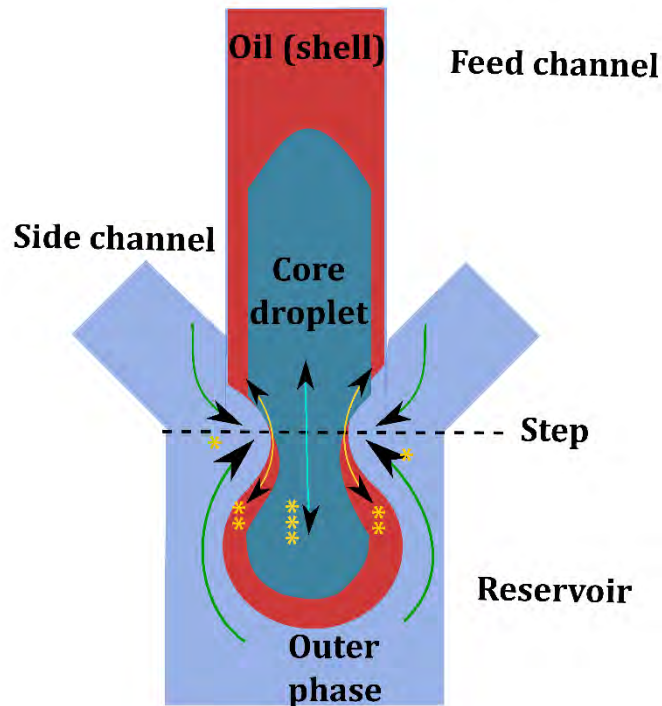
Figure 51 Representation of the liquid movements during emulsification of a single W/O emulsion into W/O/W using the hydrophilic step emulsificator. Green arrows with a single asterisk (*) indicate movement of the outer phase, yellow arrows denoted with two asterisks (**) denote movement of the shell phase, and bright blue arrow with three asterisks (***) denotes movement of the core phase.

Thickness of produces DE was around 20% of double emulsion diameter, more than in actively produced DE[115,161] or DE made in systems where very large core splits into subsequent double emulsions[172]. My solution, however, guarantees that the core content of double emulsion comes from a single core droplets. Such property minimizes the risk of cross-contamination when carrying out biological assays (e.g. core droplets contain single cells and are encapsulated into DE for sorting in directed evolution experiment[128]).

8. Summary, conclusions and perspectives

In this chapter I present the summary of the projects carried out within my doctoral dissertation. I also provide my insight into the future of the passive droplet microfluidic system in use for analytical assays.

8.1.   Research overview

Analytical assays, especially digital ones such as ddPCR, benefit from utilizing droplets as microreactors. Using droplets instead of traditional microwell plates leads to increasing the applicability and dynamic ranges of the assays, at the same reducing the cost (see Table 1, page 19). Passive emulsification is a group of methods in which the droplet formation process is governed mainly by the geometry of the droplet forming unit, not the flow actuation[100].

In order to provide monodisperse emulsions for the analytical assays, I optimized passive step emulsificators. My research objectives were:

i)   To decouple the droplet size from the flow rate,

ii)   To increase the throughput of the passive step emulsificator,

iii)   To investigate the mechanism of the mechanism of passive formation of double emulsions.

Each problem was researched as a stand-alone project. As a result, I presented the modified geometry of step emulsification junction that produced droplets of defined volume despite varying flow rate of to-be-dispersed phase (see chapter 5 Decoupling droplet volume from flow rate in step emulsificator). Using the findings from this project I designed another system that upscaled the number of droplet forming units, and characterized the mechanism of droplet formation within that system (see chapter 6 Increasing throughput of step emulsificator). Then, further exploring the step emulsificator with non-standard geometry I produced double emulsions in a passive manner. I designed a system for passive double emulsion production that enabled investigation of the mechanism of DE production and influence of the viscosity of the core droplet on the DE composition (see Chapter 7 Passive microfluidic production of multiple emulsions).

8.1.1.   Stabilizing droplet volume against varying flow rate

In the first part of results of my dissertation I focused on the dependence of droplet size on the flow rate of the to-be-dispersed phase. Breaking off a droplet in passive step emulsification systems is caused by the Laplace pressure that collapses the neck of the to-be-dispersed phase stream. Laplace pressure change is induced by changing the geometry of the step emulsification system, usually realized with a step – an

abrupt change of the height (or depth) of the channel. The thread of to-be-dispersed phase reaches the step and starts growing, due to release of spatial confinement. Growth of the head of the thread draws even more liquid from the bulk of the thread due to the Laplace pressure difference. The region of the thread from which the liquid is drawn is thinning, and is called a neck. Necking time is the time the thinning of the interface takes, before the thread is ruptured by the Rayleigh-Plateau instability. The necking time depends on the value of interfacial tension and on the rates of flow of the two immiscible liquids. The droplet liquid needs to be evacuated from the neck, while the continuous liquid needs to be supplied to the space immediately surrounding the collapsing neck. Thus the rate of collapse depends on the viscosities of the two liquids and on the geometry of the junction. In standard step emulsification junction the outer phase must compete with the flowing out to-be-dispersed phase. The hypothesis of presented work was that modification of chip geometry would enable outer phase easy access to the neck of the to-be-dispersed phase and decouple the necking time from the time it takes outer phase to invade the microchannel.

To test this hypothesis, together with coworkers I modified the geometry of the standard step emulsificator. I introduced new types of step nozzles, comprising constrictions and bypasses upstream of the step. Constriction allows spatial localization of the neck of the thread and facilitates droplet formation. The bypasses allow outer phase easy, continuous access to the necking area. Modification of nozzle geometry with those elements allowed production of monodisperse nanoliter emulsions in a wide range of volumetric flow rates. Moreover, I showed that the device can be operated using single source of flow. The electronic pipette was a sufficient tool to perform emulsification of microliter sample into the monodisperse library of nanoliter-sized droplets. Complete set of fluids needed for emulsification can be injected a sequence of plugs in one pipetting step. The composition of the to-be-dispersed phase did not influence the emulsification results, even if the sample had viscosity 10 times higher than the viscosity that of the pure water.

8.1.2. **High throughput passive droplet production**

In the second part of my dissertation I focused on the issue of the throughput of the step emulsificators. Passive droplet production schemes yield tightly monodisperse emulsions, but often at a price of reduced throughput, when compared to active methods. The common solution to this problem is to increase the number of the droplet forming units (DFUs) in the passive microfluidic device. Techniques utilizing this approach, namely MCE and EDGE, offer high throughput emulsion production. However, MCE and EDGE differ in mode of production – MCE produces more uniform droplet populations than EDGE, but at lower throughput. Since the MCE and EDGE nozzle architectures differ I assumed that the reason for the distinction lies in the geometry of the step. My hypothesis was that an intermediate geometry between MCE and EDGE should combine their advantages such as high throughput and monodispersity of the produced emulsions.

To test this hypothesis, I designed, fabricated and tested microfluidic devices that created continuum of geometries, ranging from MCE to EDGE devices. Introducing partitions of different heights to a wide step emulsification junction allowed screening of geometries, and identification of the geometrical variants yielding the highest throughput. The intermediate geometries, named grooved step emulsifiers, yielded monodisperse emulsions at higher throughput then state of the art architectures. Grooved step emulsifiers also stabilized the droplet size to the flow rate changes. To compare the grooved geometry with MCE: the volume of the produced droplets increased by just 75% for 260-fold increase of the flow rate in the grooved step emulsifier, as compared to 91% increase in volume over a 180-fold increase of flow rate of to-be-dispersed phase in MCE.

I characterized the grooved step emulsifier using dimensionless quantities, which allows scaling of the geometry. The transition between two distinct droplet generation modes, EDGE and MCE, is a function of the geometrical parameters of the nozzle, namely height of partitions between DFUs in relation to the nozzle height (PGR, partition-to-groove ratio). I showed that size and monodispersity of the produced emulsion can be tuned by changing the PGR value of the device.

The optimized grooved geometry combines advantages of both MCE and EDGE, i.e. spatial localization of droplet forming units (DFUs), high-throughput formation of tightly monodisperse droplets from parallel DFUs, and low sensitivity to variation in the flow rate of the dispersed phase. Moreover, grooved devices show lower dependence on the flow rate than the compared MCE and EDGE geometries. Grooved geometries allows fine tuning of the interplay between emulsion monodispersity, size, and device throughput on the level of device fabrication.

8.1.3. **Passive production of double emulsions**

In the third part of my dissertation I focused on producing double emulsions in step emulsificator. I investigated whether core composition influences the mechanism of droplet formation and the shell thickness of the produced DE. My hypothesis was that viscous core present in the necking area could withstand the closing of the interface during the necking process and slip into DE without splitting.

In order to verify my hypothesis I designed the tandem emulsification system comprising two microfluidic devices connected with tubing. First device, rendered fluorophilic, produced single W/O emulsion that was fed to the second, hydrophilic device. I characterized both devices for used liquids that were solutions of PVA 2%wt. and 10%wt., and two fluorinated oils of different viscosity (HFE7500 and FC40).

Having characterized the devices, their operational flowrates and produced single emulsions I prepared a number of double emulsions of varying composition. I observed that core droplets composed of PVA 2%wt. (μ=2 mPa*s) tended to split if W/O was emulsified into W/O/W at the step. Core droplets made of PVA 10%wt. (μ=23 mPa*s) did not split during the emulsification of W/O into W/O/W, slipping whole into the newly-formed double emulsion.

Double emulsions containing PVA 2%wt. cores due to the splitting tended to be the size of the nominal droplet size for the device (i.e. a size of empty O/W droplet for given flow conditions). DE shell thickness varied significantly between subsequent droplets. Double emulsions produced with large and viscous cores of PVA 10%wt. due to their resistance to splitting were larger than the nominal droplet size for the device (i.e. a size of empty O/W droplet for given flow conditions). Shell size for the cores

larger than nominal droplet size was quite stable, and constituted around 20-25% of double emulsion diameter.

Reason of the different behaviors of the cores, namely splitting or slipping, lies in the viscous resistance to deformation of the core droplet. Highly viscous core droplet of PVA 10%wt. could withstand the force exerted by the thinning shell-outer phase interface and slipped into the double emulsion. I expect that even highly viscous cores would eventually split if the sufficient force was applied for long enough. One way to increase the time of squeezing the core would be to use very viscous outer phase, which would greatly increase the necking time of the fed W/O emulsion. Further studies are required to confirm that claim.

8.2. **Perspectives and future applications**

Droplet microfluidic systems are currently widespread in laboratory research, mainly in biochemistry and molecular biology assays[218,219]. The range of the performed assays is very vast and is used to investigate many different chemical and biological processes. Droplet-based assays can be applied to almost any biomedical and diagnostic application, starting from investigation of the protein crystallization[220], through nucleic acid amplification[177], bacteria enumeration[221], to transcriptome profiling (mRNA-seq[5]) and genome profiling (ChIP-seq[222])of large populations of cells. Some assays, such as directed evolution of bacteria, may require more restrictions on the sample partitioning, which can be realized by encapsulating single emulsions in droplets – i.e. making double emulsions[128].

Most of the aforementioned assays utilize active droplet generation schemes. They offer high throughput and satisfying monodispersity of the produced emulsion. However, they use excess of the continuous phase and require great degree of actuation. Those nuisances can be overcome by using alternative way of droplet generation – passive emulsification. Produced emulsion can be very dense (dispersed phase can constitute up to 97% of emulsion volume[187]), and can be operated using common laboratory equipment, such as centrifuges[71,78,100,223] or pipettes[224,225].

The focus of my dissertation was on exploiting interfacial phenomena to produce monodisperse single and double emulsions. I researched the physics of the droplet generation in step emulsificators, which complemented the state of the knowledge on

128

passive droplet formation. Due to ease of operation and robustness of monodisperse droplet production I expect that passive step emulsificators of my or similar design will be incorporated into bioanalytical schemes.

In my opinion the most exciting is the perspective of integration of the passive microfluidic devices into disposable, pipette-attached cartridges. First prototypes are being described in the literature, however they are not passive systems – they require battery-powered electromagnetic actuation to break the sample into droplets[226]. I can imagine an engineered pipette tip, with the nozzle shaped into a passive step emulsificator. Operation of such device would boil down to three steps – filling the container (e.g. a disposable vial) with continuous phase, filling the pipette tip with the sample, and manual injection of the sample into the continuous phase-containing container. Passive emulsification should yield monodisperse library of droplets within seconds, with no dead volume and expensive equipment. Solutions on how to decouple droplet size from the flow rate of the sample shown in this dissertation could greatly improve the design process.

Performing the assay in droplets is often the least effort-demanding part of the procedure. Readout of the assay can take a lot of time relatively to droplet generation, e.g. droplet sorters can read and sort up to 30 000 droplets per second[227,228]. Sorting the library containing 10^7 cells/enzymes would take at least half an hour[229], and larger libraries could take hours to process. An interesting alternative is to use passive methods. Recently Schmitt and coworkers proposed passive ultra-high throughput sorting based on density difference between the bacteria-laden hydrogel microbeads[77]. The investigated bacteria were encapsulated in the sodium alginate beads and sunk to the bottom of reservoir filled with paraffin. If the bacteria could synthesize gaseous product from the supplied substrates, the resulting increasing buoyancy caused the droplets to float to the surface of the container. Operation was highly parallel and allowed to analyze in one minute 10 million nanoliter reactors and separate gas-producers from non-producers. One can easily imagine coupling high-throughput step emulsifier presented in my dissertation with the passive sorting of the produced droplet populations. After the integration of the systems one could obtain a fully passive system for screening large libraries of biological agents in short time.

III. Literature

1   P. Sykes, S. Neoh, M. Brisco, E. Hughes, J. Condon and A. A. Morley, *Biotechniques*, 1992, **3**, 444–449.

2   M. Baker, *Nat. Methods*, 2012, **9**, 541–544.

3   A. A. Morley, *Biomol. Detect. Quantif.*, 2014, 1, 1–2.

4   P. R. Debski and P. Garstecki, *Biomol. Detect. Quantif.*, 2016, **10**, 24–30.

5   E. Z. Z. Macosko, A. Basu, R. Satija, J. Nemesh, K. Shekhar, M. Goldman, I. Tirosh, A. R. Bialas, N. Kamitaki, E. M. Martersteck, J. J. Trombetta, D. A. Weitz, J. R. Sanes, A. K. Shalek, A. Regev and S. A. McCarroll, *Cell*, 2015, **161**, 1202–1214.

6   D. J. Eastburn, A. Sciambi and A. R. Abate, *Nucleic Acids Res.*, 2014, **42**, 1–10.

7   T. S. Kaminski and P. Garstecki, *Chem. Soc. Rev.*, 2017, **46**, 6210–6226.

8   J. J. Agresti, E. Antipov, A. R. Abate, K. Ahn, A. C. Rowat, J.-C. Baret, M. Marquez, A. M. Klibanov, A. D. Griffiths and D. A. Weitz, *Proc. Natl. Acad. Sci.*, 2010, **107**, 4004–4009.

9   A. S. Opalski, T. S. Kaminski and P. Garstecki, *KONA Powder Part. J.*, 2019, **36**, 50–71.

10 D. A. A. McNaught and A. Wilkinson, *IUPAC Goldbook*, Blackwell Scientific Publications, Oxford, 2008.

11 S. Neethirajan, I. Kobayashi, M. Nakajima, D. Wu, S. Nandagopal and F. Lin, *Lab Chip*, 2011, **11**, 1574–1586.

12 E. K. Sackmann, A. L. Fulton and D. J. Beebe, *Nature*, 2014, **507**, 181–189.

13 A. Rakszewska, R. J. Stolper, A. B. Kolasa, A. Piruska and W. T. S. Huck, *Angew. Chemie - Int. Ed.*, 2016, **55**, 6698–6701.

14 H. Hinrichsen and D. E. Wolf, *Phys. Granul. Media*, 2005, **49**, 1–347.

15 T. M. Allen and P. R. Cullis, *Adv. Drug Deliv. Rev.*, 2013, 65, 36–48.

16 F. Fontana, M. P. A. Ferreira, A. Correia, J. Hirvonen and H. A. Santos, *J. Drug Deliv. Sci. Technol.*, 2016, **34**, 76–87.

17 S. N. Kale and S. L. Deore, *Syst. Rev. Pharm.*, 2016, **8**, 39–47.

18 P. Garstecki, I. Gitlin, W. Diluzio, G. M. Whitesides, E. Kumacheva and H. A. Stone, *Appl. Phys. Lett.*, 2004, **85**, 2649–2651.

19 J.-C. Baret, *Lab Chip*, 2012, **12**, 422–433.

20 A. S. Opalski, K. Makuch, Y.-K. K. Lai, L. Derzsi and P. Garstecki, *Lab Chip*, 2019, **19**, 1183–1192.

21   Y. Levin, *J. Stat. Phys.*, 2003, **110**, 825–834.

22   T. F. Tadros, in *Emulsion Formation and Stability*, ed. T. F. Tadros, WILEY-VCH Verlag GmbH, Hoboken, 1st edn., 2013, pp. 1–75.

23   H. N. Joensson and H. Andersson Svahn, *Angew. Chemie - Int. Ed.*, 2012, **51**, 12176–12192.

24   P.-G. de Gennes, F. Brochard-Wyart and D. Quéré, *Phys. Scr.*, 2004, **1987**, 369–374.

25   P. Jankowski, D. Ogonczyk, A. Kosinski, W. Lisowski and P. Garstecki, *Lab Chip*, 2011, **11**, 748–752.

26   L. Derzsi, P. Jankowski, W. Lisowski and P. Garstecki, *Lab Chip*, 2011, **11**, 1151–1156.

27   P. Jankowski, D. Ogończyk, L. Derzsi, W. Lisowski and P. Garstecki, *Microfluid. Nanofluidics*, 2013, **14**, 597–604.

28   M. Bokharaei, K. Saatchi and U. O. Häfeli, *Int. J. Pharm.*, 2017, **521**, 84–91.

29   B. Dai and L. G. Leal, *Phys. Fluids*, 2008, **20**, 1–13.

30   N. Bremond, A. R. Thiam and J. Bibette, *Phys. Rev. Lett.*, 2008, **100**, 024501.

31   C. Holtze, A. C. Rowat, J. J. Agresti, J. B. Hutchison, F. E. Angilè, C. H. J. Schmitz, S. Köster, H. Duan, K. J. Humphry, R. A. Scanga, J. S. Johnson, D. Pisignano and D. A. Weitz, *Lab Chip*, 2008, **8**, 1632–1639.

32   M. H. Rausch, L. Kretschmer, S. Will, A. Leipertz and A. P. Fröba, *J. Chem. Eng. Data*, 2015, **60**, 3759–3765.

33   US Patent Office, US 2010/0105112 A1, 2010.

34   M. Pan, L. Rosenfeld, M. Kim, M. Xu, E. Lin, R. Derda and S. K. Y. Tang, *ACS Appl. Mater. Interfaces*, 2014, **6**, 21446–21453.

35   M. Pan, F. Lyu and S. K. Y. Tang, *Anal. Chem.*, 2015, **87**, 7938–7943.

36   T. Sakai, *Curr. Opin. Colloid Interface Sci.*, 2008, **13**, 228–235.

37   E. Ruckenstein and J. C. Chi, *J. Chem. Soc. Faraday Trans. 2 Mol. Chem. Phys.*, 1975, **71**, 1690–1707.

38   J. Guzowski, P. M. Korczyk, S. Jakiela and P. Garstecki, *Soft Matter*, 2012, **8**, 7269.

39   L. D. Zarzar, V. Sresht, E. M. Sletten, J. A. Kalow, D. Blankschtein and T. M. Swager, *Nature*, 2015, **518**, 520–524.

40   L. D. Landau and E. M. Lishitz, *Fluid Mechanics*, Elsevier Ltd, Moscow, Second., 1987.

41   V. S. Kim and S. J. Karrila, *Microhydrodynamics: Principles and Selected Applications*,

Butterworth-Heinemann Ltd, Boston, London, Singapore, 1992, vol. 64.

42   T. Thorsen, R. W. Roberts, F. H. Arnold and S. R. Quake, *Phys. Rev. Lett.*, 2001, **86**, 4163–4166.

43   P. Garstecki, M. J. Fuerstman, H. A. Stone and G. M. Whitesides, *Lab Chip*, 2006, **6**, 437–446.

44   M. De Menech, P. Garstecki, F. Jousse and H. A. Stone, *J. Fluid Mech.*, 2008, **595**, 141–161.

45   A. S. Utada, A. Fernandez-Nieves, H. A. Stone and D. A. Weitz, *Phys. Rev. Lett.*, 2007, **99**, 094502.

46   A. R. Abate, J. Thiele and D. A. Weitz, *Lab Chip*, 2011, **11**, 253–258.

47   N. L. Jeon, S. K. W. Dertinger, D. T. Chiu, I. S. Choi, A. D. Stroock and G. M. Whitesides, *Langmuir*, 2000, **16**, 8311–8316.

48   D. R. Reyes, D. Iossifidis, P. A. Auroux and A. Manz, *Anal. Chem.*, 2002, **74**, 2623–2636.

49   E. Berthier, E. W. K. Young and D. Beebe, *Lab Chip*, 2012, **12**, 1224–1237.

50   M. A. Unger, H. P. Chou, T. Thorsen, A. Scherer and S. R. Quake, *Science.*, 2000, **288**, 113–116.

51   A. Manz, D. J. Harrison, E. M. J. Verpoorte, J. C. Fettinger, A. Paulus, H. Lüdi and H. M. Widmer, *J. Chromatogr. A*, 1992, **593**, 253–258.

52   D. J. Harrison, K. Fluri, K. Seiler, Z. Fan, C. S. Effenhauser and A. Manz, *Science.*, 1993, **261**, 895–897.

53   T. M. Squires and S. R. Quake, *Rev. Mod. Phys.*, 2005, **77**, 977–1026.

54   A. Persat, M. E. Suss and J. G. Santiago, *Lab Chip*, 2009, **9**, 2454–2469.

55   A. Persat, R. D. Chambers and J. G. Santiago, *Lab Chip*, 2009, **9**, 2437–2453.

56   J. Melin and S. R. Quake, *Annu. Rev. Biophys. Biomol. Struct.*, 2007, **36**, 213–231.

57   T. Thorsen, S. J. Maerkl and S. R. Quake, *Science.*, 2002, **298**, 580–584.

58   G. Taylor, *Proc. R. Soc. A Math. Phys. Eng. Sci.*, 1953, **219**, 186–203.

59   R. Aris, *Proc. R. Soc. A Math. Phys. Eng. Sci.*, 1960, **259**, 370–376.

60   H. Song, D. L. Chen and R. F. Ismagilov, *Angew. Chemie - Int. Ed.*, 2006, **45**, 7336–7356.

61   X. Casadevall i Solvas and A. deMello, *Chem. Commun.*, 2011, **47**, 1936–1942.

62   Y. Temiz, R. D. Lovchik, G. V. Kaigala and E. Delamarche, *Microelectron. Eng.*, 2015, **132**, 156–175.

63   H. Gu, M. H. G. Duits and F. Mugele, *Int. J. Mol. Sci.*, 2011, **12**, 2572–2597.

64   J. D. Tice, H. Song, A. D. Lyon and R. F. Ismagilov, *Langmuir*, 2003, **19**, 9127–9133.

65   J. D. Tice, A. D. Lyon and R. F. Ismagilov, *Anal. Chim. Acta*, 2004, **507**, 73–77.

66   S.-Y. Teh, R. Lin, L.-H. Hung and A. P. Lee, *Lab Chip*, 2008, **8**, 198–220.

67   J. Guzowski, P. M. Korczyk, S. Jakiela and P. Garstecki, *Lab Chip*, 2011, **11**, 3593–3595.

68   M. Leman, F. Abouakil, A. D. Griffiths and P. Tabeling, *Lab Chip*, 2015, **15**, 753–765.

69   A. Sciambi and A. R. Abate, *Lab Chip*, 2015, **15**, 47–51.

70   T. H. Kim, C. J. Kim, Y. Kim and Y. K. Cho, *Sensors Actuators, B Chem.*, 2018, **256**, 310–317.

71   S. Haeberle, D. Mark, F. Von Stetten and R. Zengerle, *Microsystems Nanotechnol.*, 2012, **9783642182**, 853–895.

72   A. R. Abate, T. Hung, P. Mary, J. J. Agresti and D. A. Weitz, *Proc. Natl. Acad. Sci.*, 2010, **107**, 19163–19166.

73   T. S. Kaminski, S. Jakiela, M. A. Czekalska, W. Postek and P. Garstecki, *Lab Chip*, 2012, **12**, 3995–4002.

74   M. Horka, S. Sun, A. Ruszczak, P. Garstecki and T. Mayr, *Anal. Chem.*, 2016, **88**, 12006–12012.

75   K. Churski, T. S. Kaminski, S. Jakiela, W. Kamysz, W. Baranska-Rybak, D. B. Weibel and P. Garstecki, *Lab Chip*, 2012, **12**, 1629–1637.

76   S. Jakiela, T. S. Kaminski, O. Cybulski, D. B. Weibel and P. Garstecki, *Angew. Chemie - Int. Ed.*, 2013, **52**, 8908–8911.

77   S. Schmitt, M. Walser, M. Rehmann, S. Oesterle, S. Panke and M. Held, *Sci. Rep.*, 2018, **8**, 1–9.

78   F. Schuler, M. Trotter, M. Geltman, F. Schwemmer, S. Wadle, E. Domínguez-Garrido, M. López, C. Cervera-Acedo, P. Santibáñez, F. von Stetten, R. Zengerle and N. Paust, *Lab Chip*, 2016, **16**, 208–216.

79   P. Mair, F. Gielen and F. Hollfelder, *Curr. Opin. Chem. Biol.*, 2017, **37**, 137–144.

80   H. H. Jeong, D. Issadore and D. Lee, *Korean J. Chem. Eng.*, 2016, **33**, 1757–1766.

81   S. Yadavali, H. H. Jeong, D. Lee and D. Issadore, *Nat. Commun.*, 2018, **9**, 1222.

82   T. Nisisako and T. Torii, *Lab Chip*, 2008, **8**, 287–293.

83   A. S. Utada, E. Lorenceau, D. R. Link, P. D. Kaplan, H. A. Stone and D. A. Weitz, *Science.*, 2005, **308**, 537–541.

84   M. V. Bandulasena, G. T. Vladisavljević and B. Benyahia, *J. Colloid Interface Sci.*, 2019, **542**, 23–32.

85   J. C. McDonald, D. C. Duffy, J. R. Anderson, D. T. Chiu, H. Wu, O. J. A. Schueller and G. M. Whitesides, *Electrophoresis*, 2000, **21**, 27–40.

86   D. C. Duffy, J. C. McDonald, O. J. A. Schueller and G. M. Whitesides, *Anal. Chem.*, 1998, **70**, 4974–4984.

87   J. C. McDonald and G. M. Whitesides, *Acc. Chem. Res.*, 2002, **35**, 491–499.

88   J. N. Lee, C. Park and G. M. Whitesides, *Anal. Chem.*, 2003, **75**, 6544–6554.

89   K. J. Regehr, M. Domenech, J. T. Koepsel, K. C. Carver, S. J. Ellison-Zelski, W. L. Murphy, L. A. Schuler, E. T. Alarid and D. J. Beebe, *Lab Chip*, 2009, **9**, 2132–2139.

90   A. Zuchowska, P. Kwiatkowski, E. Jastrzebska, M. Chudy, A. Dybko and Z. Brzozka, *Electrophoresis*, 2016, **37**, 536–544.

91   Y. Xia and G. M. Whitesides, *Angew. Chemie - Int. Ed. Int. Ed.*, 1998, **37**, 550–575.

92   K. Haubert, T. Drier, D. Beebe, D. Duffy, J. McDonald, O. Schueler, G. Whitesides, B. Jo, L. Van Lerberghe, K. Motsegood, D. Beebe, B. Ginn, O. Steinbock, D. Eddington, J. Puccinelli and D. Beebe, *Lab Chip*, 2006, **6**, 1548–1549.

93   D. J. Guckenberger, T. E. De Groot, A. M. D. Wan, D. J. Beebe and E. W. K. Young, *Lab Chip*, 2015, **15**, 2364–2378.

94   R. Ortiz, J. L. Chen, D. C. Stuckey and T. W. J. Steele, *Micro Nano Eng.*, 2019, **2**, 92–103.

95   D. Ogończyk, J. Węgrzyn, P. Jankowski, B. Dąbrowski and P. Garstecki, *Lab Chip*, 2010, **10**, 1324–1327.

96   D. Conchouso, D. Castro, S. A. Khan and I. G. Foulds, *Lab Chip*, 2014, **14**, 3011–3020.

97   T. B. Stachowiak, D. A. Mair, T. G. Holden, L. J. Lee, F. Svec and J. M. J. Fréchet, *J. Sep. Sci.*, 2007, **30**, 1088–1093.

98   H. Li, Y. Fan, R. Kodzius and I. G. Foulds, *Microsyst. Technol.*, 2012, **18**, 373–379.

99   T. Femmer, A. Jans, R. Eswein, N. Anwar, M. Moeller, M. Wessling and A. J. C. Kuehne, *ACS Appl. Mater. Interfaces*, 2015, **7**, 12635–12638.

100   P. Zhu and L. Wang, *Lab Chip*, 2017, **17**, 34–75.

101   H. Van Nguyen, H. Q. Nguyen, V. D. Nguyen and T. S. Seo, *Sensors Actuators B Chem.*, 2019, **296**, 126676.

102   J. Zhou, D. A. Khodakov, A. V. Ellis and N. H. Voelcker, *Electrophoresis*, 2012, **33**, 89–104.

103   A. R. Abate, D. Lee, T. Do, C. Holtze and D. A. Weitz, *Lab Chip*, 2008, **8**, 516–518.

104   A. R. Abate, J. Thiele, M. Weinhart and D. A. Weitz, *Lab Chip*, 2010, **10**, 1774–1776.

105   S. C. Kim, D. J. Sukovich and A. R. Abate, *Lab Chip*, 2015, **15**, 3163–3169.

134

106   B. H. Jo, L. M. van Lerberghe, K. M. Motsegood and D. J. Beebe, *J. Microelectromechanical Syst.*, 2000, **9**, 76–81.

107   W.-A. C. Bauer, M. Fischlechner, C. Abell and W. T. S. Huck, *Lab Chip*, 2010, **10**, 1814–1819.

108   J. Yan, W. A. C. Bauer, M. Fischlechner, F. Hollfelder, C. F. Kaminski and W. T. S. Huck, *Micromachines*, 2013, **4**, 402–413.

109   K. M. Kovach, J. R. Capadona, A. Sen Gupta and J. A. Potkay, *J. Biomed. Mater. Res. - Part A*, 2014, **102**, 4195–4205.

110   S. Deshpande and C. Dekker, *Nat. Protoc.*, 2018, **13**, 856–874.

111   Y. J. Chuah, Y. T. Koh, K. Lim, N. V. Menon, Y. Wu and Y. Kang, *Sci. Rep.*, 2015, **5**.

112   H. Liu, J. Huang, Z. Chen, G. Chen, K. Q. Zhang, S. S. Al-Deyab and Y. Lai, *Chem. Eng. J.*, 2017, **330**, 26–35.

113   L. Derzsi, T. S. Kaminski and P. Garstecki, *Lab Chip*, 2016, **16**, 893–901.

114   L. A. Filla, D. C. Kirkpatrick and R. S. Martin, *Anal. Chem.*, 2011, **83**, 5996–6003.

115   A. Vian, B. Reuse and E. Amstad, *Lab Chip*, 2018, **18**, 1936–1942.

116   R. Ortiz, J. L. Chen, D. C. Stuckey and T. W. J. Steele, *ACS Appl. Mater. Interfaces*, 2017, **9**, 13801–13811.

117   K. Bazaka and O. Bazaka, *Superhydrophobic Polymers*, WILEY-VCH Verlag GmbH, 2015.

118   L. Rayleigh, *Proc. R. Soc. London*, 1879, **29**, 71–97.

119   J. Plateau, *Statique expérimentale et théorique des liquides soumis aux seules forces moléculaires*, Gauthier-Villars, Paris, 1873.

120   A. A. Fragkopoulos, P. W. Ellis and A. Fernandez-Nieves, *Eur. J. Phys.*, 2015, **36**.

121   P. Garstecki, H. A. Stone and G. M. Whitesides, *Phys. Rev. Lett.*, 2005, **94**, 164501.

122   P. M. Korczyk, L. Derzsi, S. Jakieła and P. Garstecki, *Lab Chip*, 2013, **13**, 4096–4102.

123   G. Amselem, C. Guermonprez, B. Drogue, S. Michelin and C. N. Baroud, *Lab Chip*, 2016, **16**, 4200–4211.

124   R. Dangla, S. C. Kayi and C. N. Baroud, *Proc. Natl. Acad. Sci.*, 2013, **110**, 853–858.

125   M. A. Czekalska, T. S. Kaminski, K. Makuch and P. Garstecki, *Sensors Actuators B Chem.*, 2019, **286**, 258–265.

126   S. L. Anna, N. Bontoux and H. A. Stone, *Appl. Phys. Lett.*, 2003, **82**, 364–366.

127   P. B. Umbanhowar, V. Prasad and D. A. Weitz, *Langmuir*, 2000, **16**, 347–351.

128   A. Zinchenko, S. R. A. Devenish, B. Kintses, P. Y. Colin, M. Fischlechner and F. Hollfelder, *Anal. Chem.*, 2014, **86**, 2526–2533.

129   P. Garstecki, M. J. Fuerstman and G. M. Whitesides, *Phys. Rev. Lett.*, 2005, **94**, 234502.

130   P. M. Korczyk, V. van Steijn, S. Blonski, D. Zaremba, D. A. Beattie and P. Garstecki, *Nat. Commun.*, 2019, **10**, 2528.

131   S. L. Anna, *Annu. Rev. Fluid Mech.*, 2016, **48**, 285–309.

132   L. Derzsi, Institute of Physical Chemistry of Polish Academy of Sciences, 2012.

133   F. Dutka, A. S. Opalski and P. Garstecki, *Lab Chip*, 2016, **16**, 2044–2049.

134   N. Mittal, C. Cohen, J. Bibette and N. Bremond, *Phys. Fluids*, 2014, **26**, 082109.

135   T. Nakashima, M. Shimizu and M. Kukizaki, *Adv. Drug Deliv. Rev.*, 2000, **45**, 47–56.

136   S. Sugiura, M. Nakajima, S. Iwamoto and M. Seki, *Langmuir*, 2001, **17**, 5562–5566.

137   T. Kawakatsu, Y. Kikuchi and M. Nakajima, *J. Am. Oil Chem. Soc.*, 1997, **74**, 317–321.

138   S. Sugiura, M. Nakajima, J. Tong, H. Nabetani and M. Seki, *J. Colloid Interface Sci.*, 2000, **227**, 95–103.

139   R. Dangla, E. Fradet, Y. Lopez and C. N. Baroud, *J. Phys. D. Appl. Phys.*, 2013, **46**, 114003.

140   I. Kobayashi, M. Nakajima, K. Chun, Y. Kikuchi and H. Fujita, *AIChE J.*, 2002, **48**, 1639–1644.

141   A. Montessori, M. Lauricella, S. Succi, E. Stolovicki and D. Weitz, *Phys. Rev. Fluids*, 2018, **7**, 1–7.

142   M. Hein, S. Afkhami, R. Seemann and L. Kondic, *Microfluid. Nanofluidics*, 2015, **18**, 911–917.

143   Z. Li, A. M. Leshansky, L. M. Pismen and P. Tabeling, *Lab Chip*, 2015, **15**, 1023–1031.

144   I. Chakraborty, J. Ricouvier, P. Yazhgur, P. Tabeling and A. M. Leshansky, *Lab Chip*, 2017, **17**, 3609–3620.

145   E. Amstad, M. Chemama, M. Eggersdorfer, L. R. Arriaga, M. P. Brenner and D. A. Weitz, *Lab Chip*, 2016, **16**, 138–155.

146   A. G. Håti, T. Szymborski, M. Steinacher and E. Amstad, *Lab Chip*, 2018, **18**, 648–654.

147   G. T. Vladisavljević, E. E. Ekanem, Z. Zhang, N. Khalid, I. Kobayashi and M. Nakajima, *Chem. Eng. J.*, 2018, **333**, 380–391.

148   F. Spyropoulos, D. M. Lloyd, R. D. Hancocks and A. K. Pawlik, *J. Sci. Food Agric.*, 2014, **94**, 628–638.

149   K. van Dijke, G. Veldhuis, K. Schroën and R. Boom, *Lab Chip*, 2009, **9**, 2824–2830.

150   S. Sugiura, M. Nakajima and M. Seki, *Langmuir*, 2002, **18**, 5708–5712.

151   E. Crestel, L. Derzsi, H. Bartolomei, J. Bibette and N. Bremond, *Phys. Rev. Fluids*, 2019, **4**, 073602.

152   S. Sugiura, M. Nakajima and M. Seki, *Langmuir*, 2002, **18**, 3854–3859.

153   S. Sugiura, M. Nakajima, N. Kumazawa, S. Iwamoto and M. Seki, *J. Phys. Chem. B*, 2002, **106**, 9405–9409.

154   K. van Dijke, R. de Ruiter, K. Schroën and R. Boom, *Soft Matter*, 2010, **6**, 321–330.

155   K. C. van Dijke, K. Schroën, A. van der Padt and R. Boom, *J. Food Eng.*, 2010, **97**, 348–354.

156   D. T. Chong, X. S. Liu, H. J. Ma, G. Y. Huang, Y. L. Han, X. Y. Cui, J. J. Yan and F. Xu, *Microfluid. Nanofluidics*, 2015, **19**, 1071–1090.

157   G. T. Vladisavljević, R. Al Nuumani and S. Nabavi, *Micromachines*, 2017, **8**, 75.

158   N. Garti, *Colloids Surfaces A Physicochem. Eng. Asp.*, 1997, **123–124**, 233–246.

159   C. H. Choi, H. Lee, A. Abbaspourrad, J. H. Kim, J. Fan, M. Caggioni, C. Wesner, T. Zhu and D. A. Weitz, *Adv. Mater.*, 2016, **28**, 3340–3344.

160   S.-H. Kim, J. W. Kim, J.-C. Cho and D. A. Weitz, *Lab Chip*, 2011, **11**, 3162–3166.

161   A. Vian, V. Favrod and E. Amstad, *Microfluid. Nanofluidics*, 2016, **20**, 159.

162   L. R. Arriaga, E. Amstad and D. A. Weitz, *Lab Chip*, 2015, **15**, 3335–3340.

163   K. Akamatsu, S. Kanasugi, S. I. Nakao and D. A. Weitz, *Langmuir*, 2015, **31**, 7166–7172.

164   C. S. Ho, J. W. Kim and D. A. Weitz, *J. Am. Chem. Soc.*, 2008, **130**, 9543–9549.

165   S. H. Kim, J. W. Kim, D. H. Kim, S. H. Han and D. A. Weitz, *Small*, 2013, **9**, 124–131.

166   N. N. Deng, M. Yelleswarapu and W. T. S. Huck, *J. Am. Chem. Soc.*, 2016, **138**, 7584–7591.

167   T. Nisisako, S. Okushima and T. Torii, *Soft Matter*, 2005, **1**, 23–27.

168   C.-H. H. Choi, H. Wang, H. Lee, J. H. Kim, L. Zhang, A. Mao, D. J. Mooney and D. A. Weitz, *Lab Chip*, 2016, **16**, 1549–1555.

169   S. Van Der Graaf, C. G. P. H. Schroën and R. M. Boom, *J. Memb. Sci.*, 2005, **251**, 7–15.

170   S. Sugiura, M. Nakajima, K. Yamamoto, S. Iwamoto, T. Oda, M. Satake and M. Seki, *J. Colloid Interface Sci.*, 2004, **270**, 221–228.

171   M. L. Eggersdorfer, W. Zheng, S. Nawar, C. Mercandetti, A. Ofner, I. Leibacher, S. Koehler and D. A. Weitz, *Lab Chip*, 2017, **17**, 936–942.

172   A. Ofner, I. Mattich, M. Hagander, A. Dutto, H. Seybold, P. A. Rühs and A. R. Studart, *Adv. Funct. Mater.*, 2018, **1806821**, 1806821.

173   J. Guzowski, S. Jakiela, P. M. Korczyk and P. Garstecki, *Lab Chip*, 2013, **13**, 4308–4311.

174   J. Guzowski and P. Garstecki, *Phys. Rev. Lett.*, 2015, **114**, 188302.

175   R. K. Saiki, S. Scharf, F. Faloona, K. B. Mullis, G. T. Horn, H. A. Erlich and N. Arnheim, *Science.*, 1985, **230**, 1350–1354.

176   P. R. Debski, K. Gewartowski, S. Bajer and P. Garstecki, *Sci. Rep.*, 2017, **7**, 44854.

177   B. J. Hindson, K. D. Ness, D. A. Masquelier, P. Belgrader, N. J. Heredia, A. J. Makarewicz, I. J. Bright, M. Y. Lucero, A. L. Hiddessen, T. C. Legler, T. K. Kitano, M. R. Hodel, J. F. Petersen, P. W. Wyatt, E. R. Steenblock, P. H. Shah, L. J. Bousse, C. B. Troup, J. C. Mellen, D. K. Wittmann, N. G. Erndt, T. H. Cauley, R. T. Koehler, A. P. So, S. Dube, K. A. Rose, L. Montesclaros, S. Wang, D. P. Stumbo, S. P. Hodges, S. Romine, F. P. Milanovich, H. E. White, J. F. Regan, G. A. Karlin-Neumann, C. M. Hindson, S. Saxonov and B. W. Colston, *Anal. Chem.*, 2011, **83**, 8604–8610.

178   Q. Zhu, Y. Xu, L. Qiu, C. Ma, B. Yu, Q. Song, W. Jin, Q. Jin, J. Liu and Y. Mu, *Lab Chip*, 2017, **17**, 1655–1665.

179   A. C. Hatch, J. S. Fisher, A. R. Tovar, A. T. Hsieh, R. Lin, S. L. Pentoney, D. L. Yang and A. P. Lee, *Lab Chip*, 2011, **11**, 3838–3845.

180   T. S. Kaminski, Institute of Physical Chemistry of Polish Academy of Sciences, 2016.

181   J. Kehe, A. Kulesa, A. Ortiz, C. M. Ackerman, S. G. Thakku, D. Sellers, S. Kuehn, J. Gore, J. Friedman and P. C. Blainey, *Proc. Natl. Acad. Sci.*, 2019, 201900102.

182   W. Postek, P. Gargulinski, O. Scheler, T. S. Kaminski and P. Garstecki, *Lab Chip*, 2018, **18**, 3668–3677.

183   P. Neužil, S. Giselbrecht, K. Länge, T. J. Huang and A. Manz, *Nat. Rev. Drug Discov.*, 2012, **11**, 620–632.

184   A. Kulesa, J. Kehe, J. E. Hurtado, P. Tawde and P. C. Blainey, *Proc. Natl. Acad. Sci. U. S. A.*, 2018, 201802233.

185   F. Lan, B. Demaree, N. Ahmed and A. R. Abate, *Nat. Biotechnol.*, 2017, **35**, 640–646.

186   M. Stoeckius, C. Hafemeister, W. Stephenson, B. Houck-Loomis, P. K. Chattopadhyay, H. Swerdlow, R. Satija and P. Smibert, *Nat. Methods*, 2017, **14**, 865.

187   F. Schuler, N. Paust, R. Zengerle and F. von Stetten, *Micromachines*, 2015, **6**, 1180–1188.

188   J. M. de Rutte, J. Koh and D. Di Carlo, *Adv. Funct. Mater.*, 2019, **1900071**, 1900071.

189   Stilla Technologies, *Appl. note*, 2016, https://www.stillatechnologies.com/application-not.

190   Z. Z. Chong, S. B. Tor, A. M. Gañán-Calvo, Z. J. Chong, N. H. Loh, N. T. Nguyen and S. H. Tan, *Microfluid. Nanofluidics*, 2016, **20**, 1–14.

191   C. T. Rueden, J. Schindelin, M. C. Hiner, B. E. DeZonia, A. E. Walter, E. T. Arena and K. W. Eliceiri, *BMC Bioinformatics*, 2017, **18**, 1–26.

192   J. Schindelin, I. Arganda-Carreras, E. Frise, V. Kaynig, M. Longair, T. Pietzsch, S. Preibisch, C. Rueden, S. Saalfeld, B. Schmid, J. Y. Tinevez, D. J. White, V. Hartenstein, K. Eliceiri, P. Tomancak and A. Cardona, *Nat. Methods*, 2012, **9**, 676–682.

193   O. Cybulski and P. Garstecki, in *19th International Conference on Miniaturized Systems for Chemistry and Life Sciences (MicroTAS 2015)*, 2015, pp. 1398–1400.

194   P. M. Korczyk, O. Cybulski, S. Makulska and P. Garstecki, *Lab Chip*, 2011, **11**, 173–175.

195   C. A. Schneider, W. S. Rasband and K. W. Eliceiri, *Nat. Methods*, 2012, **9**, 671–675.

196   M. L. Eggersdorfer, H. Seybold, A. Ofner, D. A. Weitz and A. R. Studart, *Proc. Natl. Acad. Sci.*, 2018, 201803644.

197   M. Nakajima, *Lab Chip*, 2017, **17**, 2330–2331.

198   E. Amstad and D. A. Weitz, *Lab Chip*, 2017, **17**, 2332–2333.

199   G. M. Walker, *Nat. Chem.*, 2011, **3**, 428–429.

200   N. S. Cheng, *Ind. Eng. Chem. Res.*, 2008, **47**, 3285–3288.

201   E. Stolovicki, R. Ziblat and D. A. Weitz, *Lab Chip*, 2018, **18**, 132–138.

202   W. Postek, T. S. Kaminski and P. Garstecki, *Lab Chip*, 2017, **17**, 1323–1331.

203   S. A. Byrnes, T. C. Chang, T. Huynh, A. Astashkina, B. H. Weigl and K. P. Nichols, *Anal. Chem.*, 2018, **90**, 9374–9380.

204   D. J. Sukovich, S. C. Kim, N. Ahmed and A. R. Abate, *Analyst*, 2017, **142**, 4618–4622.

205   Z. Zhu and C. J. Yang, *Acc. Chem. Res.*, 2017, **50**, 22–31.

206   V. Eisinaite, D. Juraite, K. Schroën and D. Leskauskaite, *Food Chem.*, 2016, **206**, 59–66.

207   B. Tal-Figiel, *Chem. Eng. Res. Des.*, 2007, **85**, 730–734.

208   K. Bernath, M. Hai, E. Mastrobattista, A. D. Griffiths, S. Magdassi and D. S. Tawfik, *Anal. Biochem.*, 2004, **325**, 151–157.

209   A. Vian and E. Amstad, *Soft Matter*, 2019, **15**, 1290–1296.

210   J. Petit, I. Polenz, J. C. Baret, S. Herminghaus and O. Bäumchen, *Eur. Phys. J. E*, 2016, **39**.

211   C. X. Zhao, D. Chen, Y. Hui, D. A. Weitz and A. P. J. Middelberg, *ChemPhysChem*, 2016, **17**, 1553–1556.

212   L. A. Adams, T. E. Kodger, S.-H. Kim, H. C. Shum, T. Franke and D. A. Weitz, *Soft Matter*, 2012, **8**,

10719.

213   S. A. Nabavi, G. T. Vladisavljević, S. Gu and E. E. Ekanem, *Chem. Eng. Sci.*, 2015, **130**, 183–196.

214   S. A. Nabavi, G. T. Vladisavljević and V. Manović, *Chem. Eng. J.*, 2017, **322**, 140–148.

215   3M Electronics Markets Materials Division, *Prod. Descr.*, 2010.

216   K. Van Dijke, I. Kobayashi, K. Schroën, K. Uemura, M. Nakajima and R. Boom, *Microfluid. Nanofluidics*, 2010, **9**, 77–85.

217   S. A. Nabavi, S. Gu, G. T. Vladisavljević and E. E. Ekanem, *J. Colloid Interface Sci.*, 2015, **450**, 279–287.

218   T. S. Kaminski, O. Scheler and P. Garstecki, *Lab Chip*, 2016, **16**, 2168–2187.

219   O. Scheler, W. Postek and P. Garstecki, *Curr. Opin. Biotechnol.*, 2018, **55**, 60–67.

220   M. Maeki, Y. Teshima, S. Yoshizuka, H. Yamaguchi, K. Yamashita and M. Miyazaki, *Chem. - A Eur. J.*, 2014, **20**, 1049–1056.

221   H. Lu, O. Caen, J. Vrignon, E. Zonta, Z. El Harrak, P. Nizard, J. C. Baret and V. Taly, *Sci. Rep.*, 2017, **7**, 1366.

222   K. Grosselin, A. Durand, J. Marsolier, A. Poitou, E. Marangoni, F. Nemati, A. Dahmani, S. Lameiras, F. Reyal, O. Frenoy, Y. Pousse, M. Reichen, A. Woolfe, C. Brenan, A. D. Griffiths, C. Vallot and A. Gérard, *Nat. Genet.*, 2019, **51**, 1060–1066.

223   M. Madou, J. Zoval, G. Jia, H. Kido, J. Kim and N. Kim, *Annu. Rev. Biomed. Eng.*, 2006, **8**, 601–628.

224   Z. Chen, Y. Fu, F. Zhang, L. Liu, N. Zhang, D. Zhou, J. Yang, Y. Pang and Y. Huang, *Lab Chip*, 2016, **16**, 4512–4516.

225   K. Langer, N. Bremond, L. Boitard, J. Baudry and J. Bibette, *Biomicrofluidics*, 2018, **12**.

226   J. Fan, Y. Men, H. Tseng, Y. Ding and Y. Ding, *Biomicrofluidics*, 2018, **12**, 034107.

227   J.-C. Baret, O. J. Miller, V. Taly, M. Ryckelynck, A. El-Harrak, L. Frenz, C. Rick, M. L. Samuels, J. B. Hutchison, J. J. Agresti, D. R. Link, D. A. Weitz and A. D. Griffiths, *Lab Chip*, 2009, **9**, 1850–1858.

228   S. S. Schütz, T. Beneyton, J.-C. Baret and T. M. Schneider, *Lab Chip*, 2019, 2220–2232.

229   P. Y. Colin, B. Kintses, F. Gielen, C. M. Miton, G. Fischer, M. F. Mohamed, M. Hyvönen, D. P. Morgavi, D. B. Janssen and F. Hollfelder, *Nat. Commun.*, 2015, **6**.